5-2014

Understanding the Influence of Interfacial Chemistry in Core, Core/Shell and Core/Shell/Shell Quantum Dots on their Fluorescence Properties

Omondi Bernard Omogo
University of Arkansas, Fayetteville

Understanding the Influence of Interfacial Chemistry in Core, Core/Shell and Core/Shell/Shell Quantum Dots on their Fluorescence Properties

Understanding the Influence of Interfacial Chemistry in Core, Core/Shell and Core/Shell/Shell Quantum Dots on their Fluorescence Properties

A dissertation submitted in partial fulfillment
of the requirements for the degree of
Doctor of Philosophy in Chemistry

by

Omondi Benard Omogo
The Catholic University of Eastern Africa
Bachelors of Education (Science) in Mathematics & Chemistry, 2008

May 2014
University of Arkansas

This dissertation is approved for recommendation to the Graduate Council.

_____
Dr. Colin Heyes
Dissertation Director

_____
Dr. Paul Adams
Committee Member

_____
Dr. Jingyi Chen
Committee Member

_____
Dr. Feng Wang
Committee Member

ABSTRACT

Colloidal semiconductor nanocrystals (quantum dots) have received a great deal of attention due to their superior size tunable properties and promising applications in many areas. Some of the most practical areas of their applications include light emitting diodes (LED), photovoltaic and biological studies. Synthetic methods of these crystals is becoming more established with new strategies being reported every now and then. However, quantitative studies connecting the processes at the interface, namely core-ligand, core-shell and shell-shells, to the overall quantum dots fluorescence properties are not well understood. Specifically for cores, relating surface-atoms interactions, solvents, ligands nature, density and functional groups on quantum yields have not been exhaustively carried out. Furthermore, for the core/shell counterparts, the connection between the qualities of the starting core on its resulting core/shell quality have been left trivial without experimental back up. Here, we summarize the reports of experiments that have systematically investigated these effects on the properties of quantum dots. Combining systematic synthetic approach with characterization tools such as FTIR, X-ray photoelectron and diffraction together with time resolved visible spectroscopies, we observed that the density, nature and the orientation of the ligand functional groups play significant roles in determining the charge carrier dynamics that results on the various quantum yields and quality of the quantum dots. The experimental results also contradicted the trivial belief that starting with a high quality core material should result into high quality core/shell quantum dots. We further extended these studies by controlling both lattice mismatch and exciton confinement potential to design small, biologically friendly and highly stable core/shell/shell material. Blinking studies confirmed an interplay of both lattice strain and exciton confinement as the major factors responsible for the blinking dynamics of these core/shell/shell quantum dots. Therefore, by controlling these parameters, we were able to observe

reduced blinking quantum dots with relatively moderate shell thickness. These observations will provide a useful insight while designing these particles and enhance their future applications.

ACKNOWLEDGMENTS

This journey has been very phenomenal. It had several ups and downs, some very challenging but I realized that I had wonderful people around me. I'm fortunate to have reached this far to be able to recognize a few of them here. First of all, I would like to thank the Almighty God for His blessings throughout these years. Second, the late Dr. Robert E Gawley for his advice anytime I stopped by his office and during committee meetings that greatly motivated me. He left us so early but he remained as an inspiration in my heart; may he rest in peace. My special thanks also goes to my advisor Dr. Colin Heyes, if it was not for his positive direction, understanding and encouragement, things may be different now. His approach to advising made me discover so much potential, which I did not realize before.

I would like to thank my current committee members: Dr. Paul Adams, Dr. Jingyi Chen and Dr. Wang Feng. Their continuous advice and stimulating discussions challenged me to do more. Dr. Xiaogang Peng and Dr. Min Xiao, even though their transfers could not allow them continue serving in my committee, for the foundation they laid that helped keep this project going. I am grateful to both Dr. Bill Durham and Dr. Dan Davis for their continuous advice and recommendations while making decisions regarding the graduate school requirements. I would like to express my regards to Ms. Liz Williams, Ms. Heather Jorgensen, and Ms. Leslie Johnson for their countless professional help to me as a student, as well as to the rest of Chemistry department faculty, staff and students that I was fortunate to meet and work with. To all my lab group members, their friendship turned the lab into a home where I could walk in and feel always welcome. Special thanks go to Dr. Jose Aldana who gave me the initial hands on training with making these nanoparticles.

I am also grateful to Dr. Feng Gao for the help with training on single molecule experiments and discussions. Dr. Madhuri Mukhopadhyay and Dr. Gopa Mandal for collaboration and discussions. Thanks also go to Derrel Walters for setting up the vacuuming system that opened the way for successful synthesis. Additional thanks are extended to Dr. Mourad Benamara for overall training with TEM and specifically Dr. Ryan for intensive training on handling the TEM which equipped me with skills to be an independent operator.

I would like to thank all my family members, especially my parents Peter and Leonida Omogo, their prayers and constant encouragement gave me the motivation to carry on. Special thanks go my uncle, Fr. John Agala for prayers and bro Camlus Omogo, for words of encouragement and advise when things got tough. Both their selflessness to pay part of my college fee was the background for this achievement. Also, special thanks go to my girlfriend, Dorine Munyasia Kisiangani (Dolphine). Even though she came to my life during the final years of this journey, she was very supportive and encouraging, especially with reading through the document for spelling errors. I would like to also thank my brothers Leonard Omogo and Maurice Omogoh for constantly calling and chatting to check on how things are going on with me. Special thanks to my sister-law Millicent Adhiambo Oganga for wonderful hospitality whenever I came home for holidays. I was fortunate to have a wonderful host family who made life simple and quickly transformed Fayetteville to a home; thanks to Mr. Murl, May and Grant Meredith and the family. Finally my regards go to all my friends who have been part of my life over this time especially JeanMarie Bikorimana, Antony Ndugo, Francis Oloo (Walala), Pooja, Winnie Nyambok, Maryanne Gachukia, Sarah Hamilton, Jane Achando, Felix Rotich, Gordon Ochieng, Mildred Otieno, Immaculate Otieno, John and Anne Magugu, and George Ondier, they were all motivating in different ways during this journey.

DEDICATION

This dissertation is dedicated to three groups as follow. Firstly, to my parents Peter and Leonida Omogo. Even though you never had any formal education, you still remain as my best teachers ever. Mum, I promise to start an educational foundation with your name to promote your belief in education. Secondly, to my late family members especially to my grandmother Agnes Okeya Agala, The pocket money you were giving me when I was in high school was very helpful and is still highly appreciated. My late sister Annastasia Akinyi. You told me when I was little that there were good things ahead for me and twenty years later I am writing this dissertation. I still live with that conversation and hope for better things ahead. My late brother Paul Oduor Omogo and his wife Jane Auma Oduor, I admired and still try to imitate your simple way of approaching life. May you all R.I.P. Lastly, to all the children from the larger K'agala family. This is the second Ph.D. from this big family but I challenge you to bring more Ph.Ds or any other educational excellence to this family.

TABLE OF CONTENTS

CHAPTERS

LIST OF TABLES

LIST OF FIGURES

LIST OF PUBLICATIONS

Chapter 2. Published: Omogo, B., Aldana, J.F and Heyes, C.D. Radiative and Nonradiative Lifetime Engineering of Quantum Dots in Multiple Solvents by Surface Atom Stoichiometry and Ligands. The Journal of Physical Chemistry C, 2013. 117(5): p. 2317-2327

Chapter 3. To Be Submitted: Omogo, B and Heyes**,** C. D. How the Quality of the CdSe Core affects the Optical Properties of CdSe/CdS Core/Shell Quantum Dots.

Chapter 4. To Be Submitted: Omogo, B, Gao, F., Kaneko, M and Heyes**,** C. D. Effect of Outer Shell Thickness in Core/Shell/Shell Quantum Dots on Blinking

Chapter 1. Introduction

Colloidal semiconductor nanocrystals also known quantum dots are tiny materials with their sizes ranging in a nanometer scale.[1] One of the unique feature of these crystals is that their optical and electronic properties can be tuned depending on the material, shape or the size.[2] Photo-excitation of these materials with energy equal to or greater than their band gap energy (E_g), leads to the migration of electron to the conduction band leaving back the hole in valence band. This creates an electrostatically bound electron and hole pair with their lowest energy state known as exciton.

1.1. Classification of semiconductor nanomaterials

The number of confinement dimensions of excitons in these nanomaterials leads to three major classifications, as follows.

1.1.1. Quantum well. A Quantum well is the structure whereby the electrons and holes are confined in only one dimension and are thus free to move in two dimensions. They are referred to as two dimensional nanomaterials (2D)

1.1.2. Quantum wire. A Quantum wire is a nanomaterial in which the electrons and holes are confined in two dimension, leaving only one free dimension. They are hence called one dimensional materials (1D).

1.1.3. Quantum Dot (QD). A Quantum dot is a structures in which the holes and electrons are confined in all the three dimensions leaving zero dimension of movement. They are hence called zero dimension (OD) or three dimension (3D). Typically the dimensions of QDs range between 1 to 100 nm. This work will focus on this class of semiconductor nanocrystals.

1.2. Quantum confinement effects

Photo-excitation of quantum dots, generates an exciton pair as explained above. For a material to experience quantum effects, it must be confined into a limited distance smaller than the Bohr exciton radius which is a constant specific to each type of material. For example, from table 1.1 the most commonly studied quantum dots is CdSe with a Bohr exciton radius of 4.9 nm. This means that as the size of bulk CdSe is reduced towards nanometer regime, it only begin to undergo quantum confinement when its dimensions reach 9.8 nm, the Bohr Exciton diameter. Like a particle in a box, when the exciton is confined to this limited space, its energy exhibits discrete values that depends to the mass of the particle and the dimensions of the confining area according to equation 1.1:

$$E_n = \frac{n^2 h^2}{8mL^2} \qquad \textbf{1.1}$$

where *n* and *L* are the wave function quantum number of the particle in the box and the length of the box, respectively, and correspond to the mass and the diameter for the case of quantum dots. At the same time, its band gap energy (E_g), which is the minimum energy needed to excite and electron from the valence band to the conduction band, increase as the size diminishes as shown in (figure 1.1a.). This effect is known as 'quantum confinement' and is the cause of the different optical and electrical properties exhibited by quantum dots as their sizes are varied. However, when the length of the material is greater than this constant, it exhibits bulk properties which are characterized by a continuum of bands with a corresponding smaller band gap energy. Therefore, quantum dots show properties that are neither of their molecular or bulk counterparts, but size-dependent properties that lie in between. (figure1.1b)

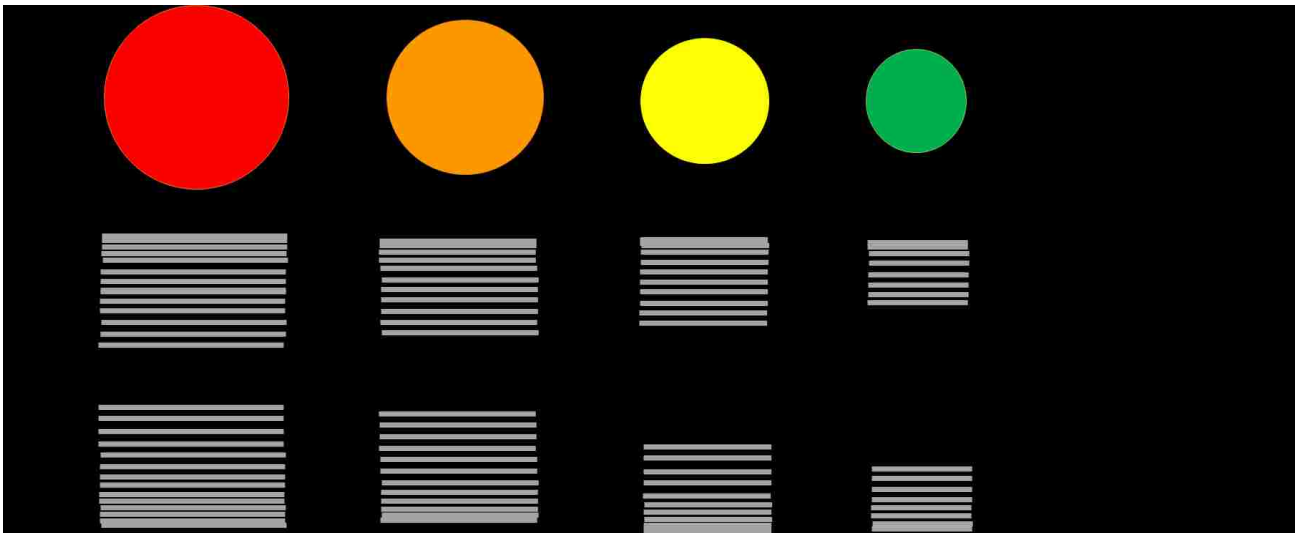

Figure 1.1a: Evolution of quantum dots color, bands and band gaps as size decreases showing quantum confinement effect.

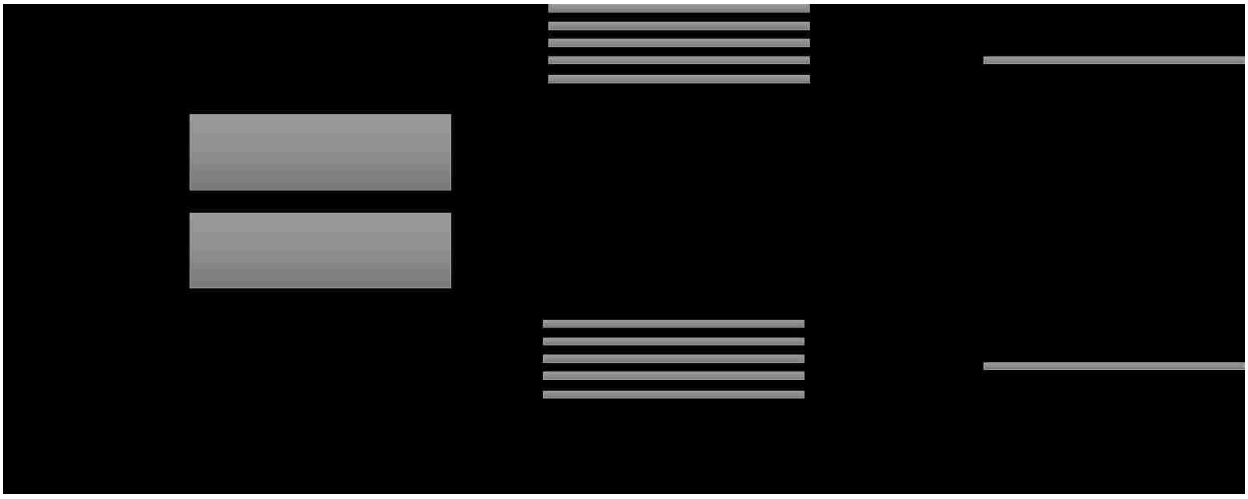

Figure 1.1b: Differences in nature of band energies of bulk, nanomaterial and molecules.

1.3. Optical Properties of quantum dots

Due to the quantum confinement effects, absorption and emission spectra can be tuned by the size of quantum dots. For example, quantum dots composed of the prototypical material CdSe[3] can be tuned to emit light from red to blue as the particle size becomes smaller (figure 1.1a). Also, given that a typical quantum dot consist of about 10^2- 10^5 atoms, resulting in large

surface area to volume ratios, surface effects also contribute significantly to the optical properties. Therefore, for superior optical properties, both quantum confinement and surface effects must be optimized.

Different types of quantum dots have been classified depending on the position of the elements used in the periodic table (table 1.1). Therefore, type II-VI semiconductors include, CdE (E = Se, S, Te)[4] and type III-V include InP and InAs. Also, ternary types such as CuInE [5], I-III-VI, have been reported. Because of the different Bohr radius and band gap energy (table 1.1) each of these types of quantum dots undergo different degrees of exciton confinement resulting in different properties, which can be used for a variety of different applications. For instance, high chemically stable quantum dots with monodisperse size distribution, high photoluminescence quantum yields (QYs) for optimized brightness and narrow emission spectra are advantageous for biologically related applications.[6] Furthermore, the arrangements of atoms in each of these types of quantum dots into either hexagonally or cubic structures results into further classification as either wurtzite or zinc blende, respectively (table 1.1), which also affect their optical properties. [7, 8]

This dissertation was focused on type II-VI quantum dots, specifically CdTe and CdSe, since these are the most promising for bioimaging applications due to their unique photoluminescence spectra.[9-12] Even though, quantum dot cores can be related to a particle in a box system, exciton confinement is never perfect due to their finite potential energy barrier leading to the possibility of quantum mechanical tunneling of the hole and/or the electron to the surface of the quantum dots upon excitation. The available dangling bonds from the ligands and atoms at the surface these materials act as surface trap states which require passivation to increase radiative pathways. Otherwise, these trap states act as non-radiative pathways through which excited electrons or holes decay thereby reducing their photoluminescence quantum yield.

Table 1.1. Material Parameters for a few Selected Semiconductors

Material	Common Structure (300K)	Type	Band gap Energy (eV)	Exciton Bohr Radius (nm)	Lattice Constant (nm)
CdSe	Wurtzite	II-VI	1.76	4.9	0.430
CdS	Wurtzite	II-VI	2.42	2.8	0.414
CdTe	Zinc blende	II-VI	1.43	7.5	0.610
ZnS	Zinc blende	II-VI	3.61	2.5	0.541
GaAs	Zinc blende	III-V	1.42	12.5	0.565
GaN	Wurtzite	III-V	3.42	2.8	0.319
InN	Wurtzite	III-V	0.8	3.4	0.355
InSb	Zinc blende	III-V	0.23	65	0.648
PbS	Rocksalt	IV-VI	0.41	18	0.594
PbTe	Rocksalt	IV-VI	0.31	150	0.646

To reduce these surface trap states, the quantum dots are usually coated using a shell material resulting into a core/shell system. Furthermore, a proper choice of a shell material relative to the core may be used to further tune their properties for a specific application as the extent of exciton confinement varies. Currently, there are four major classes of core/shell systems (figure 1.2) that can be engineered depending on the band gap position of the core relative to that of the shell material used. Type I e.g. CdSe/ZnS results when the valence and conduction bands of the shell are lower and higher, respectively, than those of the core, therefore, both electron and hole are confined within the core thus increasing their wave function overlap which results into high fluorescence quantum yield.[13] Type II e.g. CdTe/CdSe results when either the conduction or valence band of the shell is situated within the band gap of the core thus forming two staggered systems.

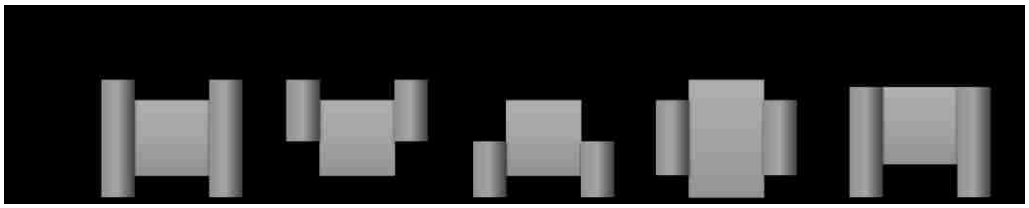

Figure 1.2. Schematic of band gap energy overlap in different types of core/shell quantum dots. The inner rectangular blocks represent the cores while the outer ones represent the shell band-gap energies, respectively.

This is where the electron and the hole are confined in the shell and hole, respectively or vice versa, lowering the energy required for the exciton recombination. The separation of charges lowers the fluorescence quantum yields but makes them more advantageous for application in solar cells. On the other hand, reverse type I e.g. ZnSe/CdSe results when the valence and conduction bands of the shell are higher and lower, respectively, than those of the core, therefore, both electron and hole are confined within the shell. These systems are more useful as NIR emitters as the recombination energy is minimized, therefore, the electron and hole recombination leads to emission in longer wavelengths. Recently reported [14] is the Quasi-type II in whereby the conduction band energy of either the core or the shell are of the same energy while that of the valence varies. Similar to Type II, one charge carrier is delocalized over all the system while the other is confined in the core. Another interesting but rather challenging parameter that can also be used to tune the properties of quantum dots are the lattice constants of the core and shell [2] materials. Table 1.1 lists some of the common lattice constants. Similar to the band gap energy consideration, proper choice of materials with minimized lattice mismatch is critical to optimize the optical properties.[6, 15] In other words, a balance between confinement from the band gap offset and lattice mismatch is necessary when engineering both core/shell and core/shell/shell quantum dots.

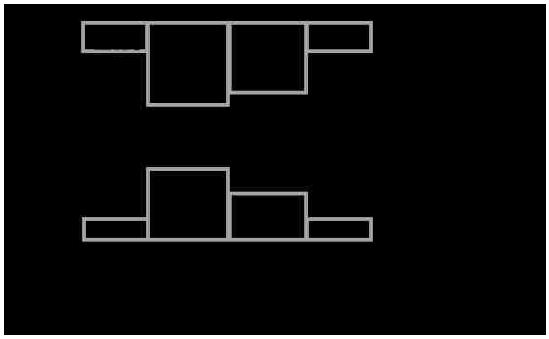

Figure 1.3. Lattice mismatch and band gap overlap of semiconductor quantum dots as used in chapter 4.

For instance, among type II-VI quantum dots, coating CdSe core with several layers of ZnS shell is the most commonly studied core/shell system.[16, 17] Given the larger band gap of ZnS compared to CdSe (table 1.1 and figure 1.3), the charge carries are both confined within the core, thus improving their wavefunction overlap, and thus radiative rate. However, the lattice mismatch between CdSe and ZnS is ~ 12 % (figure 1.3) and significantly limits the thickness of the shell that can be grown on the core. As the shell grows thicker, the pressure between the core and the shell induce interfacial defects which consequently leads to deformation of the shape as shown in figure 1.4. Also, these defects may further act as trap states that promote nonradiative pathways that lead to a reduced quantum yield as the shell thickness increases as observed by several studies.[1, 16-18] Dabbousi et al, [1] reported on a dramatic increase in the photoluminescence quantum yield followed by a steady decline after ~ 1.3 monolayers of ZnS shell thickness grown over a CdSe core.

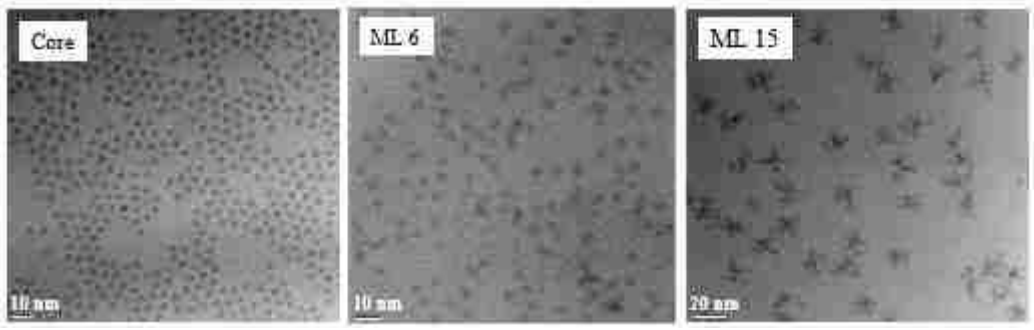

Figure 1.4. TEM Images for CdSe/ZnS. The QDs shape deviates from the original spherical as the shell thickness increases probably due to accumulation of strain between CdSe and ZnS. (Scale bar is 10 nm)

Here a monolayer thickness of ZnS refers to a shell of ZnS that is 3.1 Å long (the distance between consecutive planes along the [002] axis in bulk wurtzite ZnS).[1] Also, another feature observed was the elimination of a broad deep trap emission of bare CdSe upon ZnS shell growth. Furthermore, they observed a small red shift with shell thickness which is attributed to the partial tunneling of the exciton wavefunction into the ZnS shell

On other related studies, Talapin et al [18] reported on a maximum PL quantum yield of about 66 % after ~ 1.6 ML of ZnS shell on CdSe core. Also, Nguyen et al [13] investigated the effect of shelling CdSe core with ZnS and found the same trend of increase in intensity followed by a steady decrease. Their study involved changes in PL quantum yield as a function of reaction time after annealing at 150^{o}C.They observed that the best PL quantum yield was after 5 min reaction and longer times reduced the yield even though the size increased. This trend was also reported by Heyes et al [16] who found that their maximum QY was with 3.5ML ZnS.

On the other hand, adding a CdS shell instead of ZnS shell on CdSe core is known to minimize the lattice mismatch and provide better crystalline particles. The lattice mismatch between CdSe and CdS is ~ 4% (figure 1.4) and a thicker shell, even more than 5 nm (14 monolayers) can easily

be grown.[15, 19] However, since CdSe/CdS is a quasi-type II system, the electron wave function in CdSe/CdS core/shell system is delocalized in the whole core/shell structure, as explained above. Consequently, the degree of electron-hole wave function overlap is minimized, therefore reducing radiative recombination rates compared to the ZnS shell. Despite this limitation, a number of studies have focused on the smaller lattice mismatch to grow highly crystalline particles which consequently had almost unity fluorescence quantum yields, [6, 15, 20] highlighting the importance of controlling non-radiative pathways in core-shell quantum dots.

Recently, Peng et al [20] reported on zinc blende CdSe/CdS core/shell quantum dots with fluorescence quantum yield of 80 % at 4 monolayers shell thickness, and Bawendi et al[6] reported up to 97 % fluorescent QY CdSe/CdS QDs. The latter report used the common Cd-oleate as the Cd precursor but used octanethiol as the source of S precursor. The low reactivity of the S precursor, induced by the strong carbon-sulfur bond, enabled them to grow high crystalline quantum dots. Both studies, observed a decline in quantum yield with increasing shell thickness after some optimum. This observation can be attributed to the generated trap states that results from the lattice strain at the interface between the core and the shell as the shell thickness increases. Burda *et al*[21] reported that, due to the coherency strain at the interface between the core and the shell, the shell material adopts the lattice parameters of the core when the shell is thin but, as the shell thickness increases, it reverts to the lattice parameters of the shell material, resulting in dislocations between the shell and the core due to the lattice differences which act as trap states and lowers the fluorescence quantum yields. By extension, for core/shell/shell systems, without a proper strategy, it may result in quantum dots with compromised optical properties as the additional shell further spreads the defects. Therefore, considering the discussion above, this thesis is focused on systematically controlling these parameters, namely the band gap and lattice

mismatch to synthesize high quality quantum dots in various core, core-shell and core-shell-shell configurations.

Apart from the photoluminescence, the quality of quantum dots are also verified using their absorption features. In fact, the initial information about the quantum dots is revealed by the absorption spectra whereby well resolved peaks associated with the band-edge absorption signifies highly-crystalline particles.[3] It is well-known that the broad absorption spectra of quantum dots facilitates excitation at various wavelengths and offers more advantage over organic fluorescence dyes in bioimaging applications.[14] Furthermore, the size distribution of the quantum dots can be estimated using full-width at half maximum, calculated from the emission spectra. Similar to both absorption and emission, the quantum dots fluorescence lifetime (τ) is another measurable optical properties of quantum dots. Generally, the excited state lifetime of quantum dots tend to be longer (> 10 ns) than those of the organic fluorescence dyes and autofluorescence [5, 14] which makes them better candidates for bioimaging applications.

1.4. Structural Properties of quantum dots

In order to conclusively understand the nature of quantum dots, their structural characterization needs to be carried out effectively. Even though shelling of quantum dots has been shown to improve their optical properties, especially their photoluminescence quantum yields,[1, 22] evidence also exits that the passivation provided by the shell material is not perfect[23] and sometimes results in completely dark particles.[24]

Several factors, such as reaction conditions, lattice mismatch and variation in reactivity of some crystal planes (facets) leads to uncontrollable shell distributions. For instance, it was reported that the most reactive facet in CdSe cores is the (001) plane and the proper choice of the initial shell layer, whether cationic or anionic, dictates the overall quality of the quantum dots. [25] Also

another study relating trap-states to the distribution of the shell material [26] emphasized that the growth of a simple ZnS shell on CdSe is not enough for optimal properties, as it leads to highly anisotropic shell growth.[26] Therefore, in order to obtain clear information about quantum dots shape, size and structure, further characterization tools such as transmission electron microscopy (TEM), high resolution-(HRTEM) and X-ray diffraction techniques are required. In fact, successful shell growth has been quantified using HRTEM in certain studies.[2, 20, 27-30]

On the other hand, the X-ray diffraction patterns or HRETEM images are usually used to study the crystallinity and structure of quantum dots. Nevertheless, limitations still exist to accurately verify the difference before and after the shell growth using TEM, which depends on the material used as well as the size distribution.[13] In such cases, more advanced techniques have proved more reliable. For instance, scanning transmission electron microscopy (STEM) coupled with electron energy loss spectroscopy (EELS) are more advanced techniques that are used to identify the elemental distribution across quantum dots.[27, 28, 30-33] Other useful techniques for quantification are energy dispersive x-ray spectroscopy(EDX) and x-ray photoelectron spectroscopy(XPS).While the former can give information about the core/shell structure, the latter is more sensitive to the surface structural properties and can also be used to investigate the shell thickness.[34] The details of operation for these instruments are discussed in chapters 2 to 5.

1.5. Blinking

At the single particle level, quantum dots, under continuous illumination, show intermittency in their fluorescence emission, a behavior commonly known as blinking. They fluctuate between *fluorescent* and *dark* states, referred to as *on* and *off,* respectively. After its discovery in quantum dots by Nirmal *et al* in 1996,[35] this behavior was also reported in molecular dyes and fluorescent

proteins.[36] There is a general agreement so far that this limiting behavior is a consequence of charge carrier trapping, however, the exact mechanism is a big area of debate and still undergoing extensive research. Some groups[37, 38] defend the charging model, which was the first model proposed, whereby the trapping of a charge carrier is believed to leave a charged quantum dot which undergoes fast non-radiative Auger recombination. On the other hand, other groups [15, 19] support the non-radiative recombination model in whereby a trapped charge carrier can recombine non-radiatively with its counter charge carrier promptly after each excitation event causing the low fluorescent quantum yield.

Klimov *et al* [39] recently reported two types of blinking, A-type (conventional) and B-type whereby the former is associated with the charging and discharging of the quantum dots core resulting into lower photoluminescence intensities which correlate with the shorter photoluminescence lifetimes. B-type on the other hand was attributed to the charge fluctuations in the electron accepting surface sites. By applying appropriate voltage, they were able to control and completely suppress blinking of the quantum dots. They found that even on the same quantum dots, B-type blinking can be eliminated by thicker shells while A-type could still blink even at shell thickness of about 19 ML implying that blinking phenomenon is a consequence of the nature of the physical mechanisms and not the variations from quantum dot to quantum dot.[39]

Cordones and Leone[40], recently summarized three ways of blinking analysis methods as namely: Change point detection, autocorrelation, and bin and threshold methods. The first one, which was originally reported by Watkins and Yang[41] uses the Bayesian information criterion (without thresholding). This method allocates each duration at a given intensity to an emissive state determined from the statistically-relevant intensity change points from individual photon arrival times (without binning). The second method uses the photon autocorrelation function,

which is commonly used when shorter timescale dynamics are of more interest. In the last method, blinking traces are obtained by integrating the fluorescence counts into 1-100 ms time bins. This is the most widely used method in blinking analysis and the method used in this thesis in chapter 4. Briefly, a blinking trace is binned in such a way that the signal to noise ratio is high followed by setting a threshold which separates the *on* and *off* events. From these events, a probability distribution is then calculated which is then plotted in terms of a probability distribution function (or probability density).[40] Off-state durations are usually found to follow an inverse power low distribution while the on –states are generally found to be inverse power law distributions but with an exponential decay cut off at longer timescales (usually several seconds), as described by equations 1.2 and 1.3, respectively.

$$P_{off}(\tau)\ \alpha\ \tau^{-\alpha} \quad \textbf{1.2}$$

$$P_{on}(\tau)\ \alpha\ \tau^{-\alpha} e^{-\tau/\tau_c} \quad \textbf{1.3}$$

where, α is the power law exponent with typical values between 1 and 2. The cross-over time τ_c shows the characteristic time of the exponential cut off.

1.6. Synthesis of quantum dots

Since the discovery of quantum dots, the two major methods of synthesis that have been reported involve deposition on a substrate or dispersion in a solution. The latter, which is famously known as colloidal synthesis is the most popular among chemists, since it offers exquisite processibility for a wide variety of applications. It involves chemical reaction of precursors to form an inorganic material on nanometer scales. At an appropriate temperature specific to the material being synthesized, the precursor atoms nucleate, forming a seed material on which

continuous deposition of solid products results in an increase in the size and control over the shape of the quantum dots.

1.6.1. Core synthesis

As briefly introduced above, the general colloidal synthesis of semiconductor quantum dots involves nucleation of ionic and cationic precursors. This happens in the presence of both coordinating and non-coordinating solvents to form an inorganic nanomaterial surrounded by organic ligands. Basically, the process begins by rapid chemical disintegration of the precursor at high temperature and forming a large number of nuclei once the solution becomes supersaturated. Once the concentration of precursors drops below the supersaturation condition, the precursors then continue to deposit on the nuclei until the size of the particles increase to the desired size, at which point, the temperature is quenched. The details of their synthesis are given in chapters 2 to 4 but the general competing synthesis protocols involves the use of dimethyl cadmium and CdO/oleic acid (to form Cd-oleate) as the cadmium precursors.

Before the CdO precursor was introduced by Peng in 2001[10, 42], the main precursor of cadmium was dimethyl cadmium.[4, 11] This precursor is known to produce high quality quantum dots with narrow size distribution,[43] a benefit that has seen it in still in use up to now among some groups despite its high cost, toxicity and sensitivity to air necessitating the use of a glove box. The friendlier CdO precursor is slowly taking over and has proved to also produce very high quality particles that are reproducible, once the synthetic chemist has gained some experience in the field.[43-45] Apart from the difference in the source of Cd precursor, the rest of the procedure is almost the same in most cases, whereby selenium powder is dissolved in either tributylphosphine (TBP) or trioctylphosphine (TOP) as the Se precursors or directly in octadecene (ODE). Trioctylphosphine oxide (TOPO) which is used as a reaction solvent is heated up to 300°C in an

oxygen-free environment followed by rapid injection of the liquid precursors in the reaction flask.[4] As explained earlier, CdSe quantum dots immediately begin to nucleate and grow to the desired size which can be monitored by the gradual change in the solution color or using a UV-Vis light/spectrophotometer.

1.6.2. Core/shell and core/shell/shell synthesis

Two approaches to shelling of quantum dots are the two-step and one-pot synthesis.[13] In the former method, the initial core synthesis is followed by purification before adding the shell precursors to grow the shell, while the latter involves a continuous injection of the shell precursor directly in the same pot after the core formation. For proper control of shell growth, two criteria must be taken into account. The first is that the shelling temperature must be lower than the one used during core formation to avoid nucleation of the shell material and uncontrolled ripening. Secondly, the shell precursors should be added slowly to enable for a uniform diffusion around the core as this is necessary to produce quantum dots with uniform size distribution.

In order to calculate the correct precursor amounts to grow a given shell thickness, it is necessary to know the concentration of the core material being used. The first excitonic absorption peak of quantum dots is measured using UV-vis spectroscopy and can be related directly to several parameters that leads to the calculation of the concentration. From the first excitonic peak wavelength, the size of quantum dots in diameter (D) can calculated using the empirically-derived equation 1.4 and then applying to equation 1.5 to calculate the molar extinction coefficient (ε). The example used here is specific to CdSe but similar equations are available in the same paper for other materials.[45]

$$D = (1.6122 \times 10^{-9})\lambda^4 - (2.6575 \times 10^{-6})\lambda^3 + (1.6242 \times 10^{-3})\lambda^2 - (0.4277)\lambda + (41.57) \qquad \textbf{1.4}$$

$$\varepsilon = 5857(D)^{2.65} \quad \textbf{1.5}$$

Finally, by applying the ε to the Beer-Lambert law (equation 1.6) we can then calculate the concentration of the quantum dots which then enables us to accurately calculate the required shell precursor amounts.

$$A = cl\varepsilon \quad \textbf{1.6}$$

where A is the absorbance, ε is the molar extinction coefficient (L mol cm^{-1}), c is the molar concentration (mol L^{-1}), and *l* is the cuvette path length (cm). While both precursors can be added simultaneously, which was the method used for several years (Hines, Guyot-sionnest and Daboussi, Bawendi Refs), successive ion layer adsorption and reaction (SILAR) and Thermal Cycling (CT) methods were introduced by Peng in 2003[44] and 2007[46], respectively, and are particularly useful techniques to optimize the quality of core-shell quantum dots. SILAR requires that an exactly-calculated shell precursor is added to grow one monolayer of shell at a time, with the cationic and anionic species alternately added in a sequential mannerand allowed to grow before the next precursors are added. It was later found that injection at a lower temperature followed by growth of the shell monolayer at higher temperature (usually 20-40 °C higher) allows for the diffusion of the precursors to the particle surface at the lower temperature before actual shell growth at the higher temperature, and called thermal cycling.

1.6.3. Ligands

The use of organic ligands as capping agents in quantum dots synthesis dates back to 1980s when the word "quantum dots" was first coined by Reed at Texas Instruments when reporting on structures that were produced by lithographic method.[47] At the same time, Bard[48] and Brus [49] published the use methylviologen and phenyl-TMS as surfactants, respectively. While

methylviologen was capped around CdS suspension to act as electron acceptor (mediator) for photocoulometric studies, the phenyl groups that bonded to CdSe crystallites rendered them hydrophobic and facilitated their dissolution into an organic solvent, opening the way for colloidal quantum dots.[49] Several years later, the use of organic ligands such as tri-n-octylphosphine oxide (TOPO), tryoctylphosphine (TOP), hexadecylamine (HDA) and octadecylamine (ODA), among others, (figure 1.5) as both solvent and capping ligands during quantum dots synthesis became extremely popular.[50]

Besides providing colloidal stability to the quantum dots, some of this ligands have other benefits. For instance, because of the high boiling point of TOPO, it facilitates precursor decomposition and allowsnanoparticle annealing at high temperature. Furthermore, its long hydrophobic chains renders it completely compatibile with otherorganic solvents which allows further manipulation in different organic solvents. TOP and TBP on the other hand are commonly used both as surfactants and as Selenium or Tellurium delivery agents in the form of TOP-Se or TBP-Te. They have been shown to bind on the QDs surface at anionic sites, thus providing more passivated particles than the cationic-binding phosphine oxide and amine ligands alone.

Comparing the role of primary, secondary and tertiary amines as QDs ligands , Mulvaney et al[51] reported that primary amines significantly enhanced the emission of the QDs while both secondary and tertiary had no effect. This was attributed to the less steric effect by the primary amines and passivation of the electron trap sites by the lone pair of electrons from the amine. Work on amine ligands was expounded upon further on by Peng et al[52] who reported that among the primary amines, hexadecylamine (HDA) produces the highest quality particles with highest PL quantum yields.

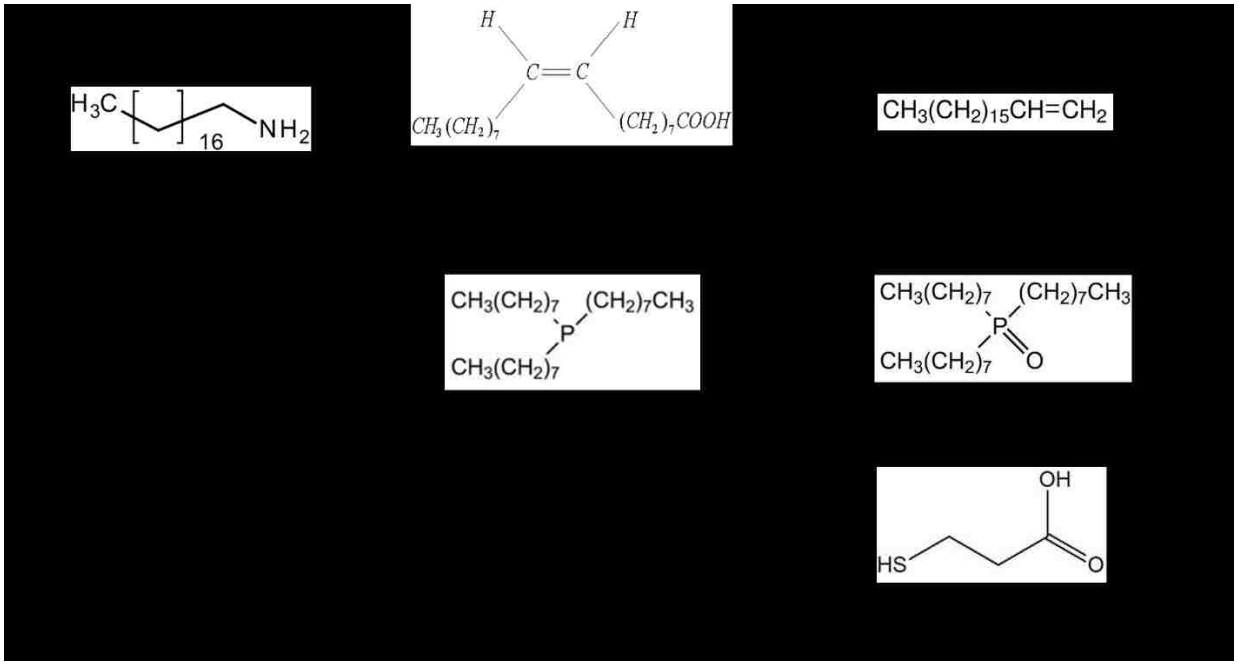

Figure 1.5. Common ligands used as coordinating and non-coordinating ligands during synthesis and ligand exchange of quantum dots.

When it comes to QDs morphology, phosphonic acid based ligands have been reported to play the lead role. For instance, the growth of nanorods was regulated by using different concentrations of hexyl-phosphonic acid (HPA).[53]

Furthermore, rods with aspect ratios of up to 30, as well as arrows, teardrops, and tetrapods morphologies were formed by controlling the ratio of HPA : TOPO injection rates and number of injections.[54] The current trend in literature is geared towards using specific ligands to control the growth of quantum dots to achieve desired structures and unity PL quantum yields. For instance in 2013, Using single-source precursor cadmium diethyldithiocarbamate ($Cd(DDTC)_2$) which also acted as a surfactant ligand Peng et al[20] compared the properties of CdSe/CdS core/shell nanocrystals with zinc blend or wurtzite structures and found that zinc blende showed higher-quality. In the same year, Bawendi et al[6] used octanethiol ligands to slow the growth of shells at

higher temperature and produced QDs with high crystallinity and uniformity showing narrow emission linewidth and suppressed blinking.

1.7. Purification and ligand exchange

One way of transferring quantum dots capped with organic ligands to aqueous medium for various application is by perform ligand exchange. Two common strategies employed in achieving these are polymer coating [55, 56] and ligand exchange. [12, 57-60] The former involves the coating of the original hydrophobic ligands with an amphiphilic polymer that renders them soluble in aqueous solution. The latter on the other hand, involves the substitution of the original hydrophobic ligand with new hydrophilic ligands.

One important step during ligand exchange and which applies to any other purification of quantum dots is to remove any unreacted precursors and loosely-bound ligands prior to the reaction. This is accomplished by several cycles of dispersion and centrifugation in two immiscible solvents of which one phase extracts the polar material leaving quantum dots dissolved in the nonpolar phase. Since the quantum dots are usually dissolved in either toluene[10] or hexane[9] after synthesis, the common extraction solvents are either methanol or acetone. For ligand exchange purposes, the quantum dots are further precipitated out of these solvents to enhance the removal of most of the ligands.

After purification and precipitation, quantum dots are re-dissolved into a solution containing the new hydrophilic ligands. Hydrophilic ligands such as MPA (figure 1.4) with thiol (-SH) group at one end of the molecule for binding to the surface of QDs and a carboxylic (-COOH) functional group on the other end to dissolve in polar solvents are commonly used.[57-59] Refluxing of the resulting quantum dots solution facilitates binding of the ligands to produce stable and water-soluble quantum dots for biological applications.

1.8. Objectives and overview of the dissertation

This dissertation was divided into three parts with each part presenting the findings from the three major projects conducted. The first part (chapter 2) involves a controlled synthesis of CdTe core quantum dots which were prepared by varying the Cd:Te ratio from 5:1 to 1:5 resulting in quantum dots which are Cd-rich to Te-rich on the surface, respectively. CdTe quantum dots have unique characteristics that are promising for applications in photoluminescence, photovoltaics or optoelectronics. For example, given the position of the conduction band of CdTe relative to the HOMO of thiol ligand, CdTe is easily exchanged with thiol based ligands without the need for a shell unlike CdSe which is easily quenched by the thiol ligands. However, wide variations of the reported quantum yields exist and the influence of ligand-surface interactions that are expected to control the excited state relaxation processes remains unknown. It is important to thoroughly understand the fundamental principles underlying these relaxation processes to tailor the QDs properties to their application

The main aim of this project was to systematically investigate the roles of the surface atoms, ligand functional groups and solvent on the radiative and non-radiative relaxation rates. Combining a systematic synthetic approach with X-ray photoelectron, quantitative FT-IR and time-resolved visible spectroscopies, we found that CdTe QDs can be engineered with average radiative lifetimes ranging from nanoseconds up to microseconds. The non-radiative lifetimes are anticorrelated to the radiative lifetimes, although they show much less variation. The density, nature and orientation of the ligand functional groups and the dielectric constant of the solvent play major roles in determining charge carrier trapping and excitonic relaxation pathways.

The second part (chapter 3) discusses the effects of shelling a variety of CdSe core quantum dots that show various qualities of fluorescence quantum yield. Specifically, this study involved

synthesis of five sets of CdSe cores with photoluminescence quantum yields (PL QYs) ranging from 52% to 9 % resulting into quantum dots with different optical and structural properties. The fluorescence quality of the CdSe core is controlled by varying the ratio of the coordinating ligands, and using both thermal cycling (TC) and successive ion layer adsorption and reaction method (SILAR) in shelling, the CdS shell growth was monitored up to 8 monolayer (ML) for each set of the samples. Apart from the prominent absorbance spectral redshift monitored by both UV-Vis spectrophotometer and fluorometer, the shell growth was further proved by the TEM images and ligand exchange results. Surprisingly, the lower quality core samples (in terms of quantum yield) exhibited the general CdSe/CdS shelling trend whereby the initial quantum yield increases with addition of shell thickness then declined as the shell becomes thicker, on the other hand the higher PL QY (high quality core) showed a reverse trend whereby the initial shell thickness reduced the PL QYs before increasing but not exceeding that of the core. The quality, crystallinity and wurtzite structure of these particles were verified by both HRTEM and XRD. It was found from quantifying the radiative and nonradiative rates that nonradiative recombination pathways are more responsible for the observed trends in PL QY.

The last part (chapter 4) is an extension of the core/shell to a core/shell/shell system to design small, less toxic and reduced blinking quantum dots. A lot of effort has been directed towards the suppression and elimination of blinking of quantum dots. However, these reports rely on using either very thick[15, 19] or highly-crystalline, medium thickness CdS shells[6] or interfacial alloying,[61] while using only ZnS as a shell on CdSe does not suppress blinking.[16] Even though, there have been reports of blinking suppression with multishell configurations, particularly with CdS and ZnS,[19] the role that interfacial trap states play in these systems is not so well understood. Therefore, the project presented in this part was aimed at addressing the above

limitations while still focusing on the suppression of blinking on quantum dots. Briefly, we examined how increasing the outer shell (ZnS) thickness on CdSe/CdS/ZnS quantum dots leads to a reduction in blinking. Time resolved fluorescence, TEM and STEM/EELS were used to follow the shelling process. The different shells affect the radiative and non-radiative rates differently due to the competing effects of degree of charge carrier confinement and lattice mismatch. Using only a 3 monolayer (ML) CdS inner-shell, we find that we can greatly reduce blinking by adding just 3ML of a ZnS outer shell – thereby maintaining a relatively small QDs. However, by making the ZnS shell thicker, blinking is increased again, which we attribute to induced lattice strain from the ZnS as discussed above. We anticipate that the reported QDs will be useful in bio-imaging applications due to their suppressed blinking, smaller size, and lower toxicity of the outer shell (compared to CdSe-CdS core-shells).

1.9. References

[1]. Dabbousi, B.O., et al., (CdSe)ZnS (Core)Shell Quantum Dots: Synthesis and Characterization of a Size Series of Highly Luminescent Nanocrystallites. The Journal of Physical Chemistry B, 1997. 101(46): p. 9463-9475.

[2]. Smith, A.M., A.M. Mohs, and S. Nie, Tuning the optical and electronic properties of colloidal nanocrystals by lattice strain. Nat Nano, 2009. 4(1): p. 56-63.

[3]. Smith, A.M. and S. Nie, Semiconductor Nanocrystals: Structure, Properties, and Band Gap Engineering. Accounts of Chemical Research, 2009. 43(2): p. 190-200.

[4]. Murray, C.B., D.J. Norris, and M.G. Bawendi, Synthesis and characterization of nearly monodisperse CdE (E = sulfur, selenium, tellurium) semiconductor nanocrystallites. Journal of the American Chemical Society, 1993. 115(19): p. 8706-8715.

[5]. Mandal, G., et al., Cadmium-free quantum dots as time-gated bioimaging probes in highly-autofluorescent human breast cancer cells. Chemical Communications, 2013. 49(6): p. 624-626.

[6]. Chen, O., et al., Compact high-quality CdSe/CdS core/shell nanocrystals with narrow emission linewidths and suppressed blinking. Nat Mater, 2013. 12(5): p. 445-451.

[7]. Subila, K.B., et al., Luminescence Properties of CdSe Quantum Dots: Role of Crystal Structure and Surface Composition. The Journal of Physical Chemistry Letters, 2013. 4(16): p. 2774-2779.

[8]. Mohamed, M.B., et al., Synthesis of High Quality Zinc Blende CdSe Nanocrystals. The Journal of Physical Chemistry B, 2005. 109(21): p. 10533-10537.

[9]. Omogo, B., J.F. Aldana, and C.D. Heyes, Radiative and Nonradiative Lifetime Engineering of Quantum Dots in Multiple Solvents by Surface Atom Stoichiometry and Ligands. The Journal of Physical Chemistry C, 2013. 117(5): p. 2317-2327.

[10]. Peng, Z.A. and X. Peng, Nearly Monodisperse and Shape-Controlled CdSe Nanocrystals via Alternative Routes:Nucleation and Growth. Journal of the American Chemical Society, 2002. 124(13): p. 3343-3353.

[11]. Peng, X., et al., Epitaxial Growth of Highly Luminescent CdSe/CdS Core/Shell Nanocrystals with Photostability and Electronic Accessibility. Journal of the American Chemical Society, 1997. 119(30): p. 7019-7029.

[12]. Breus, V.V., C.D. Heyes, and G.U. Nienhaus, Quenching of CdSeâˆ’ZnS Coreâˆ’Shell Quantum Dot Luminescence by Water-Soluble Thiolated Ligands. The Journal of Physical Chemistry C, 2007. 111(50): p. 18589-18594.

[13]. Reiss, P., M. Protière, and L. Li, Core/Shell Semiconductor Nanocrystals. Small, 2009. 5(2): p. 154-168.

[14]. Petryayeva, E., W.R. Algar, and I.L. Medintz, Quantum Dots in Bioanalysis: A Review of Applications Across Various Platforms for Fluorescence Spectroscopy and Imaging. Applied Spectroscopy, 2013. 67(3): p. 215-252.

[15]. Mahler, B., et al., Towards non-blinking colloidal quantum dots. Nat Mater, 2008. 7(8): p. 659-664.

[16]. Heyes, C.D., et al., Effect of the shell on the blinking statistics of core-shell quantum dots: A single-particle fluorescence study. Physical Review B, 2007. 75(12): p. 125431.

[17]. Spinicelli, P., et al., Non-Blinking Semiconductor Colloidal Quantum Dots for Biology, Optoelectronics and Quantum Optics. ChemPhysChem, 2009. 10(6): p. 879-882.

[18]. Talapin, D.V., et al., Highly Luminescent Monodisperse CdSe and CdSe/ZnS Nanocrystals Synthesized in a Hexadecylamine, Trioctylphosphine Oxide and Trioctylphospine Mixture. Nano Letters, 2001. 1(4): p. 207-211.

[19]. Chen, Y., et al., "Giant" Multishell CdSe Nanocrystal Quantum Dots with Suppressed Blinking. Journal of the American Chemical Society, 2008. 130(15): p. 5026-5027.

[20]. Nan, W., et al., Crystal Structure Control of Zinc-Blende CdSe/CdS Core/Shell Nanocrystals: Synthesis and Structure-Dependent Optical Properties. Journal of the American Chemical Society, 2012. 134(48): p. 19685-19693.

[21]. Chen, X., et al., Coherency Strain Effects on the Optical Response of Core/Shell Heteronanostructures. Nano Letters, 2003. 3(6): p. 799-803.

[22]. Hines, M.A. and P. Guyot-Sionnest, Synthesis and Characterization of Strongly Luminescing ZnS-Capped CdSe Nanocrystals. The Journal of Physical Chemistry, 1996. 100(2): p. 468-471.

[23]. Ebenstein, Y., T. Mokari, and U. Banin, Fluorescence quantum yield of CdSe/ZnS nanocrystals investigated by correlated atomic-force and single-particle fluorescence microscopy. Applied Physics Letters, 2002. 80(21): p. 4033-4035.

[24]. Nazzal, A.Y., et al., Environmental Effects on Photoluminescence of Highly Luminescent CdSe and CdSe/ZnS Core/Shell Nanocrystals in Polymer Thin Films. The Journal of Physical Chemistry B, 2004. 108(18): p. 5507-5515.

[25]. Soni, U. and S. Sapra, The Importance of Surface in Coreâ^'Shell Semiconductor Nanocrystals. The Journal of Physical Chemistry C, 2010. 114(51): p. 22514-22518.

[26]. Yu, Z., et al., Shell Distribution on Colloidal CdSe/ZnS Quantum Dots. Nano Letters, 2005. 5(4): p. 565-570.

[27]. Abel, K.A., et al., Probing the Structure of Colloidal Core/Shell Quantum Dots Formed by Cation Exchange. The Journal of Physical Chemistry C, 2012. 116(6): p. 3968-3978.

[28]. Hughes, S.M. and A.P. Alivisatos, Anisotropic Formation and Distribution of Stacking Faults in IIâ€“VI Semiconductor Nanorods. Nano Letters, 2012. 13(1): p. 106-110.

[29]. Saha, A., et al., Near-Unity Quantum Yield in Semiconducting Nanostructures: Structural Understanding Leading to Energy Efficient Applications. The Journal of Physical Chemistry Letters, 2013. 4(20): p. 3544-3549.

[30]. Zorn, G., et al., Method for Determining the Elemental Composition and Distribution in Semiconductor Coreâ^'Shell Quantum Dots. Analytical Chemistry, 2011. 83(3): p. 866-873.

[31]. Abel, K.A., et al., Analysis of the Shell Thickness Distribution on NaYF4/NaGdF4 Core/Shell Nanocrystals by EELS and EDS. The Journal of Physical Chemistry Letters, 2010. 2(3): p. 185-189.

[32]. Carlson, L.J., et al., Fluorescence Efficiency of Individual Carbon Nanotubes. Nano Letters, 2007. 7(12): p. 3698-3703.

[33]. Coxon, P.R., et al., Electron energy loss spectroscopy on alkylated silicon nanocrystals. Journal of Applied Physics, 2008. 104(8):

[34]. Borchert, H., et al., Investigation of ZnS Passivated InP Nanocrystals by XPS. Nano Letters, 2001. 2(2): p. 151-154.

[35]. Nirmal, M., et al., Fluorescence intermittency in single cadmium selenide nanocrystals. Nature, 1996. 383(6603): p. 802-804.

[36]. Cichos, F., C. von Borczyskowski, and M. Orrit, Power-law intermittency of single emitters. Current Opinion in Colloid & Interface Science, 2007. 12(6): p. 272-284.

[37]. Jones, M., S.S. Lo, and G.D. Scholes, Signatures of Exciton Dynamics and Carrier Trapping in the Time-Resolved Photoluminescence of Colloidal CdSe Nanocrystals. The Journal of Physical Chemistry C, 2009. 113(43): p. 18632-18642.

[38]. Frantsuzov, P.A. and R.A. Marcus, Explanation of quantum dot blinking without the long-lived trap hypothesis. Physical Review B, 2005. 72(15): p. 155321.

[39]. Galland, C., et al., Two types of luminescence blinking revealed by spectroelectrochemistry of single quantum dots. Nature, 2011. 479(7372): p. 203-7.

[40]. Cordones, A.A. and S.R. Leone, Mechanisms for charge trapping in single semiconductor nanocrystals probed by fluorescence blinking. Chemical Society Reviews, 2013. 42(8): p. 3209-3221.

[41]. Watkins, L.P. and H. Yang, Detection of Intensity Change Points in Time-Resolved Single-Molecule Measurements. The Journal of Physical Chemistry B, 2004. 109(1): p. 617-628.

[42]. Peng, X., science/technology concentrates. Chemical & Engineering News Archive, 2001. 79(2): p. 25.

[43]. Wang, Q., et al., Luminescent CdSe and CdSe/CdS core-shell nanocrystals synthesized via a combination of solvothermal and two-phase thermal routes. Journal of Luminescence, 2006. 118(1): p. 91-98.

[44]. Li, J.J., et al., Large-Scale Synthesis of Nearly Monodisperse CdSe/CdS Core/Shell Nanocrystals Using Air-Stable Reagents via Successive Ion Layer Adsorption and Reaction. Journal of the American Chemical Society, 2003. 125(41): p. 12567-12575.

[45]. Yu, W.W., et al., Experimental Determination of the Extinction Coefficient of CdTe, CdSe and CdS Nanocrystals. Chemistry of Materials, 2004. 16(3): p. 560-560.

[46]. Blackman, B., et al., Control of the Morphology of Complex Semiconductor Nanocrystals with a Type II Heterojunction, Dots vs Peanuts, by Thermal Cycling. Chemistry of Materials, 2007. 19(15): p. 3815-3821.

[47]. Reed, M.A., et al., Observation of discrete electronic states in a zero-dimensional semiconductor nanostructure. Physical Review Letters, 1988. 60(6): p. 535-537.

[48]. White, J.R. and A.J. Bard, Electrochemical investigation of photocatalysis at cadmium sulfide suspensions in the presence of methylviologen. The Journal of Physical Chemistry, 1985. 89(10): p. 1947-1954.

[49]. Bawendi, M.G., M.L. Steigerwald, and L.E. Brus, The Quantum Mechanics of Larger Semiconductor Clusters ("Quantum Dots"). Annual Review of Physical Chemistry, 1990. 41(1): p. 477-496.

[50]. Green, M., The nature of quantum dot capping ligands. Journal of Materials Chemistry, 2010. 20(28): p. 5797-5809.

[51]. van Embden, J., J. Jasieniak, and P. Mulvaney, Mapping the Optical Properties of CdSe/CdS Heterostructure Nanocrystals: The Effects of Core Size and Shell Thickness. Journal of the American Chemical Society, 2009. 131(40): p. 14299-14309.

[52]. Qu, L. and X. Peng, Control of Photoluminescence Properties of CdSe Nanocrystals in Growth. Journal of the American Chemical Society, 2002. 124(9): p. 2049-2055.

[53]. Qian, C., et al., Solution-Phase Synthesis of Single-Crystalline Iron Phosphide Nanorods/Nanowires. Journal of the American Chemical Society, 2004. 126(4): p. 1195-1198.

[54]. Manna, L., et al., Epitaxial Growth and Photochemical Annealing of Graded CdS/ZnS Shells on Colloidal CdSe Nanorods. Journal of the American Chemical Society, 2002. 124(24): p. 7136-7145.

[55]. Gao, X., et al., In vivo cancer targeting and imaging with semiconductor quantum dots. Nat Biotech, 2004. 22(8): p. 969-976.

[56]. Wu, X., et al., Immunofluorescent labeling of cancer marker Her2 and other cellular targets with semiconductor quantum dots. Nat Biotech, 2003. 21(1): p. 41-46.

[57]. Aldana, J., Y.A. Wang, and X. Peng, Photochemical Instability of CdSe Nanocrystals Coated by Hydrophilic Thiols. Journal of the American Chemical Society, 2001. 123(36): p. 8844-8850.

[58]. Breus, V.V., et al., Zwitterionic Biocompatible Quantum Dots for Wide pH Stability and Weak Nonspecific Binding to Cells. ACS Nano, 2009. 3(9): p. 2573-2580.

[59]. Takeuchi, H., B. Omogo, and C.D. Heyes, Are Bidentate Ligands Really Better than Monodentate Ligands For Nanoparticles? Nano Letters, 2013. 13(10): p. 4746-4752.

[60]. Woehrle, G.H., L.O. Brown, and J.E. Hutchison, Thiol-Functionalized, 1.5-nm Gold Nanoparticles through Ligand Exchange Reactions:Scope and Mechanism of Ligand Exchange. Journal of the American Chemical Society, 2005. 127(7): p. 2172-2183.

[61]. Wang, X., et al., Non-blinking semiconductor nanocrystals. Nature, 2009. 459(7247): p. 686-689.

Chapter 2. Radiative and Non-Radiative Lifetime Engineering of Quantum Dots in Multiple Solvents by Surface Atom Stoichiometry and Ligands

Benard Omogo, Jose F. Aldana and Colin D. Heyes*

Department of Chemistry and Biochemistry, University of Arkansas, Fayetteville, AR, 72701

* To whom correspondence should be addressed: cheyes@uark.edu

2.1. Abstract

CdTe quantum dots have unique characteristics that are promising for applications in photoluminescence, photovoltaics or optoelectronics. However, wide variations of the reported quantum yields exist and the influence of ligand-surface interactions that are expected to control the excited state relaxation processes remains unknown. It is important to thoroughly understand the fundamental principles underlying these relaxation processes to tailor the QDs properties to their application. Here, we systematically investigate the roles of the surface atoms, ligand functional groups and solvent on the radiative and non-radiative relaxation rates. Combining a systematic synthetic approach with X-ray photoelectron, quantitative FT-IR and time-resolved visible spectroscopies, we find that CdTe QDs can be engineered with average radiative lifetimes ranging from nanoseconds up to microseconds. The non-radiative lifetimes are anticorrelated to the radiative lifetimes, although they show much less variation. The density, nature and orientation of the ligand functional groups and the dielectric constant of the solvent play major roles in determining charge carrier trapping and excitonic relaxation pathways. These results are used to propose a coupled dependence between hole-trapping on Te atoms and strong ligand coupling, primarily *via* Cd atoms, that can be used to engineer both the radiative and non-radiative lifetimes.

Keywords: Cadmium telluride, fluorescence lifetime, infrared spectroscopy, surface states, ligand exchange, quantum dot synthesis

2.2. Introduction

Colloidal semiconductor nanocrystals (also called quantum dots, QDs) are showing great potential for a range of applications including photovoltaics [1], lasers[2], pH[3] and chemical[4-6] sensors and biophysical fluorescent probes.[7, 8] The commercialization of QDs as biological fluorescent probes is commonly based on CdSe, using a ZnS shelling procedure introduced in 1996.[9] Shelling allowed subsequent water solubilization for biological labeling applications.[7, 8, 10] In general, it is not possible to transfer CdSe to water using thiols and maintain a reasonable amount of fluorescence without using a shell.[11] If particularly small QDs are needed, such as for labeling small proteins, imaging small intracellular or intercellular regions like mitochondria or neural synapses, or in quantitative FRET assays, CdTe may be a better choice, since they can retain their fluorescence in water using thiolated ligands without a shell.[12, 13] This effect was attributed to thiols acting as strong hole acceptors for CdSe but not for CdTe QDs.[14] Furthermore, to use CdTe in photovoltaic applications where interfacial charge carrier transfer is necessary, a shell may reduce its efficiency.

CdTe QDs can be synthesized directly in water but typically require long reaction times under reflux,[15-17] but can be shortened by the use of an autoclave[18] or by a microwave-assisted procedure.[19] Some of the reports of CdTe synthesized by aqueous routes are very promising, although the reported properties can be variable – even for those prepared by essentially identical procedures.[16, 20] Organometallic-based synthetic procedures for CdSe are, by far, the most prevalent due to high reproducibility and particle quality[21] and have evolved to use more environmentally friendly and safer-to-handle precursors.[22, 23] CdTe can be synthesized by these same routes but the details have not been optimized as they have for CdSe.[24] Wuister *et al.* did use an organometallic approach for CdTe and have reported that thiol ligand-exchanged

CdTe QDs in water can have higher luminescence than trioctylphosphine/dodecylamine-capped CdTe QDs in chloroform, while the opposite is true for CdSe.[12, 14] However, the degree of quantum yield (QY) enhancement for CdTe in water over organic solvents seems to be rather variable, which may be a result of different CdTe synthetic parameters.[12, 14, 25, 26]

Qu and Peng performed an in-depth study of synthesis parameters for the organometallic synthesis of CdSe, using CdO and elemental Se as precursors.[24] They found that using higher Se:Cd ratios in the reaction mixture resulted in a higher QY for organic-soluble QDs, which was attributed more to the organization of the passivating ligands on the surface rather than surface atomic stoichiometry. Jasienak and Mulvaney later found that post-preparative modifying of the surface atomic stoichiometry played a major role in determining the QY through the passivating ligands.[27] CdTe synthesized by Wuister et al. used the more difficult $Cd(Me)_2$ approach and only one Cd:Te synthesis ratio of ~1.2:1 ,[12] but these QDs had high fluorescence after transferring to water. In all these reports, it has not been clearly identified if the QY variations arise from changes in the radiative or non-radiative relaxation rates. Furthermore, there is a general lack of quantification of how the ligands bind to the QD surfaces and, in particular, their effect on the charge carrier relaxation processes.

The aim of this study was to evaluate the details underlying how the coupling of surface atoms to ligand binding affects the radiative and non-radiative relaxation pathways. We use the more accessible CdO precursor approach to organometallic CdTe synthesis and subsequent water solubilization by ligand exchange. We determine how the Cd:Te synthesis ratio affects the resulting surface atom ratio and, in turn, how they determine the binding of different ligands and, consequently, control the optical properties. These properties are investigated first with their native phosphonic acid/phosphine ligands and upon exchange with hydrophobic thiols in the same

solvent, and then hydrophilic thiols in methanol and water. This systematic progression allows us to quantify the individual roles of the surface atoms, the coordinating and functional groups of the ligands, and the solvent in controlling the electronic relaxation pathways of CdTe QDs. Our results provide a deeper understanding of the relaxation pathways of the excited state so that one can optimize the synthetic conditions and ligand coupling to produce QDs tailored for specific applications.

2.3. Experimental Section

2.3.1. Chemicals. Cadmium oxide (CdO – Puratronic, 99.998%), 1-Tetradecylphosphonic acid (TDPA - 98%), 1-Octadecene (ODE – tech 90%), Tellurium powder (Te – 99.99%), Tri-n-butylphosphine (TBP – 95%, 1-Propanethiol (PPT – 98%), 3-Mercaptopropionic acid (MPA – 99%), and Tetramethyl ammonium hydroxyde pentahydrate (TMAH – 98%) were all purchased from Alfa Aesar. Hexanes, acetone and anhydrous diethyl ether were all ACS grade and purchased from EMD. Methanol was purchased from BDH through VWR Scientific. Fluorescein from the Reference Dye Sampler Kit (R14782, Invitrogen, Eugene, OR) was used for the photoluminescence quantum yield measurements.

2.3.2. QD Synthesis. The nanoparticles were prepared using 5 different Cd to Te molar ratios: 5:1, 2:1, 1:1, 1:2 and 1:5 by hplding Cd constant at 0.2 mmol. As an example of the synthesis protocol for 5:1 Cd:Te with 0.2 mmol Cd was prepared as follows: 0.0256 g (0.2 mmol Cd) of CdO was mixed with 0.114 g of TDPA (0.41 mmol) and placed in 3.93 g of ODE in a three neck round bottom flask. This mixture was vacuum purged for ~30 minutes then, after turning off the vacuum, was placed under argon flow, and heated to 300°C with a heating mantle. At this temperature, the tellurium was injected, consisting of a mixture of 1.90 g of ODE and 0.10 g of a Te stock solution,

prepared by dissolving 1.02 g of Te powder in 18.98 g tributylphosphine (0.04 mmol Te). After the Te was injected, the solution temperature was immediately reduced to 250°C and the nanocrystals grown to the desired size as monitored by their UV-Vis and PL spectra, usually within a couple of minutes. Once the nanocrystals had achieved the desired size, the heating mantle was removed and the reaction stopped by withdrawing a sample and dissolving into cold hexane. All synthesis times were controlled to produce similar sized QDs.

2.3.3. QD Ligand Exchange. Each of the samples was then split into 3 different aliquots; one aliquot was left as-prepared, one aliquot was ligand exchanged with propanethiol (PT), and the other aliquot was ligand exchanged with mercaptopropionic acid (MPA). The PT ligand exchange was performed as follows: 2 mL of the as-prepared nanocrystal solution was added to a vial and diluted with 2 mL of hexanes. To extract the unreacted starting materials, 4 mL of methanol were added and vigorously agitated. Then, to achieve efficient phase separation, the sample was centrifuged for 5 minutes.

After centrifugation, the methanol layer containing the unreacted starting materials was removed from the hexane layer containing the QDs. The extraction was repeated. The hexane QD solution was precipitated with acetone and the solution was centrifuged for ~15 minutes until a pellet was formed at the bottom of the vial and only clear, colorless liquid remained above. The liquid was decanted and excess solvent was removed from the pellet by tapping the vial upside down. Immediately, the ligand solution was added to the pellet, which consisted of 200 µL of PT dissolved in 10 mL of hexanes. Upon addition of the ligand solution to the pellet, the mixture was sonicated and placed in a three neck round bottom flask under argon and refluxed for 3 hours at ~68°C. After reflux, the heating mantle was removed and the solution was allowed to cool to room temperature. The same procedure was repeated for MPA ligand exchange, except that the QD

sample was precipitated from hexanes with acetone, centrifuged to a pellet and decanted. Then a ligand solution, consisting of 200 µL of MPA dissolved in 10 ml methanol adjusted to pH ~10.5 with tetramethylammonium hydroxide (TMAH), was added to the pellet. To obtain the MPA-QDs in water, a 2 mL aliquot of the MPA particles in methanol was precipitated by addition of diethyl ether and centrifuged for ~15 minutes until a pellet was obtained. The liquid was decanted and the vial was inverted and lightly tapped to remove any remaining liquid. Following this, 2 mL of 18MΩ Millipore water was added. The MPA-exchanged nanocrystals readily dissolved in the water.

2.4. Instrumentation and measurements

2.4.1. Absorption and Fluorescence Spectroscopy. To measure the spectra and photoluminescence quantum yield (QY) of the as-prepared QDs in hexane, PT-QDs in hexane, MPA-QDs in methanol and MPA-QDs in water, aliquots from each of the samples were diluted with their respective solvents to an optical density of 0.01 at a wavelength of 450 nm, measured by a Hitachi U-3900H UV-VIS absorption spectrophotometer. Their photoluminescence spectra recorded with a Perkin-Elmer LS 55 luminescence spectrometer from 470 to 800 nm upon excitation at 450 nm. The QY was calculated by comparing the integrated area of the QD emission spectrum to that of a 0.01 O.D. (@450 nm) solution of fluorescein in 0.1M NaOH, which has a 92% QY.

2.4.2. Fluorescence Microscopy. To measure the fluorescence lifetime of the QDs, aliquots were diluted in their respective solvents to ~100 nM in a powder-coated stainless steel liquid cell into which a glass coverslip was sealed using a silicone O-ring seal. Time-correlated single photon counting (TCSPC) curves were obtained using a MicroTime 200 Confocal Fluorescence Lifetime Microscope (PicoQuant GmbH, Berlin, Germany), consisting of a 485 nm picosecond DPSS laser

(LDH-P-C-485, Picoquant), controlled by the Sepia II software with 5 μW power and 5 MHz repetition rate. The excitation laser was reflected from a dichroic mirror (DCXR500, Chroma) and passed through a water-immersion objective (Olympus UPLSAPO 60×w, 1.2N_A). The emitted fluorescence was collected by the same objective, transmitted through the same dichroic mirror, a 75 μm pinhole, and a 605/55m emission filter (Chroma, Bellows Falls, VT) onto an avalanche photodiode detector (PDM, Microphoton Devices, Bolzano, Italy). The detector passed the signal to the TCSPC card (Picoharp 300, Picoquant) onto 4096 channels with 64 ps per channel, and the data was collected and analyzed with the SymphoTime software package. The width of the instrument response function was determined to be less than 0.3 ns, which greatly facilitated data fitting. The data was fit to the minimum number of exponentials, *i*, required until the chi-squared value was no-longer reduced and the residuals showed no systematic deviation (3 components were needed), and the average fluorescence lifetime, τ_{fl}, determined by equation 2.1 as follows:

$$\tau_{fl} = \frac{\sum_{i=1}^{3} c_i \tau_i^2}{\sum_{i=1}^{3} c_i \tau_i} \qquad \textbf{2.1}$$

c_i is the fractional amplitude of component *i*, and $\sum_i c_i = 1$ and τ_i is the lifetime of component *i*.

2.4.3. FT-IR Spectroscopy. The FT-IR spectra were measured on a Bruker Vertex 70 FT-IR spectrometer equipped with a deuterated tri-glyceride sulfate (DTGS) detector, and the sample chamber purged with a steady stream of dry N_2. After measuring the background spectrum of a clean, dry CaF_2 window, 40 μL of a solution of QDs with an exact OD of 0.1719 at the λ_{max} was placed in the exact center of the CaF_2 window, resulting in a drop smaller in diameter than the probe beam to ensure that the same amount of sample was measured for each sample, and then left in a horizontal position to dry overnight in the N_2-purged sample chamber. The FT-IR absorption spectrum was calculated by measuring and averaging 16 scans.

2.4.4. Transmission Electron Microscopy. TEM images were acquired on a JEOL 100cx transmission electron microscope (JEOL, Tokyo, Japan). QDs were washed of impurities by precipitating them from solution with methanol, centrifuging to a pellet and redissolving in pure hexane, which was repeated 2-3 times. A Formvar-coated copper TEM grid (Ted Pella, Redding, CA) was dipped into the well-washed QD hexane solution, and allowed to dry in air overnight. The acceleration voltage used during the measurement was 100 kV, and images were acquired on a CCD camera (low mount XR41, AMT, Danvers, MA).

2.4.5. X-Ray Photoelectron Spectroscopy. To measure the X-ray photoelectron spectra, QDs were precipitated using the same method as for ligand exchange; extraction with methanol 3 times followed by addition of acetone and centrifugation. The precipitate was placed on a carbon sticky tab, dried in a vacuum oven overnight before being inserted into the load lock of the XPS (Phi Versaprobe, Physical Electronic Inc., Chanhassen, MN) and allowed to dry for a further 24-48 hours prior to analysis. The XPS is equipped with a monochromated Al-Kα source (1486.6eV), dual-beam charge compensation and a spherical capacitance analyzer operated in fixed analyzer transmission mode. The Pass Energies used were 117eV and 23.5eV to 45eV for survey and quantification scans, respectively.

Data was collected at a 45° take-off angle relative to the analyzer lens with between 100-500 ms collection time, depending on the peak. Data analysis was performed using Phi MultiPak (Physical Electronics Inc.). Charge referencing was made to the adventitious C1s peak. Data were smoothed by the Savitzky-Golay method prior to background subtraction via the iterated Shirley model. Peak areas were related to composition via the relative sensitivity factor method, which allows for multiple pass energies to be used in the same multiplex. Nanoparticles were assumed to be equally dispersed throughout the analysis volume and as such compositions were treated

using the homogeneous quantification model. Data collection was performed using a collection angle of 45° is used to minimize errors associated with this assumption.

2.5. Results and discussion

It has previously been shown that 2 Cd-complexing ligands are needed to solubilize CdO.[18, 19, 28] We performed all reactions using a constant 0.2 mmol Cd, 0.4 mmol TDPA, and vary the Te precursor amount. The sizes of the various CdTe QDs were controlled to be as equal as possible during synthesis by monitoring the absorption spectra. Details of the syntheses are provided in the in section 2.2.2 above. The resulting absorption spectra of the samples with different Cd:Te ratios are overlaid in figure 2.1a. TEM images of three of the samples are shown in figure 2.1b, highlighting the similarity in size from Cd-rich to Te-rich, having an average of ~4nm and low size dispersion.

X-ray photoelectron spectra (XPS) of the Cd peaks for the 5:1 Cd:Te sample is shown in figure 2.2a and the Te peaks for the 1:5 Cd:Te sample is shown in figure 2.2b, exhibiting excellent signal:noise ratios, thus allowing accurate integration of the peaks in figure 2.2c. Using a 5:1 Cd:Te ratio in the reaction mixture led to an observed Cd:Te ratio of ~4:1 by XPS. With a 1:1 Cd:Te ratio, there observed ratio is ~1:1, and using 1:5 Cd:Te resulted in ~1:4 by XPS. It is important to note that these ratios are not absolute values of the surface composition, but provide comparisons between different samples of the same size.

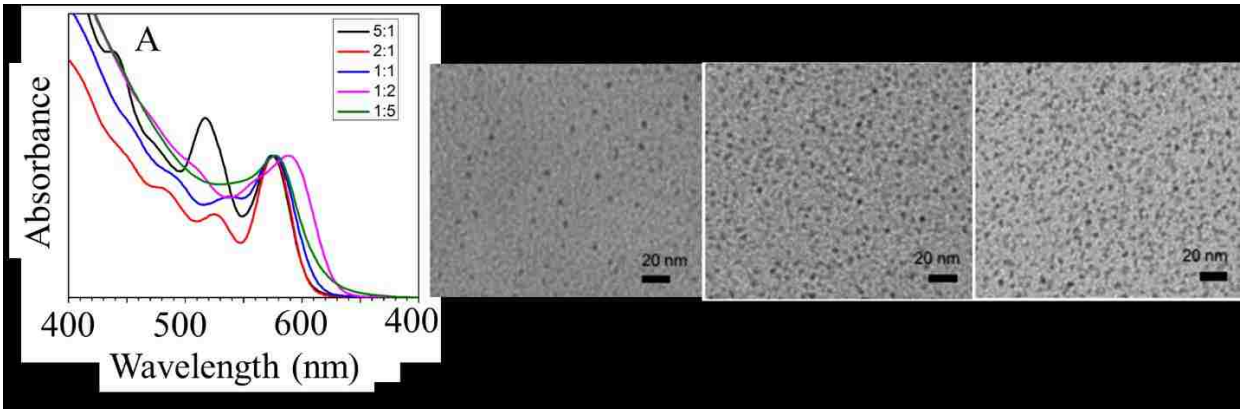

Figure 2.1. (A) Absorption spectra of CdTe QDs with varying Cd:Te ratios. (B) TEM images of Cd-rich, CdTe neutral and Te-rich CdTe QDs

XPS is generally more sensitive to surface atoms than bulk atoms, although at these length scales, XPS does probe a significant fraction of the whole particle. However, if the particle bulk were significantly more Cd-rich or Te-rich, the bandgap energy, as measured from the absorption and emission spectra, would not be in agreement with their sizing curves as previously measured,[29] suggesting that the excess atoms lie preferentially on the QD surface. This is not to say that the excess atoms are *exclusively* at the surface, and there is likely a radial "shell" of Cd-rich or Te-rich CdTe, as has been modeled for CdSe.[27] Also, the possibility of forming some pure Cd or Te nanoparticles cannot be excluded. However, in general, the atomic ratios shown here are in reasonable alignment with what was expected and primarily highlight that the surface of the samples are indeed Cd-Rich, CdTe neutral or Te-rich depending on the synthesis ratios.

Upon ligand exchange, the samples exhibited shifts in the fluorescence maximum and QYs. The fluorescence spectra for the 5:1 Cd:Te samples upon ligand exchange are shown in figure 2.3a. Upon exchange of the TDPA/TBP with PT, there is a red shift in the emission maximum, whereas upon using MPA there is a blue-shift. The solvent also played a role, with MPA showing a larger blue-shift in water compared to methanol.

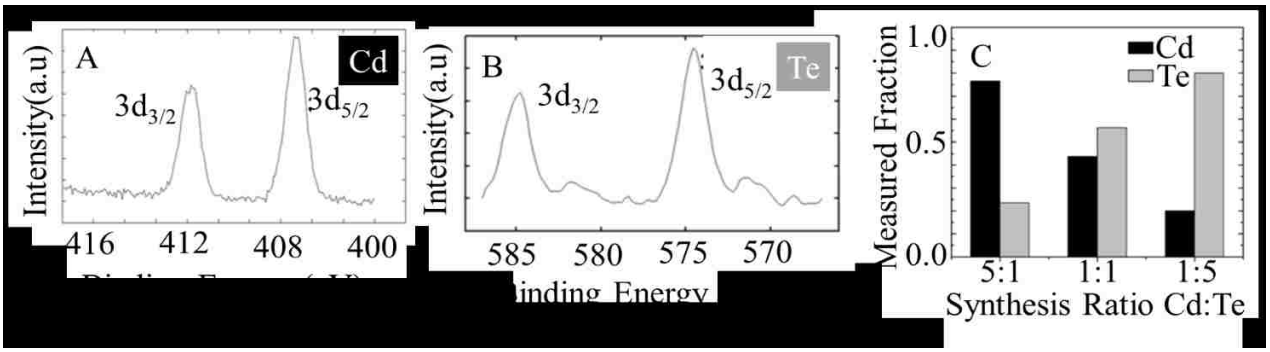

Figure 2.2. (A) XPS spectra of Cd peaks from 5:1 Cd:Te QDs. (B) XPS spectra of Te peaks from 1:5 Cd:Te QDs. (C) Integrated peak areas of Cd and Te, normalized to a total fraction of 1, for 5:1, 1:1, and 1:5 Cd:Te.

The QY results as a function of surface atom ratio, ligand and solvent are summarized in figure 2.3b. The inset of figure 2.3b shows an image of the PL as a function of surface atom ratio for the as-prepared samples, with native TDPA/TBP ligands. For the native QDs, the highest QY obtained was ~20% for QDs synthesized with a 5:1 Cd:Te molar ratio. As the ratio of Cd:Te decreased, so did the QY, with a rapid decrease occurring from 2:1 to 1:1 in which the QY decreased from ~17% to 3%, where it remains as the surface becomes Te-rich. Upon ligand exchange with PT, there is an increase in the QY for all particles as compared to the as-prepared CdTe, reaching up to 80% with 5:1 Cd:Te and decreasing with decreasing Cd:Te ratio.

However, only when the surface becomes very Te-rich does the QY drop to negligible values; at 1:2, it is still at 30%. Upon exchange of the ligands with MPA, the QY is always smaller than for PT-QDs, but is higher than the original TDPA-QDs when the surface is Cd-rich. Interestingly, the solvent plays a significant role, where methanol quenches 5:1 Cd:Te less than water, but for 2:1 Cd:Te, methanol quenches them more than water does. However, we can obtain bright water-soluble CdTe QDs with QY between 45-50% by using either 5:1 or 2:1 Cd:Te ratios. We used quantitative FT-IR absorption spectroscopy to investigate how the surface atom ratio determines the amount and type of ligand bound to each sample.

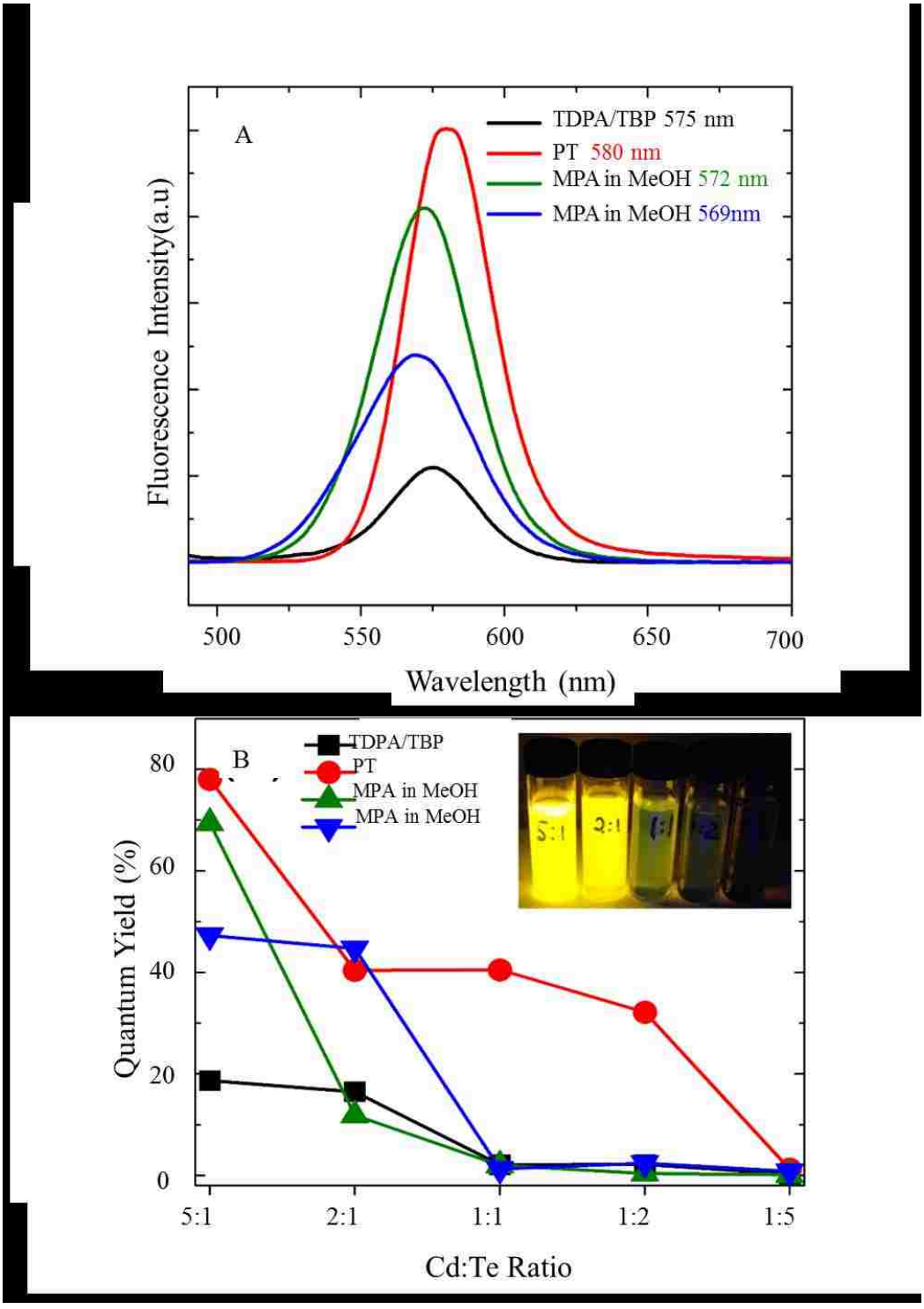

Figure 2.3. (A) Fluorescence spectra of 5:1 Cd:Te QDs for as-prepared TDPA/TBP, and after ligand exchange with PT or MPA. The MPAQDs are shown in both methanol and water. (B) Quantum yield as a function of Cd:Te surface atom ratio, ligand, and solvent. Inset: fluorescence image of TDPA-QDs in hexanes under a 366 nm UV lamp with Cd:Te ratios varying from, left to right, 5:1, 2:1, 1:1, 1:2 and 1:5.

We were extremely careful to remove excess ligands and to measure exactly the same concentration of QDs to allow quantitative comparisons of peak intensities to be made. The FT-IR absorption spectrum of the as-prepared 5:1, Cd:Te samples is shown in figure 2.4a, and the 5:1 Cd:Te MPA-exchanged QDs in figure 2.5a, together with peak assignments. For the as-prepared samples, the FT-IR spectra show strong sp3 hybridized C-H stretching peaks between 2750 and 3000 cm^{-1}, which come from all bound ligands. From the synthetic conditions, 3 possible ligands are present; TDPA, TBP and ODE. TDPA is easy to identify and quantify from the double peak of deprotonated PO_3^{2-} between 1050 and 1250 cm^{-1}.[30]

The peak at 1650 cm^{-1} is characteristic of C=C stretching and those at 990cm^{-1} and 910cm^{-1} are characteristic of monosubstituted methylinic C-H bending modes ($RHC=CH_2$), each identifying the presence of bound octadecene (ODE) on the CdTe QDs, which is quite surprising since ODE is generally considered to be a non-coordinating ligand.[31] TBP is more difficult to quantify due to the absence of characteristic peaks specific to this compound. However, the number of sp3 hybridized C-H bonds per TDPA, TBP and ODE are 29, 21 and 33 respectively, so can be indirectly inferred from the other peaks. Since the sp3 C-H peaks come from all these species, the integrated area between 2800 – 3000 cm^{-1} allows us to assess the relative amount of total ligands bound as a function of Cd:Te surface atom ratio. Comparing the change in the C-H area from sample-to-sample to the TDPA and ODE intensities allows us to determine how the surface atoms affect native ligand binding (figure 2.4b) and upon ligand exchange with PT (figure 2.4c)). The C-H peak area increases by ~50% from 5:1 Cd:Te to 1:1. Concomitantly, The TDPA peak decreases by ~50% and the ODE peaks increase by ~70%. This implies that there are more TBP ligands bound in the 1:1 sample than the 5:1 sample, as one would expect.

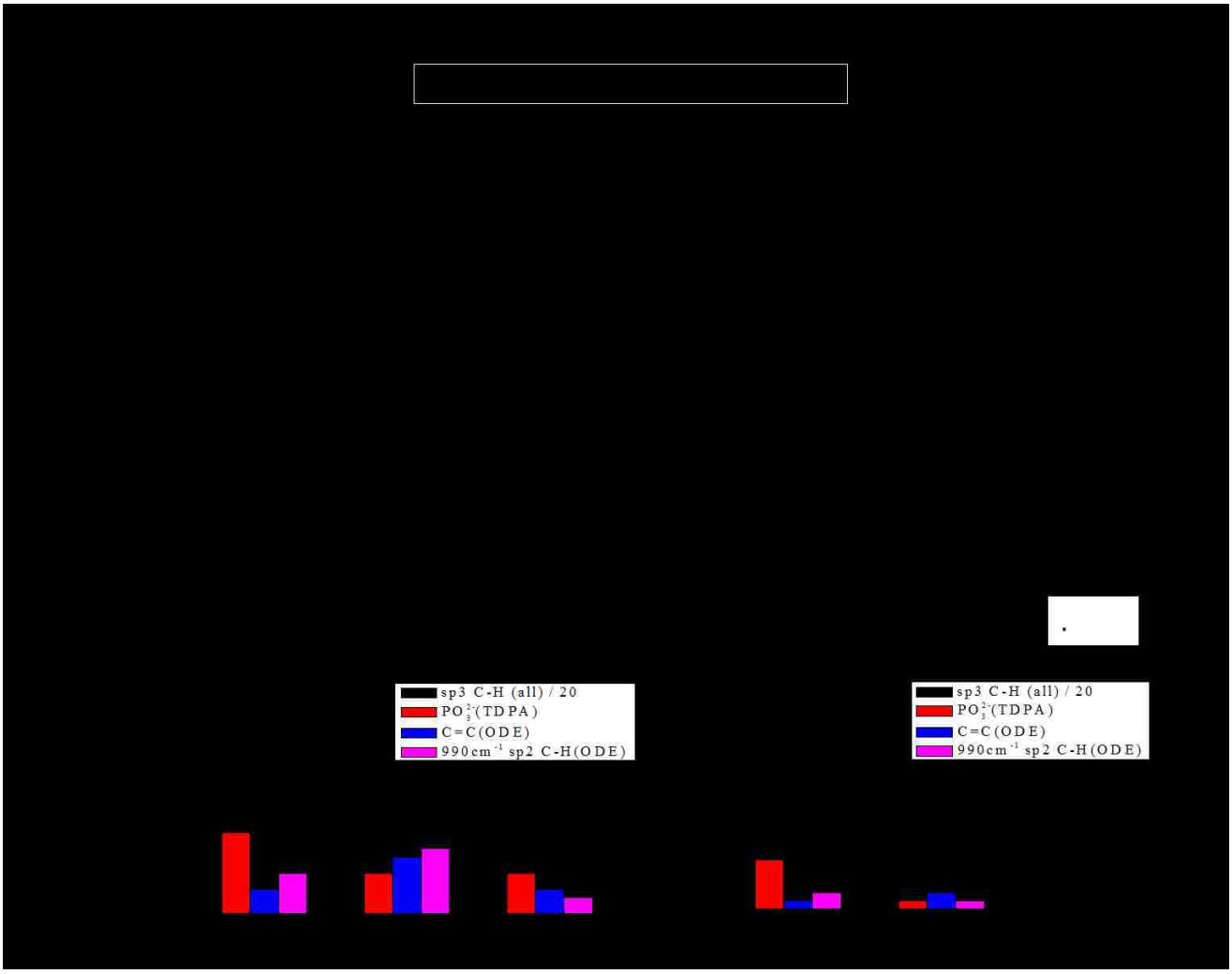

Figure 2.4. (A) FT-IR absorption spectrum of as-prepared CdTe synthesized with a Cd:Te ratio of 5:1. (B and C) Integrated peak areas of the sp3 C−H peak (black), PO_3^{2-} peak from TDPA (red), and two peaks that are representative of ODE ligands, C=C (blue) and the sp2 C−H (magenta) for as-prepared and PT-exchanged CdTe, respectively, as a function of Cd:Te ratio.

However, the large increase in the amount of ODE means that the increase in TBP is only ~30%. For 1:5 Cd:Te, the total C-H peak area is about half the value of the 1:1 Cd:Te, almost fully accounted for by the same relative decrease in the ODE peak area. It appears as though there is little-to-no extra TBP bound for the 1:5 Cd:Te compared to the 1:1. Comparing 1:5 to 5:1, there are about half the number of TDPA ligands bound to 1:5 than 5:1 and about the same amount of

ODE, with about a 25% drop in the C-H peak area; the difference coming from TBP. Taken together, we can conclude that as the surface atom ratio moves from 5:1 to 1:1, ~50% less TDPA, ~70% more ODE and up to ~30% more TBP is bound. As the ratio moves from 1:1 to 1:5, about the same amount of TDPA, ~50% less ODE and about the same amount of TBP is bound. After the 5:1 Cd:Te sample is exchanged with PT, it was found that approximately 50% of the TDPA and ~30% of the ODE ligands remained on the QDs (figure 2.4c). The number of C-H bonds per PT molecule is far less than the native ligands, significantly lowering the extinction coefficient of this peak for PT.

Therefore, inferring the amount of TBP that remains is much more difficult. Since the integrated C-H peak area for PT samples is significantly lower for PT samples than the as-prepared samples, it highlights that a significant number or ligands have been exchanged for PT. As the surface stoichiometry moves from 5:1 to 1:1, little of the TDPA remains, although about the same amount of ODE remains. The C-H peak does decrease by about 20% suggesting less PT per QD. For 1:5 Cd:Te PT-exchanges samples, no TDPA or ODE remains and the C-H peak is again reduced by a further 20-30%, implying less PT per QD for 1:5 than 1:1, showing its preference for Cd atoms, as one would expect.

After the samples are exchanged with MPA ligands, the broad O-H stretch covers the C-H stretch region, making this peak difficult to quantify. However there are no peaks associated with TDPA or ODE, suggesting complete removal of these ligands by MPA. There are characteristic strong C=O stretches for COOH at 1677 cm^{-1} and COO^- at 1582 cm^{-1} (asymmetric stretch) and at 1390 cm^{-1} (symmetric stretch). The COOH peak is slightly lower in frequency than usually observed, which may indicate that the protonated COOH group is coordinated directly to the QD surface.

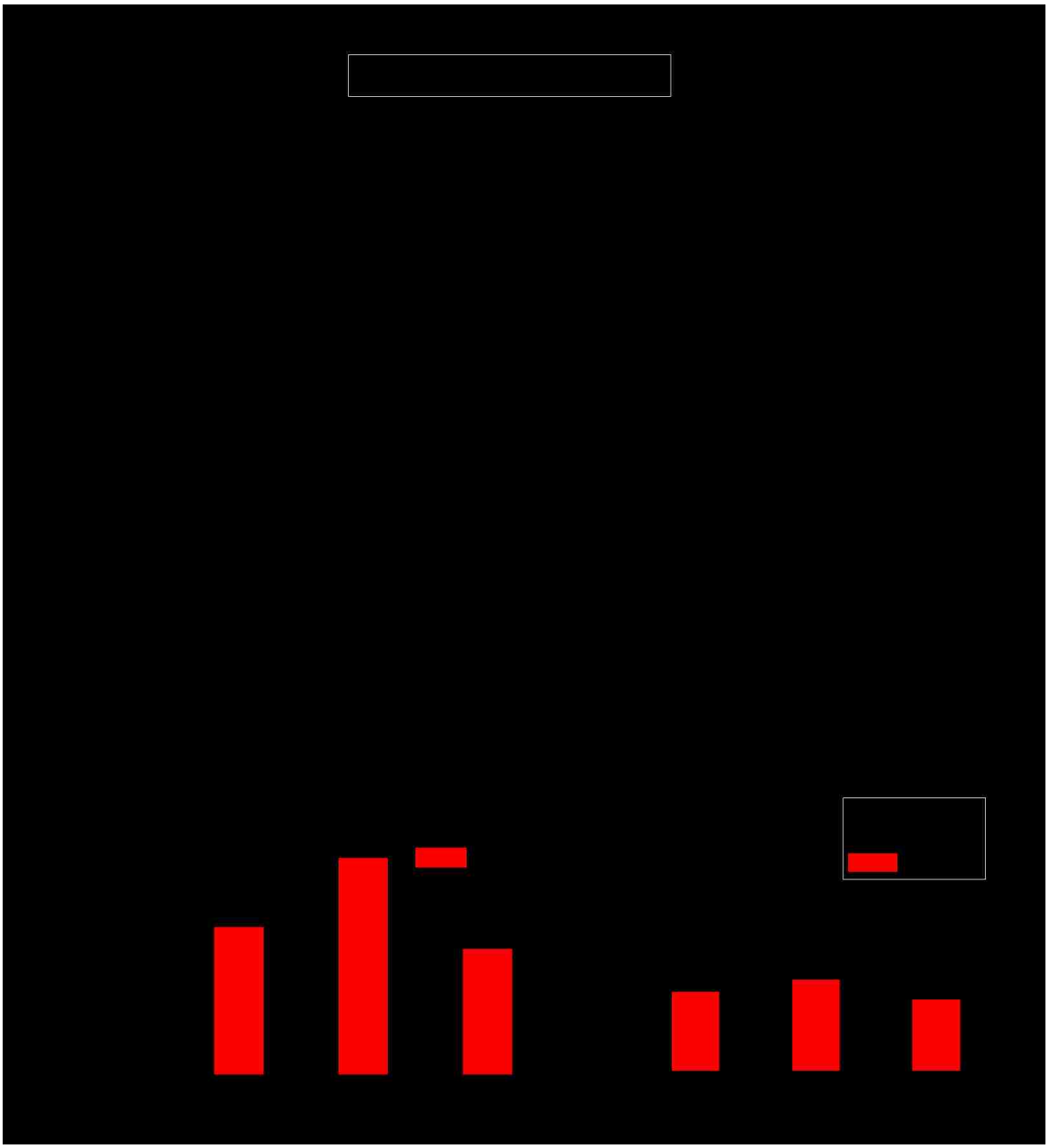

Figure 2.5. (A) FT-IR absorption spectrum of MPA exchanged CdTe in methanol, synthesized with a Cd:Te ratio of 5:1. (B and C) COOH (black) and COO^- (red) for MPA-exchanged CdTe in methanol and water, respectively, as a function of Cd:Te ratio.

The COOH and asymmetric COO^- peak areas can be used to estimate the relative number of MPA ligands bound for 5:1, 1:1 and 1:5 Cd:Te QDs, as well as the protonation state of such ligands in each solvent; methanol and water.

We must be careful when comparing the two peaks (COOH and COO^-) directly to each other, since the extinction coefficient of COOH is about half that of COO^-.[32] In methanol, the COOH peak steadily decreases as the ratio of Cd:Te decreases, suggesting that they are bound primarily, although not exclusively, to the Cd atoms. The deprotonated COO^- peak is about 30% greater for 1:1 Cd:Te than 5:1, but reduces for 1:5, to about the same area as for 5:1. As the MPA-QDs are transferred to water, there is always a lower peak area of both COOH and COO^- peaks for all Cd:Te ratios compared to the same samples in methanol. There is significant ligand removal of protonated COOH for the 5:1 ratio, which becomes less pronounced as the Cd:Te ratio reduces. This strongly supports the conclusion that the protonated COOH ligands are weakly bound to the Cd atoms, while COO- ligands are more strongly bound; implying that the deprotonated COO^- ligands coordinate via the stronger thiol group to result in the charge groups protruding into the solvent. Both the COOH and COO- peaks decrease by about the same amount (~30-40%) for the 1:5 Cd:Te. Interestingly, in water, the COO- peak area does not change as the Cd:Te ratio decreases, although the COOH peak does increase slightly for the 1:5 ratio.

In order to investigate how the surface atoms and ligands affect the electronic processes underlying the variations in quantum yield, we performed fluorescence lifetime measurements to determine the radiative and non-radiative relaxation rates. The fluorescence lifetime curve for the 5:1 sample is shown in figure 2.6a. The lifetime data are fit to a series of exponentials until the residuals showed no deviation and the chi-squared value was reduced. Usually 3 were needed, and the average fluorescence lifetime, τ_{fl}, was calculated using equation 2.1 above. The average

fluorescence lifetime values are plotted in figure 2.6b, and shows a dependence that does not directly correlate with the QY dependence, highlighting the fact that both the average radiative and average non-radiative rates are changing. These two rates (plotted as lifetimes) are calculated as follows:[33, 34]

$$\tau_r = \frac{1}{k_r} = \frac{\tau_{fl}}{QY} \quad \textbf{2.2}$$

and

$$k_{nr} = \frac{1}{\tau_{nr}} = \frac{1}{\tau_{fl}} - \frac{1}{\tau_r} \quad \textbf{2.3}$$

where τ_r is the average radiative lifetime and τ_{nr} is the average non-radiative lifetime. Strictly, equations 2.2 and 2.3 provide relationships between the radiative and non-radiative lifetimes from a single process. In our experiments, we do not separate excitonic emission from shallow trap emission, which is only slightly red-shifted and difficult to distinguish from the excitonic emission,[34, 35] due to using an emission filter in the microscopy setup. Therefore, this analysis provides average radiative and average non-radiative lifetimes that contain contributions from both excitonic and trap states, each of which will be discussed in detail below.

The average radiative and non-radiative lifetimes are plotted in figures 2.6c and 2.6d, respectively. The average radiative lifetimes span at least 2 orders of magnitude as the surface atom ratio varies from Cd-rich to Te-rich and so the data are plotted on a logarithmic scale to more clearly follow the effects. It is clear that a Te-rich surface significantly increases the average radiative lifetime compared to a Cd-rich surface with all ligands, but is more pronounced for QDs with MPA ligands. The solvent also affects the radiative lifetime, with MPA-QDs in methanol having a significantly longer radiative lifetime than in water. While the radiative lifetimes vary by

2 orders of magnitude, the non-radiative lifetimes vary by about 1 order. They do show a systematic decrease as the surface becomes more Te-rich, but show less of a ligand or solvent dependence.

The much longer average radiative lifetime of Te-rich CdTe highlights that the reason for the QY change is due more to an average decrease in the electron-hole overlap integral than to an increase in non-radiative relaxation pathways. Phosphonic acid ligands bind very strongly to Cd atoms;[36, 37] in fact, phosphonic acid ligands are used to control the reactivity of Cd-monomers for better size and shape control during synthesis than phosphine oxides or amines.[38] The strong coupling of these ligands to the QD likely suppresses electron trapping at the Cd atoms, leaving hole trapping as the primary competing process. This suggests that the Te-atoms on the surface are less-passivated than Cd atoms, or Se atoms in the case of CdSe.[39] DFT calculations have shown that the trimethylphosphine-Te bond is about 70% the strength of the trimethylphosphine-Se bond, due to a smaller donation interaction energy involving less electrons per donation.[40] It is therefore more likely that Te-P bond would break during synthesis than Se-P to result in less-passivated Te atoms on CdTe QDs.

This difference could explain the contrasting results observed between using chalcogenide-rich precursor solutions when synthesizing CdSe[24] compared to CdTe, as shown here. If less ligand molecules are coordinated to the Te-rich QDs, it is reasonable to conclude that it would lead to increased hole trapping efficiency on the Te atoms due to the presence of dangling bonds. This conclusion is strongly supported by the FT-IR absorption spectra for the as-prepared CdTe, in which the integrated C-H peak area was lower for 1:5 than 1:1 and 5:1 Cd:Te ratio QDs.

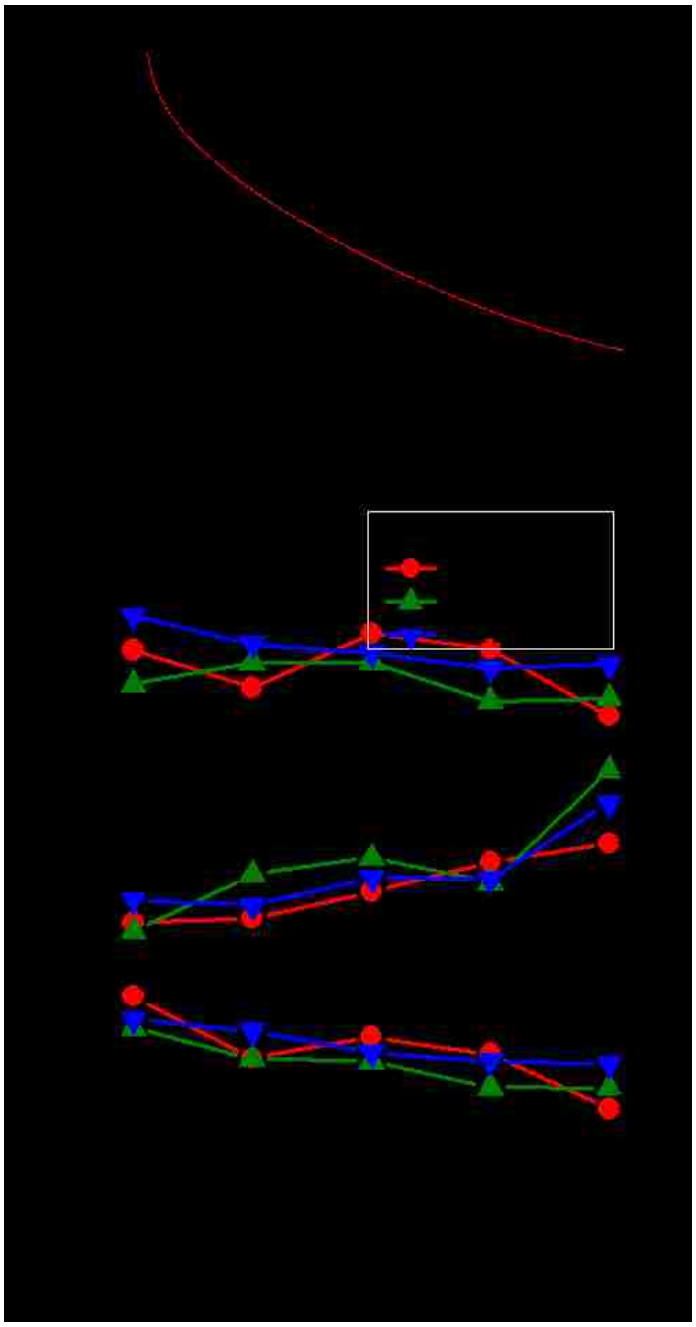

Figure 2.6. (A) Fluorescence lifetime decay (TCSPC) curve of a typical QD (5:1 with native TDPA ligands shown here) with multiexponential fit (red) and residuals. (B) Average fluorescence lifetime measured by the fit to (A). (C) Radiative lifetime calculated using eq 2.2 as a function of Cd:Te surface atom ratio, ligand, and solvent. (D) Nonradiative lifetime calculated using eq 2.3 as a function of Cd:Te surface atom ratio, ligand, and solvent.

The calculated increase in the amount of TBP bound for 1:1 Cd:Te compared to 5:1 (~30%) is far less than the increase in the number of surface Te atoms measured by XPS (up to 250%), highlighting an overall higher fraction of unpassivated Te which results in an increased radiative lifetime.As the Cd:Te ratio changes from 1:1 to 1:5, the amount of bound TBP does not increase, while the number of Te atoms does so significantly, leading to an even greater increase in radiative lifetime, as we observe. To explain these effects we propose a model that connects the structural properties of the QD surface to the energy levels, shown schematically in figure 2.7. The details of this model will be explained below. In addition to increasing the average radiative lifetime, there is a small but steady decrease in the non-radiative lifetime as the surface changes from Cd-rich to Te-rich. While holes have been shown to generally relax faster than electrons,[41, 42] the complexity of electron and hole relaxation pathways in colloidal QDs has been recently highlighted.[43]

It was proposed that confining one of the charge carriers may enhance the ligand-induced nonadiabatic transition rate due to removing the Auger relaxation channel, which was used to explain the absence of a phonon bottleneck for both charge carriers. Recent TDDFT calculations also support this hypothesis.[44] For CdTe, it has been shown that the hole is trapped on the ~1ps timescale.[45, 46] Once trapped, it would be easier for the excess electronic energy to couple to the vibrations of the ligand molecule, resulting in a shorter non-radiative lifetime (faster rate). These processes are described in figure 2.7 as k_3 and $k_{2\ (non\text{-}rad)}$ respectively. We propose that it is the balance of the rates of these two processes that are responsible for the observed effects on theaverage radiative and non-radiative lifetimes shown in figure 2.6. The rate of the surface trapping process, R_3, is

Figure 2.7. Proposed model showing the relationship between surface structure and excitonic emission, trapping, and nonradiative processes in (A) Cd-rich and (B) Te-rich CdTe, respectively. (C and D) Energy level diagrams showing the various radiative and nonradiative processes for high-energy trap states such as from TDPA/TBP ligands and lower energy trap states such as from thiol ligands, respectively. Rates, R_i, and rate constants, k_i, are related in eqs 2.4 and 2.5.

$$R_3 = k_3[Te]_s[h_X^+] \qquad \textbf{2.4}$$

where $[Te]_S$ is the concentration of unpassivated surface Te atoms and $[h^+_X]$ is the density of holes, which at the (constant and low) laser power used in these experiments should be ~ 1 per QD. Since there are few Te atoms on Cd-rich QDs, this rate is relatively slow, and the competing process of excitonic radiative recombination ($R_{1\,(rad)}$) with the excitonic hole (h^+_X) leads to a relatively high QY. Once the hole is trapped, the rate of non-radiative relaxation of the excess electronic energy via the ligand-induced nonadiabatic transition is given by the product of the trapping rate and the ligand density

$$R_{2(non-rad)} = k_2 k_3 [e^-][ligand][Te]_s[h_X^+] \quad \textbf{2.5}$$

The concentrations $[e^-]$ and $[h^+_X]$ are equal at time = 0, since the absorption of 1 photon creates 1 excitonic electron-hole pair. Since there is still some (although much reduced) overlap of the trapped-hole wave function with the electron, there is a competing radiative recombination process, $R_{2\ (rad)}$, which is expected to be relatively slow. The faster average radiative lifetime observed for Cd-rich QDs would be a result of the larger contribution from the fast excitonic emission ($R_{1\ (rad)}$) rather than the slower $R_{2\ (rad)}$ process). For Te-rich QDs, the larger $[Te]_S$ in equation 2.4 leads to a faster R_3 process compared to $R_{1(rad)}$, resulting in a strong reduction in QY.

The $R_{2(non\text{-}rad)}$ process described in equation 2.5 depends on both the ligand density and the number of hole-trap states. Since the ligands are largely bound to the fewer Cd-atoms on the surface in Te-rich QDs, $R_{2(non\text{-}rad)}$ is low and there is a larger contribution of the slower $R_{2(rad)}$ to the observed average radiative lifetime. As the surface goes from Cd-rich to Te-rich, the decrease in the observed non-radiative lifetime (i.e. increase in $R_{2(non\text{-}rad)}$) suggests that $k_3[Te]_S$ increases at a faster rate than k_2[ligand] decreases in equation 2.5. $R_{2(rad)}$ is determined by the overlap integral and is thus expected not to change. Additional non-radiative processes due to point defects within the crystal may also play a role, and will be investigated in future work. In any case, the proposed model in figure 2.7 is strongly supported by the FT-IR data; Cd-rich QDs are much more passivated by ligands than Te-rich QDs, especially by the strongly Cd-binding TDPA. The increased C-H peak area observed for 1:1 Cd:Te compared to 5:1 shows that some of the additional Te atoms are indeed passivated by ligands (most likely TBP).

It is not only the density of ligands that are important for the observed relaxation dynamics, but also their identity. This is evident from the strong dependence of ligand on QY. Upon ligand

exchange of the native ligands with PT ligands, the average radiative lifetime decreased for all surface atom ratios, suggesting that the trapping process is significantly reduced by the thiol, in agreement with previous observations.[12, 14] Even though thiols preferentially bind to Cd, they also bind to Te, as demonstrated by FT-IR; as Cd:Te varies from 5:1 to 1:5, the total intensity of the C-H peak of PT-QDs and the C=O peaks of MPA-QDs decease by only a factor of ~2. Due to the smaller footprint of PT over TBP, more of the Te atoms would likely be passivated compared to the as-prepared CdTe, resulting in less trap states and a reduced average radiative lifetime.

Furthermore, it has been proposed that the energy of thiol traps states is lower in energy than the valence band edge of CdTe.[14] This lowering of trap energy may open up a new pathway in which the trapped holes may be thermally de-trapped (R_{-3} in figure 2.7d), which competes with both $R_{2(rad)}$ and $R_{2(non\text{-}rad)}$ to increase the probability of excitonic recombination ($R_{1(rad)}$), and thus increase QY, the process of delayed fluorescence. The relative rates of R_{-3} $R_{2(rad)}$, and $R_{2(non\text{-}rad)}$ would determine the overall contribution of delayed fluorescence vs the ligand-dependent non-radiative pathways on quantum yield and average lifetime, but it is reasonable to assume that R_{-3} would be faster than $R_{2(rad)}$. This is supported by the fact that the average radiative lifetime of the PT-capped QDs is lower than the TDPA/TBP capped QDs for all Cd:Te ratios.

However, the trend of increased radiative lifetime with decreasing Cd:Te ratio is still evident, supporting the model of figure 2.7. Again this interpretation is supported by the FT-IR data, which shows a decrease in PT ligand binding between Cd-rich and Te-rich. The thiol group also increases the non-radiative lifetime compared to TDPA/TBP (i.e. decreases $R_{2(non\text{-}rad)}$ in equation 2.5, and the trend of non-radiative lifetime decreasing with increasing Te-richness persists. A weaker coupling of the ligand to the QD would serve to decrease k_2 in equation 2.5 while a stronger coupling would increase it. However, since thiol ligands are much smaller than TDPA or TBP,

one can expect that the density of ligands would be much higher for ligand-exchanged QDs, compared to the as-prepared samples.

Based on the observations of figure 2.6d, the increase in non-radiative lifetime (decrease in $R_{2(non\text{-}rad)}$) of Cd-rich samples upon ligand exchange suggests that the decrease in k_2 between thiol ligands and TDPA ligands is larger than the increase in [ligand]. The "noise" in the non-radiative lifetime trend may arise from variations in obtaining the same level of ligand exchange from sample-to-sample. It is common knowledge that the ligand exchange process is prone to variability. Furthermore, the overall trend of decreasing non-radiative lifetime with increasing Te-richness is stronger for PT ligands than for TDPA. Again, this can be explained as $k_3[Te]_S$ increasing at a faster rate than k_2[ligand] decreasing but, in addition to the ligand density, may also result from differences in k_2 upon ligand exchange. TDPA is a strongly coordinated ligand whereas TBP is much weaker, therefore replacing TDPA with thiols would reduce k_2 more than replacing TBP (on Te-rich QDs) with thiols.

The effect of the carboxylic acid group on the MPA ligand and the solvent also play significant roles in the charge carrier relaxation pathways, particularly for Te-rich surfaces, which seems to be additive to the effect of the thiol group. It was previously found that thiolated carboxylic acid ligands quench the fluorescence of CdSe-ZnS core-shell QDs more so than the hydroxyl analogues in water.[47] Here we have shown that the average radiative lifetime for Te-rich CdTe increases to several microseconds for MPA-QDs in methanol, which we have suggested to result from increased hole-trapping, but the same QDs in water have radiative lifetimes similar to the as-prepared QDs. This longer radiative lifetime correlates to the FT-IR data showing that the both forms of the MPA ligand are bound far less efficiently to the QD in the more polar solvent. The FT-IR data also suggests that the MPA ligands coordinate to the QD not just with the thiol

groups (as is the case with PT), but also with their carboxylic acid groups, evidenced by the relatively low frequency of the COOH peak. This is particularly prevalent for the QDs in methanol. The carboxylic acid groups could increase the hole-trapping lifetime compared to the thiol (i.e compared to PT), to result in similar average radiative lifetimes as for the TDPA ligands. We envision this as a reduction in the R_{-3} process in figure 2.7d. This is reasonable considering the chemical similarity of the carboxylic acid to the phosphonic acid. Even though phosphonic acids bind stronger than carboxylic acids, the smaller size of the MPA relative to TDPA, may lead to a larger number of ligands on the QD in both orientations (coordinated by the thiol group or the carboxylic acid group).

Furthermore, the FT-IR data suggests that the protonated form preferentially binds to Cd atoms, as the peak was larger for Cd-rich CdTe in methanol, and it is this form that is more efficiently removed upon transfer to water. As the Te-rich QDs are transferred to water, there is a large decrease in average radiative lifetime, consistent with the view that the R_{-3} process may be largely recovered by the preferential removal of COOH-bound ligands. As was the case for TDPA/TBP- and PT-functionalized QDs, the non-radiative lifetime for MPA-functionalized QDs decreases steadily as the Cd:Te ratio decreases, concomitant with the FT-IR data showing that [ligand] is reduced. Similar to the TDPA/TBP and PT ligands, it appears that $k_3[Te]_S$ increases at a faster rate than k_2[ligand] decreases in equation 2.5.

In addition to the effects of the ligand on the relaxation dynamics, the fluorescence spectra were red shifted for PT ligands, but blue-shifted for MPA ligands (figure 2.2a), suggesting electronic effects from both the thiol group and the carboxyl group, and further supporting the multi-functional-group binding observed by FT-IR. The red-shift for PT-QDs must be directly related to the thiol binding, since the solvent is unchanged between PT-QDs and TDPA-QDs.

However, the extent of blue-shifting for MPA-QDs was larger in water than in methanol. It may initially seem contradictory that the blue-shift is larger for MPA-QDs in water than in methanol, considering that there are less MPA ligands bound to the QD in water than in methanol. However, recent work has identified the role of the dielectric constant of the solvent on the spectral shifts in CdTe using both experimental and TDDFT calculations.[48] It appears that there are competing effects in play; roles involving the coordinating group of the ligands and roles involving the dielectric constant of the solvent.

Our systematic progression from hydrophobic thiol to hydrophilic thiol in methanol and then in water allowed us to separate some of these effects. The thiol group both helps to suppress hole trapping and causes a red-shift in the emission spectrum. Transfer of the QD into a higher dielectric constant medium is accompanied by a greater degree of deprotonation of the carboxylic acid, and so these effects cannot be directly uncoupled. However, as the QD is transferred from methanol into water, the additional blue-shift is mainly due to the increased dielectric constant. A previous report of thioglycolic acid (TGA)-capped QDs of similar emission peak position to ours and synthesized with a 5:1 Cd:Te ratio, identical to the QDs shown in figure 2.3 above, estimated an inverse dependence of wavelength shift with dielectric constant, with an ~7 nm blue shift as the dielectric constant changes from 40 to 68.[48] The blue shift observed here as the dielectric constant is changed from 32 (methanol) to 78 (water) is only ~3 nm, which may be due to the fact that MPA is a slightly longer ligand than TGA, thereby screening the solvent effect from the QD more. In any case, it appears that the dielectric constant of the solvent is responsible for reversing the red-shift caused by the thiol group. There may also be some effects from the solvent on the radiative and non-radiative rates between MPA-QDs in methanol and water and may not *just* be a result of differences in how many ligands are bound, and in which orientation, as we have

identified here, but other factors may come into play. Future work will attempt to decouple these factors.

We would like to point out that, while shell-free water-soluble quantum dots have strong advantages over core-shell quantum dots, especially concerning their size and ease of synthesis, adding a shell may still provide other advantages. For example, the shell material is usually less toxic than the core material, which reduces the fluorophore's toxicity for in vivo applications. Furthermore, blinking is a problem for single molecule fluorescence applications and it has been shown that adding a thick shell reduces, or may even eliminate, this effect.[49, 50] However, it is important to pay close attention to the core-shell interface as shells with large lattice mismatches to the core do not appear to reduce the blinking.[51] Finally, adding a shell may reduce the effect of external conditions such as pH on the optical properties of cores,[15, 52] although pH effects have also been reported for core-shell QDs as well.[53-55]

More work is needed to fully understand the role of the external environment, especially aqueous environments, on shell-free QDs with different surface compositions to take full advantage of small and bright water-soluble QDs. It was previously shown that the coordinating group and the water-soluble functional group of the ligand plays an important role in fluorescence quenching of CdSe-ZnS core-shell QDs.[47] We have shown here that these effects depend on whether the surface is Cd-rich or Te-rich, which significantly affects the ligand binding and, in turn, can be used to engineer the radiative and non-radiative lifetimes. The underlying mechanisms for the lifetime variations are complex, being related to coupled effects of charge carrier trapping and ligand-induced nonadiabatic transitions affecting both radiative and non-radiative lifetimes and originating on different surface atoms.

2.6. Conclusion.

In summary, the brightest shell-free QDs that we have synthesized have ~80% QY, with a Cd-rich surface coated with propanethiol ligands. These conditions provide the optimal balance between surface atom passivation and ligand binding strength and are among the highest QY CdTe particles reported. The QY of the same QDs with MPA ligands in polar solvents such as methanol and water show ~70% and 50%, respectively, highlighting the consistent high brightness across a range of solvents. This result is promising as MPA ligands provide a route to water solubility that results in minimal size increase but provide bright, shell-free water-soluble quantum dots. The synthesis uses the cheap, easy to handle CdO and elemental Te as precursors, and has the ability to reproducibly synthesize them without long refluxing times and, using a simple ligand exchange procedure, can be completed in less than an hour. Most importantly, we can use these results to tune both solubility and the optical properties by knowing how the coupled relaxation processes affect both radiative and non-radiative lifetimes. We have quantified that a Cd-rich surface shows higher quantum yield than a Te-rich surface primarily because the radiative lifetime is significantly increased by uncoordinated Te atoms causing hole trapping processes. In addition, strongly coordinating ligands, primarily on the Cd-atoms, increases the non-radiative lifetime. We postulated a model in which a balance between trapping rate and subsequent ligand-mediated non-radiative relaxation is controlled by surface atom stoichiometry and ligand density and coupling strength, which allows us to engineer both average radiative and non-radiative lifetimes. Quantitative FT-IR spectroscopy, together with systematic synthesis and ligand exchange, has provided strong support for this model. The implications of this study in gaining a deeper understanding of the connection between the ligand binding chemistry and the physics underlying

charge carrier relaxation processes will allow one to tailor QDs for a wide variety of applications by engineering these two lifetimes. For example, photovoltaic applications will likely benefit from a system with a long radiative lifetime combined with strong chemical coupling to conducting environments, while light emitting devices benefits from having a short radiative lifetime and weak external coupling. For near-field energy transfer processes, such as FRET, it is important to gain a more complete knowledge of how the local environment affects both the radiative and non-radiative lifetimes in order to accurately calculate the energy transfer rate, and ultimately the distance between the donor and acceptor molecules.

2.7. References

[1]. Kamat, P.V., Quantum Dot Solar Cells. Semiconductor Nanocrystals as Light Harvesters. Journal of Physical Chemistry C, 2008. 112(48): p. 18737-18753.

[2]. Klimov, V.I., et al., Optical gain and stimulated emission in nanocrystal quantum dots. Science, 2000. 290(5490): p. 314-7.

[3]. Ruedas-Rama, M.J., et al., Quantum dot photoluminescence lifetime-based pH nanosensor. Chemical Communications (Cambridge, United Kingdom), 2011. 47(10): p. 2898-2900.

[4]. Chen, Y., et al., L-cysteine-capped CdTe QD-based sensor for simple and selective detection of trinitrotoluene. Nanotechnology, 2010. 21(12): p. 125502.

[5]. Wang, C., et al., Sensitive Hg(II) ion detection by fluorescent multilayer films fabricated with quantum dots. Sensors and Actuators, B: Chemical Sensors and Materials, 2009. B139(2): p. 476-482.

[6]. Shang, L., L. Zhang, and S. Dong, Turn-on fluorescent cyanide sensor based on copper ion-modified CdTe quantum dots. Analyst (Cambridge, U. K.), 2009. 134(1): p. 107-113.

[7]. Chan, W.C. and S. Nie, Quantum Dot Bioconjugates for Ultrasensitive Nonisotopic Detection. Science, 1998. 281(5385): p. 2016-2018.

[8]. Bruchez, M., et al., Semiconductor Nanocrystals as Fluorescent Biological Labels. Science, 1998. 281: p. 2013-2016.

[9]. Hines, M.A. and P. Guyot-Sionnest, Synthesis and Characterization of Strongly Luminescing ZnS-Capped CdSe Nanocrystals. Journal of Physical Chemistry, 1996. 100(2): p. 468-471.

[10]. Alivisatos, A.P., The Use of Nanocrystals in Biological Detection. Nature Biotechnology, 2004. 22: p. 47-52.

[11]. Reiss, P., J. Bleuse, and A. Pron, Highly Luminescent CdSe/ZnSe Core/Shell Nanocrystals of Low Size Dispersion. Nano Letters, 2001. 2: p. 781-784.

[12]. Wuister, S.F., et al., Highly Luminescent Water-Soluble CdTe Quantum Dots. Nano Letters, 2003. 3(4): p. 503-507.

[13]. Gaponik, N. and A.L. Rogach, Thiol-capped CdTe nanocrystals: progress and perspectives of the related research fields. Physical Chemistry Chemical Physics, 2010. 12(31): p. 8685-8693.

[14]. Wuister, S.F., C. deMello Donega, and A. Meijerink, Influence of Thiol Capping on the Exciton Luminescence and Decay Kinetics of CdTe and CdSe Quantum Dots. J. Phys. Chem. B, 2004. 108(45): p. 17393-17397.

[15]. Gao, M., et al., Strongly Photoluminescent CdTe Nanocrystals by Proper Surface Modification. The Journal of Physical Chemistry B, 1998. 102(43): p. 8360-8363.

[16]. He, H., et al., Single nonblinking CdTe quantum dots synthesized in aqueous thiopropionic acid. Angewandte Chemie, International Edition, 2006. 45(45): p. 7588-7591.

[17]. Aldeek, F., et al., The influence of capping thioalkyl acid on the growth and photoluminescence efficiency of CdTe and CdSe quantum dots. Nanotechnology, 2008. 19(47): p. 475401/1-475401/9.

[18]. Guo, J., W. Yang, and C. Wang, Systematic Study of the Photoluminescence Dependence of Thiol-Capped CdTe Nanocrystals on the Reaction Conditions. The Journal of Physical Chemistry B, 2005. 109(37): p. 17467-17473.

[19]. He, Y., et al., Microwave-Assisted Synthesis of Water-Dispersed CdTe Nanocrystals with High Luminescent Efficiency and Narrow Size Distribution. Chemistry of Materials, 2007. 19(3): p. 359-365.

[20]. Mandal, A., et al., Optical and Dynamic Properties of Water-Soluble Highly Luminescent CdTe Quantum Dots. Journal of Physical Chemistry B, 2007. 111(44): p. 12765-12771.

[21]. Murray, C.B., D.J. Norris, and M.G. Bawendi, Synthesis and Characterization of Nearly Monodisperse CdE (E = sulfur, selenium, tellurium) Semiconductor Nanocrystallites. J. Am. Chem. Soc., 1993. 115(19): p. 8706-8715.

[22]. Peng, Z.A. and X. Peng, Formation of High-Quality CdTe, CdSe, and CdS Nanocrystals Using CdO as Precursor. J Am Chem Soc, 2001. 123(1): p. 183-184.

[23]. Qu, L., Z.A. Peng, and X. Peng, Alternative Routes toward High Quality CdSe Nanocrystals. Nano Letters, 2001. 1(6): p. 333-337.

[24]. Qu, L. and X. Peng, Control of photoluminescence properties of CdSe nanocrystals in growth. J Am Chem Soc, 2002. 124(9): p. 2049-55.

[25]. Gaponik, N., et al., Efficient Phase Transfer of Luminescent Thiol-Capped Nanocrystals: From Water to Nonpolar Organic Solvents. Nano Letters, 2002. 2(8): p. 803-806.

[26]. Emin, S., et al., Photostability of Water-dispersible CdTe Quantum Dots: Capping Ligands and Oxygen. Chemistry Letters, 2010. 39(6): p. 654-656.

[27]. Jasieniak, J. and P. Mulvaney, From Cd-Rich to Se-Rich - the Manipulation of CdSe Nanocrystal Surface Stoichiometry. Journal of the American Chemical Society, 2007. 129(10): p. 2841-2848.

[28]. Zheng, F., et al., Synthesis of highly stable dihydrolipoic acid capped water-soluble CdTe nanocrystals. Nanotechnology, 2008. 19(23): p. 235603.

[29]. Yu, W.W., et al., Experimental Determination of the Extinction Coefficient of CdTe, CdSe, and CdS Nanocrystals. Chemistry of Materials, 2003. 15(14): p. 2854-2860.

[30]. Maege, I., et al., Self-assembling adhesion promoters for corrosion resistant metal polymer interfaces. Progress in Organic Coatings, 1997. 34(14): p. 1-12.

[31]. Yu, W.W. and X. Peng, Formation of high-quality CdS and other II-VI semiconductor nanocrystals in noncoordinating solvents: tunable reactivity of monomers. Angew. Chem. Int. Ed., 2002. 41(13): p. 2368-71.

[32]. Max, J.-J. and C. Chapados, Infrared Spectroscopy of Aqueous Carboxylic Acids: Comparison between Different Acids and Their Salts. J. Phys. Chem. A, 2004. 108(16): p. 3324-3337.

[33]. Sadhu, S. and A. Patra, Lattice Strain Controls the Carrier Relaxation Dynamics in $Cd_xZn_{1-x}S$ Alloy Quantum Dots. The Journal of Physical Chemistry C, 2012. 116(28): p. 15167-15173.

[34]. Wu, F., et al., Radiative and nonradiative lifetimes of band edge states and deep trap states of CdS nanoparticles determined by time-correlated single photon counting. Chemical Physics Letters, 2000. 330(34): p. 237-242.

[35]. Wu, X.C., A.M. Bittner, and K. Kern, Synthesis, Photoluminescence, and Adsorption of CdS/Dendrimer Nanocomposites. The Journal of Physical Chemistry B, 2005. 109(1): p. 230-239.

[36]. Puzder, A., et al., The Effect of Organic Ligand Binding on the Growth of CdSe Nanoparticles Probed by Ab Initio Calculations. Nano Letters, 2004. 4(12): p. 2361-2365.

[37]. Gomes, R., et al., Binding of Phosphonic Acids to CdSe Quantum Dots: A Solution NMR Study. The Journal of Physical Chemistry Letters, 2011. 2(3): p. 145-152.

[38]. Yu, W.W., Y.A. Wang, and X. Peng, Formation and Stability of Size-, Shape-, and Structure-Controlled CdTe Nanocrystals: Ligand Effects on Monomers and Nanocrystals. Chemistry of Materials, 2003. 15(22): p. 4300-4308.

[39]. Katari, J.E.B., V.L. Colvin, and A.P. Alivisatos, X-Ray Photoelectron Spectroscopy of CdSe Nanocrystals with Applications to Studies of the Nanocrystal Surface. J. Phys. Chem, 1994. 98: p. 4109-4117.

[40]. Sandblom, N., T. Ziegler, and T. Chivers, A density functional study of the bonding in tertiary phosphine chalcogenides and related molecules. Canadian Journal of Chemistry, 1996. 74(11): p. 2363-2371.

[41]. Klimov, V.I., et al., Mechanisms for intraband energy relaxation in semiconductor quantum dots: The role of electron-hole interactions. Physical Review B, 2000. 61(20): p. 13349-13352.

[42]. Guyot-Sionnest, P., B. Wehrenberg, and D. Yu, Intraband relaxation in CdSe nanocrystals and the strong influence of the surface ligands. The Journal of Chemical Physics, 2005. 123(7): p. 074709.

[43]. Cooney, R.R., et al., Unified picture of electron and hole relaxation pathways in semiconductor quantum dots. Physical Review B, 2007. 75(24): p. 245311.

[44]. Kilina, S.V., D.S. Kilin, and O.V. Prezhdo, Breaking the Phonon Bottleneck in PbSe and CdSe Quantum Dots: Time-Domain Density Functional Theory of Charge Carrier Relaxation. ACS Nano, 2009. 3(1): p. 93-99.

[45]. Yan, Y., G. Chen, and P.G. Van Patten, Ultrafast Exciton Dynamics in CdTe Nanocrystals and Core/Shell CdTe/CdS Nanocrystals. The Journal of Physical Chemistry C, 2011. 115(46): p. 22717-22728.

[46]. Kaniyankandy, S., et al., Charge carrier dynamics in thiol capped CdTe quantum dots. Physical Chemistry Chemical Physics, 2010. 12(16): p. 4210-4216.

[47]. Breus, V.V., C.D. Heyes, and G.U. Nienhaus, Quenching of CdSe-ZnS Core-Shell Quantum Dot Luminescence by Water-Soluble Thiolated Ligands. Journal of Physical Chemistry C, 2007. 111(50): p. 18589-18594.

[48]. Xu, S., C. Wang, and Y. Cui, Influence of solvent on aqueous CdTe nanocrystals: Theoretical and experimental investigation. Journal of Molecular Structure, 2012. 1010(0): p. 26-31.

[49]. Chen, Y., et al., "Giant" Multishell CdSe Nanocrystal Quantum Dots with Suppressed Blinking. Journal of the American Chemical Society, 2008. 130(15): p. 5026-5027.

[50]. Mahler, B., et al., Towards Non-Blinking Colloidal Quantum Dots. Nature Materials, 2008. 7(8): p. 659-664.

[51]. Heyes, C.D., et al., Effect of the Shell on Blinking Statistics in Single Core-Shell Quantum Dots - A Single Particle Fluorescence Study. Phys Rev B, 2007. 75: p. 125431.

[52]. Zhang, H., et al., The Influence of Carboxyl Groups on the Photoluminescence of Mercaptocarboxylic Acid-Stabilized CdTe Nanoparticles. The Journal of Physical Chemistry B, 2003. 107(1): p. 8-13.

[53]. Gao, X., W.C. Chan, and S. Nie, Quantum-dot Nanocrystals for Ultrasensitive Biological Labeling and Multicolor Optical Encoding. J Biomed Opt, 2002. 7(4): p. 532-537.

[54]. Durisic, N., et al., Probing the "Dark" Fraction of Core-Shell Quantum Dots by Ensemble and Single Particle pH-Dependent Spectroscopy. ACS Nano, 2011. 5(11): p. 9062-9073.

[55]. Durisic, N., et al., A Common Mechanism Underlies the Dark Fraction Formation and Fluorescence Blinking of Quantum Dots. ACSNano, 2009. 3: p. 1167-1175.

2.8. Appendix 1

UNIVERSITY OF ARKANSAS

J. William Fulbright College of Arts and Sciences
Chemistry and Biochemistry

To whomever it may concern

This is to certify that Benard Omogo is the first author of the paper mentioned below and has contributed about 75% of the work reported in this paper

Benard Omogo, Jose F. Aldana, and Colin D. Heyes. Radiative and Nonradiative Lifetime Engineering of Quantum Dots in Multiple Solvents by Surface Atom Stoichiometry and Ligands J. Phys. Chem. C, (2013) **117,** 2317–2327.

Colin D. Heyes

Major Advisor

CHEM 119 • 1 University of Arkansas • Fayetteville, AR 72701-1201 • 479-575-4601 • Fax: 479-575-4049 • http://chemistry.uark.edu/

2.9. Appendix 2

6/9/2014 Rightslink® by Copyright Clearance Center

Copyright Clearance Center RightsLink®

Home | Create Account | Help

ACS Publications

Title: Radiative and Nonradiative Lifetime Engineering of Quantum Dots in Multiple Solvents by Surface Atom Stoichiometry and Ligands

Author: Benard Omogo, Jose F. Aldana, and Colin D. Heyes

Publication: The Journal of Physical Chemistry C

Publisher: American Chemical Society

Date: Feb 1, 2013

Copyright © 2013, American Chemical Society

User ID:

Password:

Enable Auto Login

LOGIN

Forgot Password/User ID?

If you're a copyright.com user, you can login to RightsLink using your copyright.com credentials. Already a RightsLink user or want to learn more?

PERMISSION/LICENSE IS GRANTED FOR YOUR ORDER AT NO CHARGE

This type of permission/license, instead of the standard Terms & Conditions, is sent to you because no fee is being charged for your order. Please note the following:

- Permission is granted for your request in both print and electronic formats, and translations.
- If figures and/or tables were requested, they may be adapted or used in part.
- Please print this page for your records and send a copy of it to your publisher/graduate school.
- Appropriate credit for the requested material should be given as follows: "Reprinted (adapted) with permission from (COMPLETE REFERENCE CITATION). Copyright (YEAR) American Chemical Society." Insert appropriate information in place of the capitalized words.
- One-time permission is granted only for the use specified in your request. No additional uses are granted (such as derivative works or other editions). For any other uses, please submit a new request.

BACK | CLOSE WINDOW

Copyright © 2014 Copyright Clearance Center, Inc. All Rights Reserved. Privacy statement.
Comments? We would like to hear from you. E-mail us at customercare@copyright.com

https://s100.copyright.com/AppDispatchServlet 1/1

Chapter 3. How the Quality of the CdSe Core affects the Optical Properties of CdSe/CdS Core/Shell Quantum Dots

Benard Omogo and Colin D. Heyes*

Department of Chemistry and Biochemistry, University of Arkansas, Fayetteville, Arkansas 72701, USA

* To whom correspondence should be addressed: cheyes@uark.edu

3.1. Abstract

CdSe/CdS core/shell quantum dots with various optical and structural properties have been reported. Starting with a known quality of CdSe core obtained by varying the ratio of the coordinating ligands, and using both thermal cycling and successive ion layer adsorption and reaction method (SILAR) in shelling, we monitored the shell growth up to 8 monolayer (ML) for each set of the samples. The sample sets comprised of quantum dots core with different photoluminescence quantum yields (PL QY) ranging from 4- 50 % with their respective core/shells. Apart from the prominent absorbance spectral redshift, the shell growth was further proved by the TEM images and ligand exchange results. Surprisingly, the low quality core samples exhibited the general CdSe/CdS shelling trend as reported in most of the literature while the higher PL QY showed a reverse trend whereby the initial shell thickness reduced the PL QYs before increasing but not exceeding that of the core. The quality, crystallinity and wurtzite structure of these particles were verified by both HRTEM and XRD. Furthermore, radiative and nonradiative rates revealed that nonradiative recombination pathways are more responsible for the observed trends in PL QY. These results highlights the need for a specific choice of core material quality while performing core/shell synthesis.

3.2. Introduction

In less than six decades, studies in nanostructure fabrication and synthesis have received tremendous advances, particularly in the area semiconductor nanocrystals. The increasing interest in these materials are motivated by their promising applications in lasers,[1] photovoltaic devices[2] and biomedicine.[3, 4] Due to the size-tunable optical properties across the visible region, CdSe nanocrystals have become the most popular. Besides controlling their size distribution [5, 6] a lot of progress has been made on controlling their fluorescence brightness,[6, 7] and photostability.[8]

Previously, by controlling the ratios of precursors and ligands, Peng et al [9] reported that using precursor amounts with a low Cd:Se ratio of 1:10 gave the highest PL quantum yiled (QY), above 70% with flat (broad) PL bright points while 1:1 resulted in QDs with about 40% QY and sharp PL bright points. Furthermore, a combination of primary amines such as octadecylamine (ODA) and tri-octylphosphine oxide (TOPO) are known to enhance the PL QY and control the crystal structure of these nanocrystals.[9] This has been attributed to the closer packing of the long chain primary amines together with the high boiling point of TOPO resulting in highly passivated particles that have annealed to high crystallinity at high temperature.[10]

However, passivating both anionic and cationic surface sites completely by organic ligands is difficult, and thus dangling bonds will remain on the surface to some extent, resulting in trap sites for the excitonic charge carriers.[11] In order to passivate these trap sites, a higher band gap shell material is required. For instance ZnSe, [12] CdS, [13-16] ZnS[17-21]and alloyed $Cd_xZn_{(1-x)}S$[11] are the most commonly used shelling materials for CdSe cores. Due to the higher band gap of these shell materials compared to CdSe core, the excitons are confined to the CdSe core and away from the surface trap sites, reducing the non-radiative pathways and hence show improved optical

properties. Besides confinement, the lattice mismatch of the shell material plays a significant role in achieving highly crystalline core/shell materials. In fact, CdSe-cores with CdS-shells that have a small lattice mismatch of 3.9% were shown to favor epitaxial growth and result in extremely high crystallinity in the resulting core/shell quantum dots.[9, 11, 22] On the other hand, CdSe core with thin ZnS shell result in high PL QY due to better confinement by the larger band offset although they show high lattice mismatch and are bad for thicker shells. Therefore, both band gap and lattice mismatch considerations in core/shell synthesis can be utilized to offer several benefits such as improved PL QY[19, 21, 23-25] reduced fluorescence lifetimes,[19]and stability against chemical degradation or photo-oxidation.[8]

Except for one study that compared shelling of CdS on amine or TOPO coated CdSe cores,[15] the majority of shelling reports have been performed on low quantum yields cores,[5, 17, 18, 21] probably to highlight how shelling significantly improves the fluorescence properties of the quantum dots. More recently, this line of research is focusing on proper selection of shell precursors control the structure of the core/shell quantum dots. For example, thin shell quantum dots with almost unity PL QYs were recently reported.[22] Here, the high crystallinity and uniformity, narrow emission linewidth and suppressed blinking of the nanocrystals observed were attributed to the optimal condition provided by the slow shell precursor infusion and relatively low reactivity of the octanethiol which acted as both source of sulfur and ligand. The source of Cd in this experiment was cadmium (II) oleate. Contrary to the expected trend when shelling a core with a higher band-gap material, an initial drop in PL QY with shell growth observed was attributed to the quenching by the octanethiol. Also, high-quality CdSe/CdS core/shell nanocrystals with either zinc blend or wurtzite structure using single-source precursor cadmium diethyldithiocarbamate ($Cd(DDTC)_2$) have been reported.[5] The key here was to reduce the reaction temperature by

applying primary amines as activation reagents and the use of dynamic ligands. As with the general trend of reports, the PL QY of the starting core used here was also very low, below 5 %, before increasing to over 80% with shell growth.

The general assumption in the literature is that a high quality core is very helpful for the growth of the core/shell structures.[8] The only contradictory study, to the best of our knowledge, was just recently published,[7], and is quite consistent with the results described later in this chapter. Taking CdSe cores with varying PL QYs, the correlation between the number of defective cores (as evidenced by high resolution TEM) and their PL QYs was found to be counterintuitive. In other words, high quality cores with little-to-no surface defects surprisingly resulted in low PL QY core/shell particles, while cores with more surface defects resulted in higher PL QY core/shells. To obtain varying quality of the starting cores, the concentrations and ratios of the surface ligands were varied, as well as changing the identity of the amine in some preparations. Higher quality cores were achieved by minimizing surface trap states, while lower quality cores were achieved by reducing the number of ligands on the surface of nanocrystals thereby availing traps states, translating to an observed decrease in average fluorescence lifetime.[7] In that study a relatively narrow range of core QYs were synthesized, varying only from 4-16%, in addition to having to change the identity of the amine ligand from oleylamine to octadecylamine (ODA) to obtain cores over 8%, which made a direct comparison of the low QY and high QY cores difficult.

In this study, we report on the effects of shelling 3.5 nm CdSe cores of different PL QYs and, using SILAR[15] and thermo-cycling [26, 27] methods, we grow epitaxial shell thickness up to ~5.5 nm. Contrary to the aforementioned study,[7] we varied the quality of our cores by only varying the ratio of ODA to TOPO and not the identity, as well as maintaining the overall ligand concentration. Apart from varying the ligands ratio above, set 2 was obtained by simply

performing the reaction without degassing the solvents and precursors (table 2.1) as perfumed for all other sets. As expected, our highest PL QYs of the CdSe cores were observed with higher ratios of ODA to TOPO, and reached much higher QYs than in the previous study.[6] While our low QY particles showed a similar trend to the previous study of increasing QY upon shelling with CdS followed by a decrease as the shell becomes thicker[6] our high QY showed a *decrease* in QY for thin CdS shells before increasing for moderately thick CdS shells. The resulting core/shell nanocrystals were then compared to the original cores for their ability to[6] show fluorescence after their transfer into water. Our observations agree with this recent study[6] which contradicts the common belief that high quality cores are necessary for superior core/shell properties but extends the study to very high QYs cores. This allowed us to postulate that the shell can actually introduce interfacial defects at the core/shell interface if the core quality is *too high* that strongly decreases the average radiative decay rate, but that these defects recover as the shell grows to moderate thickness. These results provide further criteria to consider when preforming shelling of core QDs.

3.3. Experimental Section

3.3.1. Chemicals. Cadmium oxide (CdO, 90%, Sigma-Aldrich), selenium powder (Se, 99.99%, Alfa Aesar), zinc oxide (ZnO, 99%, Sigma-Aldrich), sulfur powder (S, 99.9%, Alfa Aesar), oleic acid (OA, tech. grade, Alfa Aesar), 1-octadecene (ODE, 90%, Alfa Aesar), octadecylamine (ODA, 95%, Acros Organics), tri-butylphosphine (TBP, 95%, Alfa Aesar) 5-carboxytetramethylrhodamine dye (5-CTMR dye, Invitrogen), and tri-octylphosphine oxide (TOPO, Sigma-Aldrich) were used as purchased without further purification. Solvents: methanol, hexane, and acetone were of pure grade and were all bought from VWR international.

3.3.2. CdSe core Synthesis. CdSe core samples were synthesized by modification of the literature methods.[28, 29] Briefly, 0.04 M cadmium (Cd) precursor was prepared by degassing under vacuum and then heating a mixture of 0.02565 g of CdO, 0.4452 g OA and 2 g ODE to 200^{o}C under argon flow until the solution became clear. The temperature was then reduced to 50^{o}C at which a calculated amount of ODA and TOPO, depending on the required ratio, was added, degassed if needed and heated to 300^{o}C under argon flow. At this temperature, a pre-made solution of 0.04 M Se precursor (0.01579 g Se, 0.4653 g TBP and 1.37 g ODE) was swiftly injected and after a few seconds, the heating mantle was removed to stop the growth of the particles at a desired size. The solution was then allowed to cool to room temperature, and then purified by dissolving in approximately equal amounts of hexane and methanol. The mixture was centrifuged at 4000 rpm for about 5 min. The process was repeated 3 times or more depending on the purity of the sample and the final purified hexane solution was kept in a refrigerator at 4^{o}C until the the shelling process was performed.

3.3.3. CdSe/ CdSe core/shell synthesis. The shelling process was performed using a combination of thermal cycling[26, 27]and successive ion layer adsorption and reaction (SILAR) methods.[15] Typically, 0.04 M Cd precursors were prepared in the same way as for the core synthesis while 0.04 M S precursor followed the same method as that of Se in the core, both described above. The starting CdSe core solution for the shelling process was prepared by mixing 2 mL of CdSe of known concentration as estimated from the UV-vis absorption spectra, 1 g ODA and 2 mL ODE in the reaction flask. Pre-calculated amounts of S and Cd precursors, enough for the growth of a single monolayer (ML) were injected individually at the lower temperature of 180^{o}C, and allowed to equilibrate for 5 min each before raising the temperature to 210^{o}C for an additional 20 min for the growth of a CdS shell. The S precursor was always injected first. Approximately, 1 mL aliquots

were taken out and dissolved in hexane for optical measurements prior to lowering the temperature for subsequent injection. In total, 8 cycles of S and Cd precursor injections were carried out before stopping the reaction.

3.3.4. Ligand exchange. Ligand exchange followed our earlier reports.[30, 31] Briefly, to each sample, an equal amount of methanol was added to the hexane quantum dots solution, agitated and then centrifuged at 4000 rpm for 5 minutes. The colorless bottom layer was discarded and more methanol added. This process was repeated 3 times followed by extraction using acetone at 7000 rpm for 20 minutes. The pellets were then added in a ligand solution consisting of 200μL MPA in 10 mL of methanol adjusted to pH ~10.5 with tetramethylammonium hydroxide (TMAH),Upon addition of the ligand solution to the pellet, the mixture was sonicated and placed in a three-neck round-bottom flask under argon and refluxed for 3h at ~68 °C. After reflux, the heating mantle was removed, and the solution was allowed to cool to room temperature. To obtain the MPA-QDs in water, a 2 mL aliquot of the MPA quantum dots in methanol was precipitated by addition of diethyl ether and centrifuged for ~15 min until a pellet was obtained. The liquid was decanted and the vial was inverted and lightly tapped to remove any remaining liquid. Following this, 2 mL of 18 MΩ Millipore water was added. The MPA-exchanged nanocrystals readily dissolved in the water.

3.4. Instrumentation and measurements

3.4.1. Optical Measurements. UV- Vis and Photoluminescence (PL) spectra were measured using Hitachi U-3900H spectrophotometer and Perkin Elmer LS 55 luminescence spectrometer, respectively. The samples for PL measurements were excited at 500 nm, the wavelength at which their absorbances were normalized to 0.05 optical densities. PL percentage quantum yields (PL QYs) were measured by comparing the integrated area of each sample spectra to that of 5-CTMR dye dissolved in methanol to the same OD. Average fluorescence lifetime measurements were obtained using our previous procedure.[31] Briefly, they were taken using MicroTime 200 confocal fluorescence lifetime microscope (PicoQuant, GmbH, Berlin, Germany) equipped with PicoHarp 300 TCSPC controller. The samples were excited by 485 nm picosecond DPSS laser (LDH-P-C-485,Picoquant), controlled by the Sepia II software with a 8 MHz repetition rate. Fluorescence filters (580/60 and 605/55, Chroma, chosen depending on the emission wavelength of the samples) were placed in front of Single Photon Avalanche Diode Detector (SPAD, MPI, Microphotonic devices, Bolano, Italy) to reject background fluorescence and scattered laser light.

3.4.2. Transmission Electron Microscopy. Both transmission electron microscope (TEM) and high resolution-transmission electron microscope (HR-TEM) images were taken in Tecnai G2 TF20 transmission electron microscope (FEI) with acceleration voltage of 200kV using ultrathin carbon film on 400 mesh copper grids as the substrate.

3.4.3. Powder X-ray Diffraction (XRD). XRD patterns were obtained using Rigaku, MiniFlexII x-ray diffractometer operating at 30kV and 15 mA using Cu Kα radiation. Samples were purified by 3 cycles of centrifugation as explained above followed by precipitation using acetone. The pellets were then applied onto a glass slide and allowed to air dry before measurement.

3.5. Results and discussion

The five sample sets as presented here were basically synthesized by maintaining similar reaction conditions but varying the ligand ratio, specifically the ratio of ODA to TOPO except for set 2 where purging was not performed. The resulting core samples with varying PL QY are shown table 3.1. By decreasing the ratio and maintaining the total concentration of these ligands, we gradually decreased the percentage PL QY from 52 to 9 %. The advantages of using TOPO and ODA as ligands in quantum dots synthesis had been elaborated by several groups [9, 10, 32] Apart from high boiling points and solubility in organic solvents which is facilitated by their long alkyl chains, they are also responsible for the passivation of the electronic surface sites, therefore, minimizing non-radiative charge carrier recombination.[10]

Comparing the effect of different ligands on CdSe core, Ning et al[32] concluded that both the ligands are suitable for passivation the electron trap sites, however, TOPO having a relatively closer HOMO energy to that of CdSe valence band, lowers the PL QY by extracting the hole, therefore, reducing the degree of overlap between the hole and electron wave functions. On the other hand, ODA, being a primary amine, has been shown to yield high PL QYs CdSe quantum dots with nearly perfect wurtzite structure.[9] Our results here, were therefore modeled to control the surface trap states by either passivating most of the electron trap sites using more ODA to give higher PL QYs or using more TOPO by reducing the extent of exciton wave function overlap and yield low PL QY samples.

Table 3.1: Reaction conditions explored in synthesizing various CdSe core samples used in this experiments and respective results

Sample	ODA:TOPO[a]	Purging	PL QY of core (%)[b]	λ_{max}(nm)[c]
Set 1	4:1	Yes	52	559
Set 2	4:1	No	42	560
Set 3	1.5:1	Yes	32	565
Set 4	1:2	Yes	18	552
Set 5	1:5	Yes	9	555

[a]Ratio of octadecylamine (ODA) to triocylphosphine oxide (TOPO). [b]Percentage Photoluminescence quantum yields used to classify the samples into various sets 1-5. [c]Absorbance λ_{max} of the cores.

Most recently, Saha et al[7] reported a similar trend in the PL QYs, however, in their case the surface defects were generated by reducing the number of total surface ligands therefore leaving more trap sites unpassivated. Absorption spectra of three of the sample sets are shown in figure 3.1(a-c). In each spectra, a steady redshift of the first exciton absorption peak was observed with increase in shell thickness as shown more clearly with the respective inset figures. Systematic with all samples, the extent of these redshift is larger with earlier shells and reduces as the shell thickness increases.(figure 3.2a) Furthermore, the absorption features corresponding to transitions at different electronic states other than the band edge were also eminent, especially below 470 nm for increasing CdS shell thicknesses. The redshift with increasing shell thickness is well discussed in the literature,[5-8, 20, 21, 27] and is generally attributed to the exciton delocalization into the shell material, and signifies shell growth as opposed to alloying.[5] The larger relative red shift with thin shells has been discussed before [28] and is attributed to extensive delocalization of an electron into the surrounding shell material which then diminishes as the shell becomes thicker. The full width at half maximum (FWHM) of all sample sets are given in figure 3.2b. Interestingly, there is a small but steady decrease as the shell thickness increases indicating monodisperity as consistent with the other previous reports [5, 6]

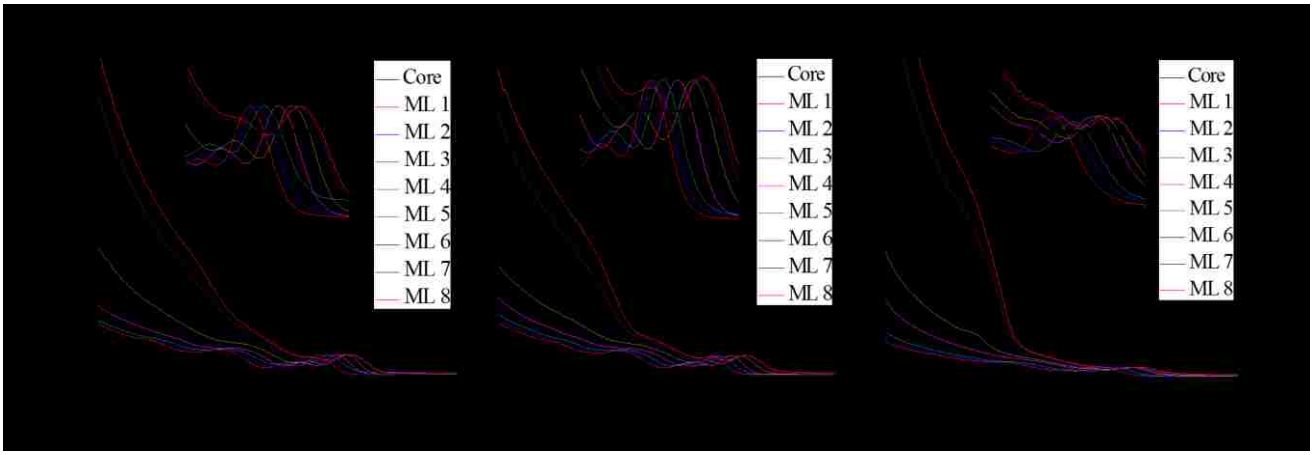

Figure 3.1. Absorbance spectra as a function of shell thickness (number of monolayers) for samples sets 1(A), 3(B) and 5(C). For each of these samples there is a steady redshift shown by the arrows depicting shell growth.

A comparative study[5] showed that the trend of FWHM for wurtzite structures, as are synthesized here (*vide infra*), may be unpredictable. The gradual decrease measured for our samples may imply that our shelling process gradually minimized the exciton separation, consistent with the observed decrease in the extent of redshift, as the monolayer number increases. The PL decay results of three samples sets 1, 3 and 5 cores are given in figure 3.3a showing the decrease of the average lifetime from higher quality sample set 1 to 3 followed by an increase for the set 5. Figure 3.2b shows the PL QY of all the sample sets as a function of monolayers of shell. As explained above, and shown in table 3.1, the number of different sets were assigned from the PL QYs of the cores where the higher PL QY sample is referred to as set 1 and the numbering goes down as the PL QYs decreases. Looking at sets 1, 2 and 3, with PL QYs of 52%, 42% and 32% respectively, there is a uniform initial decrease in PL QYs with shell thickness up to ML 3 followed by an increase to ML 5 before a final decrease. However, the extent of the increase after ML 3 depends on the original core QY, of which the increase in set 1 and 2 (the highest QY cores) did not go beyond that of the original core.

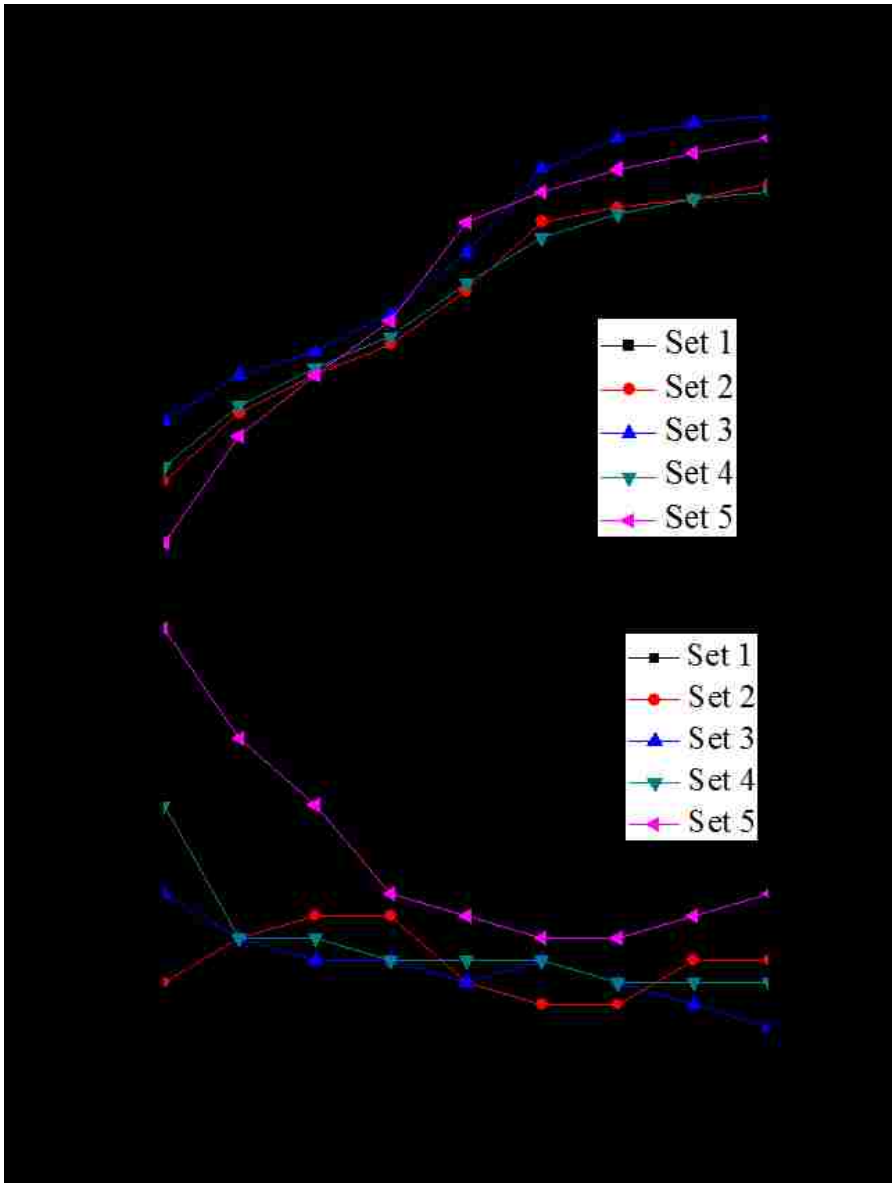

Figure 3.2. (A) Absorbance λ_{max} as a function of number of monolayers for the sample sets 1-5 illustrating the extent of redshift as the shell grows thicker. (B) Full width at half maximum (FWHM) as a function of the number of monolayers for the sample sets 1 – 5 showing a constant distribution in size before and after shelling.

On the other hand, the increase in set 3 slightly exceeded the original core before the final drop. In a systematic manner, set 4, with a PL QY of 18%, increased upon adding 1 ML of CdS then followed the same trend of decreasing with thicker shells. Finally, set 5 with the lowest PL QY of 9% showed an initial increase in PL QY as the shell thickness increases up to the bright point of 3 ML of shell, followed by a decrease, in agreement with normal expectations. It is worth mentioning here that sample sets 1-3 cores may be considered of high quality when the PL QY is compared to other CdSe cores in the literature [12, 33, 34] and also supported by high crystallinity as shown later by their TEM images and XRD. High PL QYs may be a consequence of surface defect-free quantum dots as recently reported.[7] Given that our synthesis protocol for these first three sets employed higher ODA than TOPO ratio as the main ligands to passivate the electron trap sites, we may relate these high PL QY values to the reduced nonradiative recombination pathways on the surface of the quantum dots. Most often, shelling is carried out on low PL QY cores and is known to significantly improve the quality of the quantum dots. Recently, the only group that did a quantitative study in this area[7] observed the same trend by growing relatively thicker shell on a high PL QY cores. Their observations concurred with the ones reported here that starting with poor PL QY cores is more suited for obtaining high quality core/shell quantum dots, contrary to the general intuitive belief.

The average lifetime for each sample (figure 3.3c) was obtained by fitting to a given number of exponential until the residuals showed a straight line and the chi-squared value is minimized as we reported earlier.[31] For almost all of our samples the fitting met the above criteria after 3 exponential fit from which the average fluorescence lifetimes values were derived. The general trend observed with all the samples was that the average decay lifetime (τ_{Fl}) gradually decreased as the shell thickness increased (figure 3.3c).

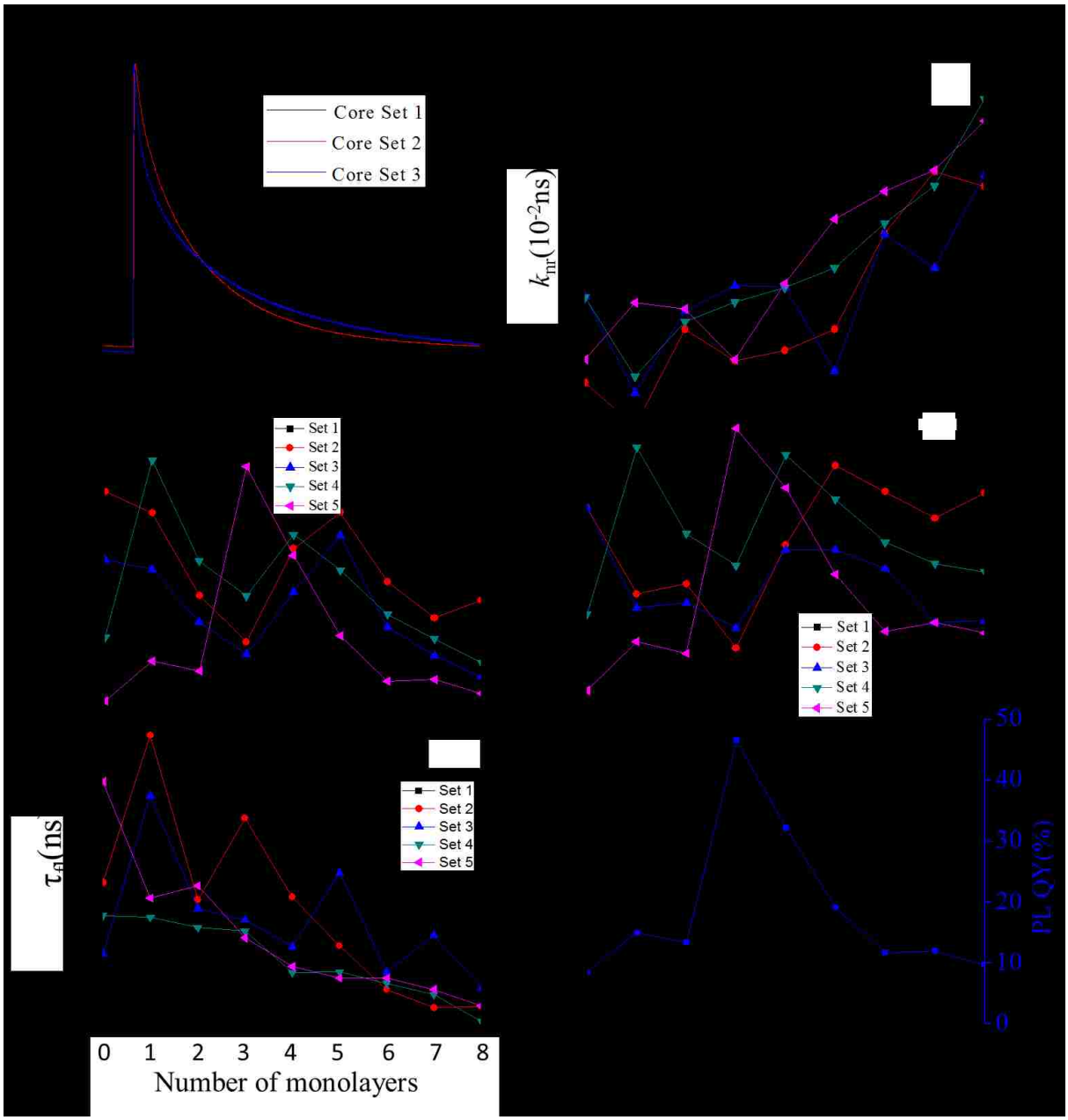

Figure 3.3. (A) Photoluminescence decay spectra of sample sets 1, 3 and 5 showing a multi-exponential decay kinetics. (B) Photoluminescence quantum yields (PL QY) as a function of increasing number monolayer for all the sample sets 1 -5. (C) Average fluorescence lifetime for all the sample sets 1-5 demonstrating a steady decrease with increasing number of monolayers. (D) and (E) Nonradiative and radiative rates, respectively calculated from equation 2.2 and 2.3 using the values from figures 3.3 (B) and (C). (F) An overly of sample set 5 from figure 3.3(B) and 3.3 (E) to illustrate the similar trend.

This may be attributed to an increase in either or both the radiative and nonradiative rates. Furthermore, the average fluorescence lifetimes of sets 2 and 3 each showed an increase in average lifetime after ML 1 followed by a decrease to ML 8 while sets 1, 4 and 5 show gradual decrease from ML 1 to Ml 8. In order to investigate in detail the processes responsible for the calculated PL QYs and the average lifetimes, we separated the nonradiative (k_{nr}) and radiative (k_r) rates using the equations 2.2 and 2.3 (chapter 2) and plotted them in figures 3.3d and e respectively. The k_r of all the samples (figure 3.3 e) follows closely the PL QYs trend (figure 3.3b) suggesting that k_r is the primary process controlling the PL QY rather than k_{nr} as is expected for interfacial defects in core/shell systems. This is further illustrated (figure 3.3f) by overlaying the k_r and PL QY of sample set 5 to highlight this similarity in trend. It is known that shelling passivates the surface trap sites hence eliminating the nonradiative recombination pathways consequently, improving the PL QYs and the overall quality of the QDs.[5-7] The small lattice mismatch of 3.9% at the interface between CdSe and CdS especially for thin shell quantum dots is known to promote high crystalline growth. [6] However, for the results reported herein, we observed that the PL QYs for the sets 1-3 with high initial core quality decreases with increase in shell thickness contrary to the expectation. A similar observation that Saha et al[7] recently referred to as counterintuitive behavior.

The initial decrease in PL QYs while the k_{nr} increases with shell thickness for the high quality samples sets 1-3, may be related to some rearrangements of both incoming and present atoms and ligands at the surface which is already been highly passivated hence generating trap sites that increases the nonradiative pathways. But as the intermediate shelling process continues, these generated pathways are gradually eliminated resulting into the observed subsequent increase in both PL QYs even though the high crystallinity is not easily recovered. For the case of the low

quality samples sets 4 and 5, however, the initially shelling process passivates the available trap sites thus increasing the observed PL QYs. As the shell becomes thicker in all the sets, some defects due to the small lattice mismatch emanates between the core and the shell which lowers the PL QYs but not strong enough to distort the crystallinity of the final core/shell sample. This argument however, may need to be investigated further.

To verify the quality of the samples as shown by the PL QYs, TEM images and high resolution TEM images were taken as shown in figure 3.4a. For each set, the core and ML 8 sample is shown highlighting the overall increase in size with shell thickness. Furthermore, the average diameter and narrow size distribution is clearly visible across all the sample sets. The The measured diameters of set 1 core and the core/shells after the last injection are 3.6±0.5 nm and 8.7±1.2 nm, respectively, while that of set 5 are 3.8±0.5 nm and 8.7±1.5 nm, respectively. Since these values agree with the calculated monolayer injections, we are to refer to the last monolayer as ML 8.

The measured size histograms are plotted in figure 3.4b, however, show that shelling slightly increased the size distribution of these samples in contrast to the narrower FWHM discussed earlier, suggesting that the narrower FWHM is not the result of size distribution, as often assumed, but due to electronic effects. As the shell becomes thicker, the exciton separation is minimized which leads to a lower FWHM, even though the size distribution may increase. Interestingly, the respective HRTEM images inset in in each TEM image sample confirms the observed trend whereby the high quality cores results into poor quality core/shell quantum dots, while the low quality cores results in higher core/shell quality. The crystallinity of sets 1-3 cores show high crystallinity, consistent with their high PL QYs values, but worsens after shell growth. On the other hand, the crystallinity of sets 4 and 5 cores which are poor at the beginning, improved significantly after shell growth.

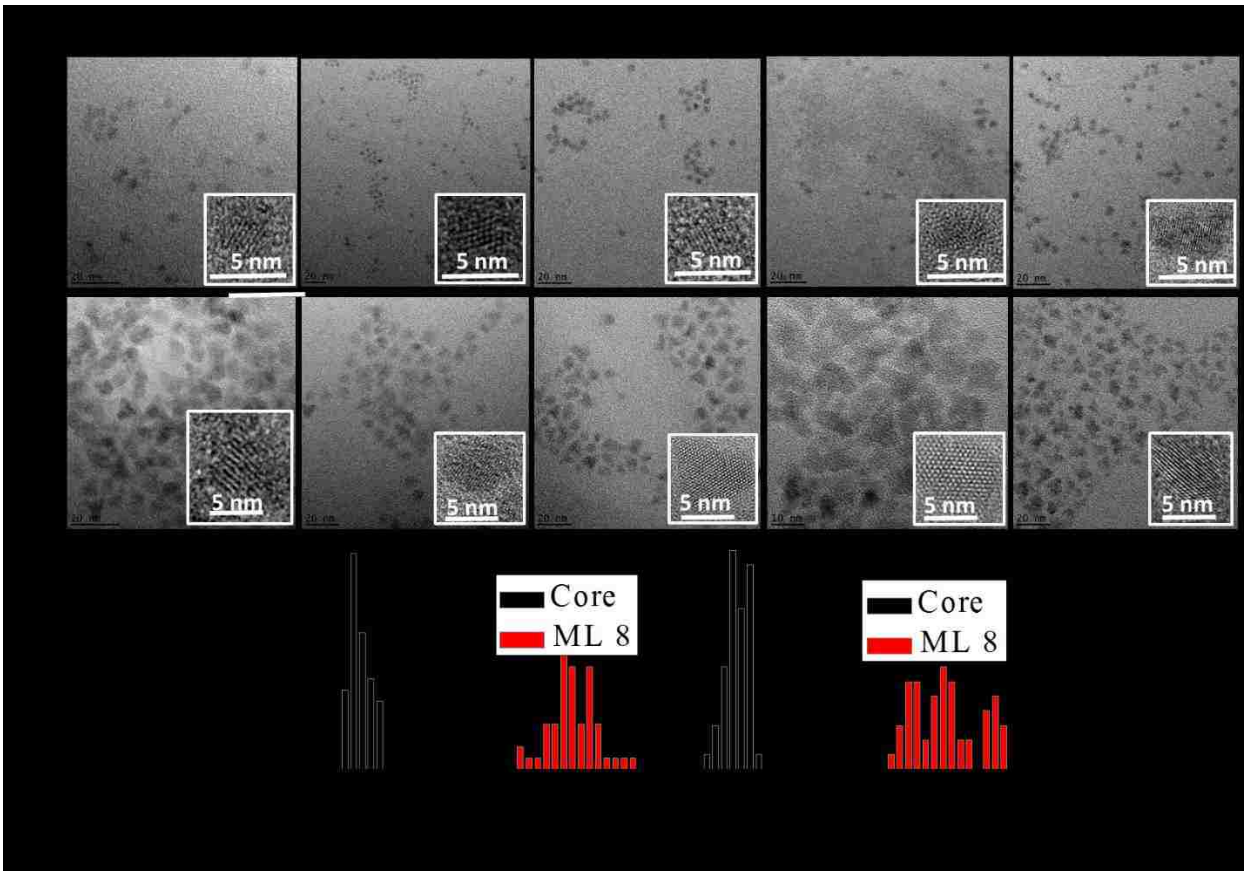

Figure 3.4. (A) TEM images of CdSe core and corresponding CdSe/8ML CdS core/shell quantum dots for all the sample sets 1- 5. Inset is the respective HRTEM image of each sample revealing high crystallinity of the samples. (B) Size distribution histograms of sets 1 and 5 for both core and ML 8 core/shells, showing the average diameter and size dispersity of the quantum dots.

Several groups [5, 35] have shown that CdSe quantum dots with zinc blende structures exhibit superior quality with high PL QYs than their wurtzite counterparts. We therefore performed XRD measurements on the two samples showing the largest PL QY difference, Set 1 core with highest PL QY and high crystallinity and set 5 with lower PL QY as shown in figure 3.5, to investigate whether high quality samples were the result of zinc blende rather than wurtzite sturecture. The results, however, revealed that both our samples exhibit wurtzite structures, highlighting that the reason for the QY difference was due to core crystallinity and/or surface trap states.

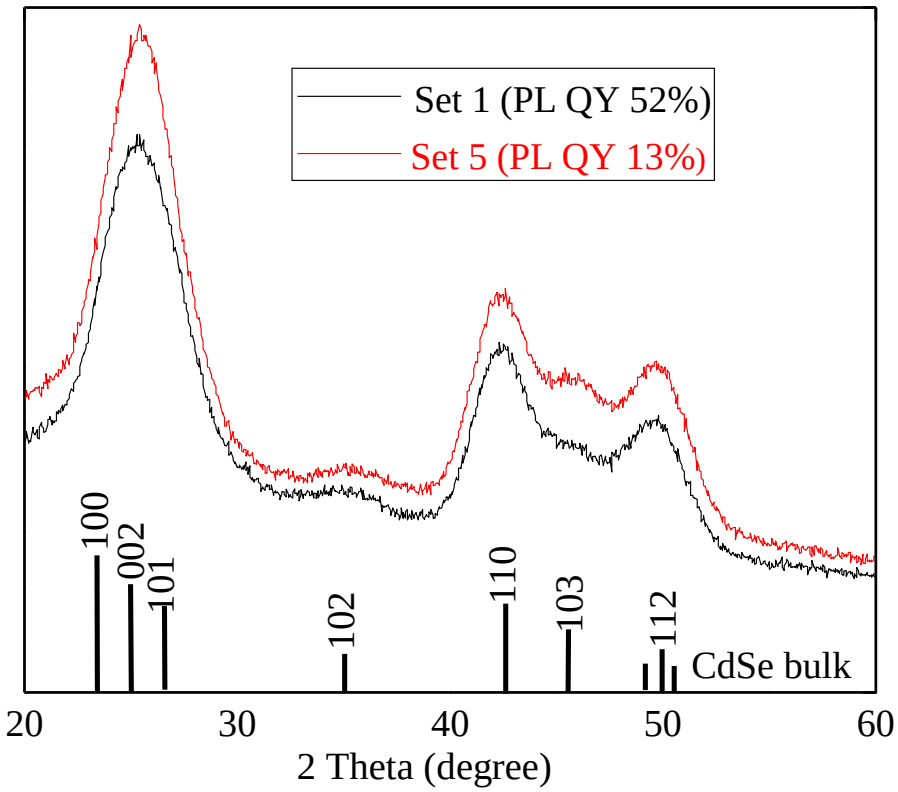

Figure 3.5. X-ray powder diffraction pattern measured from the CdSe core of the samples sets 1 and sample with PL QY 13.The diffraction peak patterns corresponds to those of wurtzite bulk CdSe showing that both the samples sets exhibit wurtzite structures.

It would have been surprising to see zinc blende even with our highest PL QY sample, given that the method used for synthesis is known to provide wurtzite structures, but the cores synthesized here are among some of the highest QYs reported for this method, so it was necessary to verify this assumption.

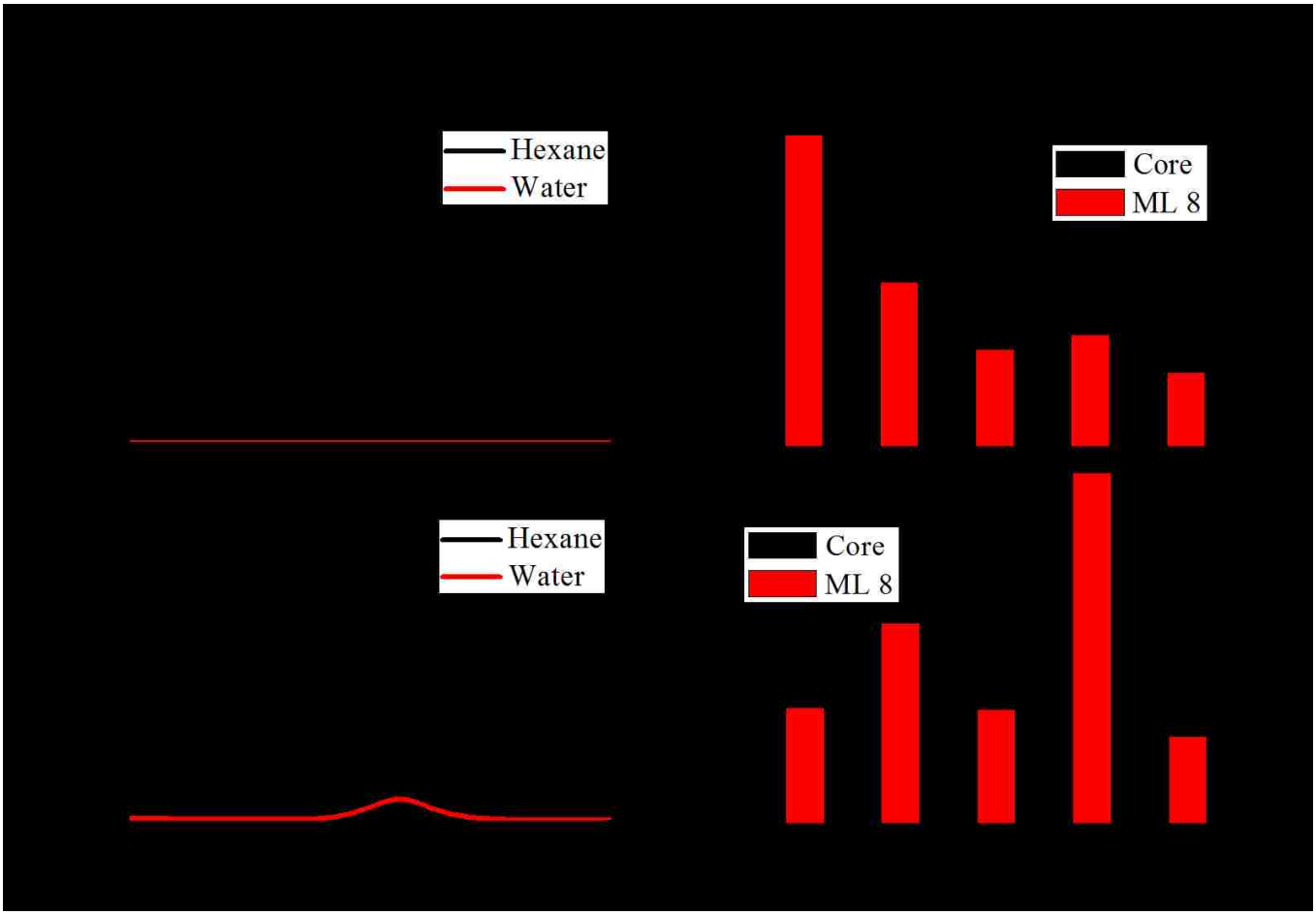

Figure 3.6. (A and B) Photoluminescence spectra of the sample set 3 for both the core and ML 8, respectively, before (hexane) and after ligand exchange (water). Photoluminescence quantum yields histograms before (C) and after ligand exchange using 3-mercaptopropionic acid (MPA) (D) for the sample sets 1- 5. There is a complete quenching of the core samples after ligand exchange compared to their ML 8 counterparts.

Most of the groups that have reported zinc blende CdSe cores [5, 35] have employed specific synthetic strategy either by utilizing appropriate ligands or temperatures. Besides the distinct diffraction peak positions corresponding to the wurtzite planes as shown by the XRD spectra, their resolution and intensity further confirmed on the quality of the samples.

In order to verify the effects of phase transfer on PL QYs or core and core/shell CdSe/CdS QDs, we performed ligand exchange and subsequent dissolution in water using 3-mercaptopropionic acid on both cores and ML 8 samples as shown in figure 3.6. Figures 3.6a and b, shows the PL spectra of the core and ML 8, respectively, for the sample set 3. Complete quenching of the core was observed, as seen before[11], as well as reduced PL QY of the core/shell, which has also previously been reported[6]. The results given in figure 3.6c shows all the PL QYs of the sample sets 1-6 both core and ML 8 dissolved in hexane while 3.6d shows the respective samples after ligand exchange and dissolution in water. Similar to the spectra 3.6a and b, the cores of all the samples were completely quenched compared to ML 8 consistent with observation reported.[11] The trend, however, is not systematic as set 4 was quenched the least followed by set 2. However, all CdSe/CdS core/shell samples showed significant reduction in PL QY, although not as much as the core-only CdSe. For the CdSe cores, the excited electron resides at the surface of the quantum dots and easily trapped during ligand exchange, particularly using thiol ligands.

However, as the shell thickness increases, the charge carriers are confined away from the surface and thus less accessible during the ligand exchange. The degree of confinement depends on the bandgap overlap with CdSe/CdS, which is small for this system , therefore experiencing less confinement of the exciton. The conduction band offset is particularly small between CdSe and CdS [29] which results in the electron wavefunction penetrating to the shell surface, with a reasonable probability of being trapped, resulting in the observed decrease in PL QYs, even after the growth 8 monolayers shell thickness. This is a major disadvantage to using only CdS as a shell material. While they result in good core/shell materials in organic solvents, they are not ideal for transfer into water with thiol ligands. For this reason, we explore the addition of adding a secondary ZnS shell in the next chapter.

3.6. Conclusion

CdSe core quantum dots with low quality i.e. low PL QY and poor crystallinity are likely to result in high quality CdSe/CdS core/shell material, while high quality cores show poor core/shell quality. The TEM images confirms this nontrivial observation, whereby the less crystalline cores resulted in highly crystalline quantum dots after shelling. The constant k_r across all the samples sets as a function of shell thickness suggests that the observed variation in PL QYs is mainly controlled by the k_r. We have also shown that PL QYs of bare CdSe cores are completely quenched through ligand exchange and phase transfer compared to their CdSe/CdS core/shell counterparts, although they show much higher quenching than ZnS shells.

3.7. References

[1]. Klimov, V.I., et al., Optical Gain and Stimulated Emission in Nanocrystal Quantum Dots. Science, 2000. 290(5490): p. 314-317.

[2]. Kamat, P.V., Quantum Dot Solar Cells. Semiconductor Nanocrystals as Light Harvestersâ€ The Journal of Physical Chemistry C, 2008. 112(48): p. 18737-18753.

[3]. Chan, W.C.W. and S. Nie, Quantum Dot Bioconjugates for Ultrasensitive Nonisotopic Detection. Science, 1998. 281(5385): p. 2016-2018.

[4]. Bruchez, M., et al., Semiconductor Nanocrystals as Fluorescent Biological Labels. Science, 1998. 281(5385): p. 2013-2016.

[5]. Nan, W., et al., Crystal Structure Control of Zinc-Blende CdSe/CdS Core/Shell Nanocrystals: Synthesis and Structure-Dependent Optical Properties. Journal of the American Chemical Society, 2012. 134(48): p. 19685-19693.

[6]. Chen, O., et al., Compact high-quality CdSe/CdS core/shell nanocrystals with narrow emission linewidths and suppressed blinking. Nat Mater, 2013. 12(5): p. 445-451.

[7]. Saha, A., et al., Near-Unity Quantum Yield in Semiconducting Nanostructures: Structural Understanding Leading to Energy Efficient Applications. The Journal of Physical Chemistry Letters, 2013. 4(20): p. 3544-3549.

[8]. Peng, X., et al., Epitaxial Growth of Highly Luminescent CdSe/CdS Core/Shell Nanocrystals with Photostability and Electronic Accessibility. Journal of the American Chemical Society, 1997. 119(30): p. 7019-7029.

[9]. Qu, L. and X. Peng, Control of Photoluminescence Properties of CdSe Nanocrystals in Growth. Journal of the American Chemical Society, 2002. 124(9): p. 2049-2055.

[10]. Green, M., The nature of quantum dot capping ligands. Journal of Materials Chemistry, 2010. 20(28): p. 5797-5809.

[11]. Xie, R., et al., Synthesis and Characterization of Highly Luminescent CdSeâˆ’Core CdS/Zn0.5Cd0.5S/ZnS Multishell Nanocrystals. Journal of the American Chemical Society, 2005. 127(20): p. 7480-7488.

[12]. Reiss, P., J.l. Bleuse, and A. Pron, Highly Luminescent CdSe/ZnSe Core/Shell Nanocrystals of Low Size Dispersion. Nano Letters, 2002. 2(7): p. 781-784.

[13]. Garcia-Santamaria, F., et al., Breakdown of Volume Scaling in Auger Recombination in CdSe/CdS Heteronanocrystals: The Role of the Coreâˆ’Shell Interface. Nano Letters, 2010. 11(2): p. 687-693.

[14]. Chen, Y., et al., "Giant" Multishell CdSe Nanocrystal Quantum Dots with Suppressed Blinking. Journal of the American Chemical Society, 2008. 130(15): p. 5026-5027.

[15]. Li, J.J., et al., Large-Scale Synthesis of Nearly Monodisperse CdSe/CdS Core/Shell Nanocrystals Using Air-Stable Reagents via Successive Ion Layer Adsorption and Reaction. Journal of the American Chemical Society, 2003. 125(41): p. 12567-12575.

[16]. Spinicelli, P., et al., Bright and Grey States in CdSe-CdS Nanocrystals Exhibiting Strongly Reduced Blinking. Physical Review Letters, 2009. 102(13): p. 136801.

[17]. Hoy, J., et al., Excitation Energy Dependence of the Photoluminescence Quantum Yields of Core and Core/Shell Quantum Dots. The Journal of Physical Chemistry Letters, 2013. 4(12): p. 2053-2060.

[18]. Talapin, D.V., et al., Highly Luminescent Monodisperse CdSe and CdSe/ZnS Nanocrystals Synthesized in a Hexadecylamine, Trioctylphosphine Oxide and Trioctylphospine Mixture. Nano Letters, 2001. 1(4): p. 207-211.

[19]. Hines, M.A. and P. Guyot-Sionnest, Synthesis and Characterization of Strongly Luminescing ZnS-Capped CdSe Nanocrystals. The Journal of Physical Chemistry, 1996. 100(2): p. 468-471.

[20]. Dabbousi, B.O., et al., (CdSe)ZnS (Core)Shell Quantum Dots:Synthesis and Characterization of a Size Series of Highly Luminescent Nanocrystallites. The Journal of Physical Chemistry B, 1997. 101(46): p. 9463-9475.

[21]. Heyes, C.D., et al., Effect of the shell on the blinking statistics of core-shell quantum dots: A single-particle fluorescence study. Physical Review B, 2007. 75(12): p. 125431.

[22]. Htoon, H., et al., Highly Emissive Multiexcitons in Steady-State Photoluminescence of Individual "Giant" CdSe/CdS Core/Shell Nanocrystals. Nano Letters. 10(7): p. 2401-2407.

[23]. Spanhel, L., et al., Photochemistry of colloidal semiconductors. 20. Surface modification and stability of strong luminescing CdS particles. Journal of the American Chemical Society, 1987. 109(19): p. 5649-5655.

[24]. Mews, A., et al., Preparation, characterization, and photophysics of the quantum dot quantum well system cadmium sulfide/mercury sulfide/cadmium sulfide. The Journal of Physical Chemistry, 1994. 98(3): p. 934-941.

[25]. Kortan, A.R., et al., Nucleation and growth of cadmium selendie on zinc sulfide quantum crystallite seeds, and vice versa, in inverse micelle media. Journal of the American Chemical Society, 1990. 112(4): p. 1327-1332.

[26]. Blackman, B., et al., Control of the Morphology of Complex Semiconductor Nanocrystals with a Type II Heterojunction, Dots vs Peanuts, by Thermal Cycling. Chemistry of Materials, 2007. 19(15): p. 3815-3821.

[27]. Blackman, B., D. Battaglia, and X. Peng, Bright and Water-Soluble Near IR-Emitting CdSe/CdTe/ZnSe Type-II/Type-I Nanocrystals, Tuning the Efficiency and Stability by Growth. Chemistry of Materials, 2008. 20(15): p. 4847-4853.

[28]. van Embden, J., J. Jasieniak, and P. Mulvaney, Mapping the Optical Properties of CdSe/CdS Heterostructure Nanocrystals: The Effects of Core Size and Shell Thickness. Journal of the American Chemical Society, 2009. 131(40): p. 14299-14309.

[29]. Mahler, B., et al., Towards non-blinking colloidal quantum dots. Nat Mater, 2008. 7(8): p. 659-664.

[30]. Takeuchi, H., B. Omogo, and C.D. Heyes, Are Bidentate Ligands Really Better than Monodentate Ligands For Nanoparticles? Nano Letters, 2013. 13(10): p. 4746-4752.

[31]. Omogo, B., J.F. Aldana, and C.D. Heyes, Radiative and Nonradiative Lifetime Engineering of Quantum Dots in Multiple Solvents by Surface Atom Stoichiometry and Ligands. The Journal of Physical Chemistry C, 2013. 117(5): p. 2317-2327.

[32]. Ning, Z., et al., Role of surface ligands in optical properties of colloidal CdSe/CdS quantum dots. Physical Chemistry Chemical Physics, 2011. 13(13): p. 5848-5854.

[33]. Aldana, J., Y.A. Wang, and X. Peng, Photochemical Instability of CdSe Nanocrystals Coated by Hydrophilic Thiols. Journal of the American Chemical Society, 2001. 123(36): p. 8844-8850.

[34]. Dethlefsen, J.R. and A. DÃ¸ssing, Preparation of a ZnS Shell on CdSe Quantum Dots Using a Single-Molecular ZnS Precursor. Nano Letters, 2011. 11(5): p. 1964-1969.

[35]. Deng, Z., et al., A New Route to Zinc-Blende CdSe Nanocrystals: Mechanism and Synthesis. The Journal of Physical Chemistry B, 2005. 109(35): p. 16671-16675.

3.8. Appendix 1

UNIVERSITY OF ARKANSAS

J. William Fulbright College of Arts and Sciences
Chemistry and Biochemistry

To whomever it may concern

This is to certify that Benard Omogo is the first author of the manuscript mentioned below and has contributed about 90% of the work reported in this paper.

Benard Omogo and Colin D. Heyes. How the Quality of the CdSe Core affects the Optical Properties of CdSe/CdS Core/Shell Quantum Dots. To Be Submitted

Colin D. Heyes

Major Advisor

CHEM 119 • 1 University of Arkansas • Fayetteville, AR 72701-1201 • 479-575-4601 • Fax: 479-575-4049 • http://chemistry.uark.edu/

Chapter 4. Effect of Outer Shell Thickness in Core/Shell/Shell Quantum Dots on Blinking

Benard Omogo, Feng Gao, Mizuho Kaneko and Colin D. Heyes*

Department of Chemistry and Biochemistry, University of Arkansas, Fayetteville, Arkansas 72701, United States of America

*Corresponding author, Email: cheyes@uark.edu Tel: 479-575-5607

4.1. Abstract

A lot of efforts towards the suppression and elimination of blinking in quantum dots have been reported, however, these reports rely on using either very thick or highly-crystalline, medium thickness CdS shells or interfacial alloying, while using only ZnS as a shell on CdSe does not suppress blinking. Even though, there have been reports of blinking suppression with multishell configurations, particularly with CdS and ZnS, the role that interfacial trap states play in these systems is not so well understood. Here, we examined how increasing the outer shell (ZnS) thickness on CdSe/CdS/ZnS quantum dots leads to a reduction in blinking. Time resolved fluorescence, TEM and STEM/EELS were used to follow the shelling process. The different shells affect the radiative and non-radiative rates differently due to the competing effects of degree of charge carrier confinement and lattice mismatch. Using only a 3 monolayer (ML) CdS inner-shell, we find that we can greatly reduce blinking by adding just 3ML of a ZnS outer shell – thereby maintaining a relatively small QDs. However, by making the ZnS shell thicker, blinking increased again, which we attribute to induced lattice strain from the ZnS as discussed above. We anticipate that the reported QDs will be useful in bio-imaging applications due to their suppressed blinking, smaller size, and lower toxicity of the outer shell (compared to CdSe-CdS core-shells).

Keywords: colloidal semiconductor, interfacial trap-states, lattice mismatch, core/shell/shell materials, and quantum dots.

4.2. Introduction

Core-shell colloidal semiconductor nanocrystals, also known as quantum dots (QDs), are one of the most researched nanomaterials because of their unique structural and optical properties. Coating of a core material with a higher band-gap shell material, for example coating CdSe with ZnS not only improves the fluorescence quantum yield of the core by passivating the surface trap-states, but also isolates the core from the effects of the external environment.[1-3] This advantage is particularly prevalent for CdSe/ZnS core/shell materials, due to the strong electron and hole confinement brought about by the higher band gap energy offset of ZnS compared to CdSe.[2] However, it has also been reported[2] that this material combination is imperfect due to the large lattice mismatch of 12% and, in fact, generates additional defects at the interface that act as trap-states and contribute to the non-radiative pathways known to lower quantum yields and promote blinking besides distorting the shape of the QDs. A study relating these trap-states to the distribution of the shell material[4] emphasized that the growth of a simple ZnS shell on CdSe is not enough for superior properties as it leads to non-uniform spherical shells. They suggested[4] that a major reason for this anisotropic distribution in CdSe/ZnS core/shell may be due the large difference in lattice constants (a = 3.81 Å and c = 6.26 Å for ZnS compared to a = 4.30 Å and c = 7.01 Å for CdSe) for the two materials.

QD blinking has been extensively studied[5-13] and reviewed,[14, 15] and is generally attributed to the trap states, which can be due to the crystal imperfections of the CdSe core, the interface between the core and the shell, the shell/shell interface for core/shell/shell QDs as well as the external surface at the inorganic/organic interface. Therefore, one of the most common ways towards suppressing blinking is to eliminate these trap states. Growing a thicker multishell material

up to ~19 MLs of a on CdSe core was reported to suppress blinking.[6] This thickness of ~19 MLs was found to be useful in confining the excitation away from surface trap states. The smaller lattice mismatch of 3.9 % between these core and shell enabled for the growth of thick shells with minimal interfacial defects, eventhough the exciton wave functions are more separated resulting in reduced radiative rates. Also, following the same strategy, a 14ML shell thickness grown on the CdSe core was reported to result in about 68% of the quantum dots studied to be non-blinking.[11] More recently, a slow shell growth method generated exceptionally high crystalline shells and reduced blinking quantum dots with only 7 MLs of CdS onto CdSe core.[5] Here, the high crystallinity and uniformity, narrow emission linewidth and suppressed blinking of the nanocrystals observed were attributed to the slow growth at higher temperature facilitated by the low reactivity of octanethiol as the shell precursor ligand.

Contrary to the reduced blinking observed in CdSe/CdS core/shell quantum dots, growing 7 ML s of ZnS shell on CdSe core [10] had been reported to have no effect on the blinking. This effect was attributed to the larger lattice mismatch, which is also known to limit the growth of very thick ZnS shell [2] unlike the CdS shell counterpart.[6] To circumvent the challenges common in CdSe/CdS and CdSe/ZnS core/shells materials, a different class of quantum dots, core/shell/shell systems are becoming more popular. Some of the superior properties of this class of quantum dots are the elimination of the toxic cadmium from the surface and maximizing the optical properties of quantum dots simply by choosing a proper material combination. Furthermore, proper control of the exciton confinement and defects (tap states) generation by the higher band gap ZnS and smaller lattice mismatch CdS shells, respectively, should enable higher quality particles that remain smaller than using only CdS. For instance, Mews *et al* [16] reported on high crystalline and almost perfectly spherical quantum dots with about 70-85% PL quantum yield obtained by

gradually changing the shell composition from CdS to ZnS in the radial direction. Using the same materials, Talapin *et al* [17] and Hai *et al*, [18] independently minimized the interfacial strain and exciton confinement to engineer very photo-stable quantum dots by growing a CdS as a buffer shell between the CdSe core and the outer ZnS shell. The former group reported PL quantum yield of up to 80 %. Also Fitzmorris *et al* [19] who reported on CdSe/ZnSe/ZnS core/shell/shell observed an increased fluorescence lifetime which was attributed to the elimination of the nonradiative recombination components by minimizing the strain in core/shell/shell quantum dots. Furthermore Xu *et al* [20] observed stability of their quantum dots both in different physiological conditions in PBS buffer and under continuous UV radiation.

However, a systematic study on blinking of these core/shell/shell systems have not been extensively carried out. Here, we particularly focus on varying the core/shell and shell/shell strain by varying the outer ZnS shell thickness and correlate it to the fluorescence blinking of CdSe/CdS/ZnS QDs. We show that both the degree of exciton confinement and the defects caused by lattice strain induced by the addition of the outer shell plays very important roles in blinking. Our strategy is to increase the confinement potential of the electron and hole wave functions by the ZnS shell, while at the same time minimizing the defect formation at the interfaces to produce high quality but still small quantum dots. Using only a 3 monolayer (ML) CdS inner-shell, we find that we can greatly reduce blinking by adding just 3ZnS outer shell – thereby maintaining a relatively small overall QD diameter, and are amongst the smallest reduced-blinking QDs reported.We found that by making the ZnS shell thicker, blinking increased again, which we attribute to induced lattice strain from the ZnS. We anticipate that the reported QDs will be useful in bio-imaging applications due to their suppressed blinking, smaller size, and lower toxicity of the outer shell.

4.3. Experimental Section

4.3.1. Chemicals. Cadmium oxide (CdO, 90%, Sigma-Aldrich), selenium powder (Se, 99.99%, Alfa Aesar), zinc oxide (ZnO, 99%, Sigma-Aldrich), sulfur powder (S, 99.9%, Alfa Aesar), oleic acid (OA, tech. grade, Alfa Aesar), 1-octadecene (ODE, 90%, Alfa Aesar), octadecylamine (ODA, 95%, Acros Organics), tri-butylphosphine (TBP, 95%, Alfa Aesar)5-carboxytetramethylrhodamine dye (5-CTMR dye, Invitrogen), poly(methyl methacrylate) (PMMA, Sigma-Aldrich) and tri-octylphosphine oxide (TOPO, Sigma-Aldrich) were used as purchased without further purification. Solvents: methanol, hexane, and acetone were of pure grade, except toluene which was of high purity grade for HPLC and were all bought from VWR international.

4.3.2. CdSe Core Synthesis. CdSe core samples were synthesized by modification of the literature methods.[2, 21-23] Briefly, 0.04 M cadmium (Cd) precursor was prepared by degassing under vacuum and then heating a mixture of 0.02565 g CdO, 0.4452 g OA and 2 g ODE to 200^{o}C under argon flow until the solution became clear. The temperature was then reduced to 50^{o}C at which point 1.5092 g of ODA and 0.5026 g of TOPO was added, degassed and heated to 300^{o}C under argon flow. At this temperature, a pre-made 0.04 M Se precursor solution (0.01579 g Se, 0.4653 g TBP and 1.37 g ODE) was swiftly injected and after a few seconds, the heating mantle was removed to stop the growth of the particles. The solution was then allowed to cool to room temperature, and then purified by dissolving in approximately equal amounts of hexane and methanol. The mixture was centrifuged at 7K rpm for about 5 to 10 min depending on the purity of the sample. The process was repeated 3 times and the final purified solution was kept in a refrigerator at 4^{o}C for storage until the the shelling process was performed.

4.3.3. Core/shell/shell synthesis. The shelling process was performed using a combination of thermal cycling (TC)[21] and successive ion layer adsorption and reaction (SILAR) methods.[22] Typically 0.04 M Cd or zinc (Zn) precursors were prepared in the same way as the Cd precursor while 0.04 M S precursor followed the same method as that of Se, both described in the previous section. The starting CdSe core solution for the shelling process was prepared by mixing 1.5 mL of CdSe in hexane, 1.5 g ODA and 4 mL ODE in the reaction flask. A pair of pre-calculated amounts of sulfur and either cadmium or zinc precursors, enough for the growth of a single monolayer (ML) were injected individually at a lower temperature of 180^{o}C and allowed to equilibrate for 5 min each before raising the temperature to 210^{o}C for an additional 20 min for the growth of a CdS shell and to 230^{o}C for a ZnS shell. The S precursor was always injected first. Approximately 1 mL aliquots were taken out and dissolved in hexane for measurements prior to lowering the temperature for subsequent injection. The first 3 ML injections were for the CdS shell while the last 5 ML injections were for the ZnS shell. Transmission electron microscope (TEM) image measurements were performed to confirm the actual thickness, as reported under the results and discussion section.

4.4. Instrumentation and measurements

4.4.1. Fluorescence and Absorption Spectroscopy. Photoluminescence (PL) and absorbance of the aliquots were measured with a Perkin Elmer LS 55 luminescence spectrometer and Hitachi U-3900H spectrophotometer, respectively. PL percentage quantum yields (PL QYs) were measured by comparing the integrated area of each ML spectra to that of 5-CTMR dye dissolved in methanol to the same optical density of 0.05 at the excitation wavelength of 500 nm.

4.4.2. Transmission Electron Microscopy. Transmission electron microscopy (TEM) and high resolution TEM (HRTEM) images were performed on a Titan TEM (FEI Company) operating

with an acceleration voltage of 300kV. Z-contrast scanning TEM (z-STEM) coupled with electron energy loss spectroscopy (EELS) results were also obtained with the same Titan instrument, but in energy-filtered mode whereby a nanoscale probe of the beam is focused at one point as it is scanned across the survey region**.** TEM samples were prepared by depositing ~ 200 µL of thoroughly purified samples on a thin film of carbon-coated copper grids. The measurements of the QDs diameter was carried out using the image J program and the EELS spectral analysis was performed using the digital micrograph software.

4.4.3. Fluorescence Microscopy. Average fluorescence lifetime and blinking measurements were carried out MicroTime 200 fluorescence microscope (PicoQuant GmbH, Berlin, Germany) which is based on an Olympus IX71.2[8, 24] and equipped with PicoHarp 300 TCSPC controller. It uses a 485 nm laser (PDL 485, Picoquant) to excite the quantum dot samples using a dichroic mirror (500dcxr, Chroma) to send the beam through a water immersion objective (Olympus, Apochromat 60x, NA 1.3) to achieve a diffraction-limited laser focus. The fluorescence is collected by the same objective and passed through the dichroic mirror and a 100 µm diameter pinhole. A fluorescence filter (605/55, Chroma) is placed in front of Single Photon Avalanche Diode Detector (SPAD, MPI, Microphotonic devices, Bolano, Italy) to reject background fluorescence and scattered laser light.

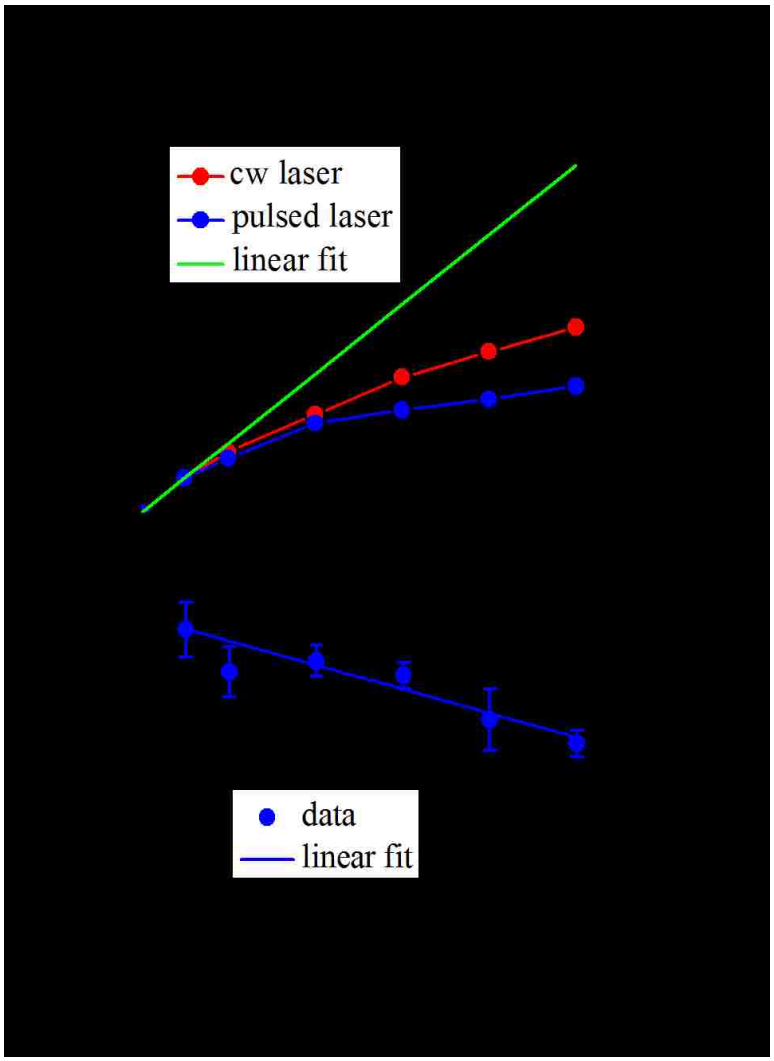

Figure 4.1. (A) The comparisons of fluorescence intensities of single QDs in PMMA matrix from cw laser or pulsed laser excitation. (B) The fluorescence lifetimes of single QDs decrease slightly over the laser power range of 5-50 μw.

The objective is positioned on a subnanometer precision 3D piezo scanning stage (PI, Berlin, Germany) and fluorescence images of 20×20 μm were recorded. For fluorescence blinking experiments, 50 μl of highly diluted quantum dot (QD) solution containing ~3% (W/V) Poly(methyl methacrylate) (PMMA) in Toluene was spin coated onto a clean No.1 glass coverslip to make a thin film for immobilizing single QDs in the PMMA matrix.

By focusing the diffraction-limited laser focus onto the individually well-isolated bright spots in the recorded fluorescence images, 5 minutes long fluorescence traces with the time resolution of 10 ms were obtained for single QDs. The fluorescence intensities of single QDs in PMMA matrix from the laser operating in either cw pulsed mode were found to be very similar to each other between 0 μw to 10 μw excitation power. Above 10 μw laser power, the average fluorescence intensity of single QDs from cw laser is higher than those for pulsed laser excitation (figure 4.1a). Furthermore, the dependence of fluorescence intensity on laser power becomes very non-linear, suggesting photophysical effects such as multiphoton absorption and multiexciton generation that may lead to Auger recombination and/or enhanced blinking plays a major role above 10 μw. The fluorescence lifetimes of single QDs were also found to decrease slightly with the laser power in the range of 5-50 μw (4.1b), in agreement with the possibility of laser-induced Auger processes.

Therefore, to minimize non-linear photophysical effects, the laser power was set to be ~10 μw for fluorescence blinking experiments, where QDs show minimal non-linearity but at the same time the signal-to-noise ratio of the obtained fluorescence traces is high enough for subsequent analysis. The SymPhoTime software was used for controlling the MicroTime 200 microscope and exporting the fluorescence traces of single QDs, which are then analyzed by a home-written Igor program for obtaining distributions of on-times, off-times, on-time fractions, as well as the relative fluorescence brightness (average fluorescence intensity of on-time events) from individual QDs. By recording the fluorescence traces with both cw and pulsed laser excitation, we are able to compare how the laser mode and particularly how multiphoton excitation affects the blinking behavior of the synthesized CdSe/CdS/ZnS core/shell/shell QDs.

4.5. Results and Discussion

4.5.1. Optical properties. The ensemble photoluminescence (PL) measurements were all performed at the same optical density of 0.05 and excited at 500 nm. The PL intensities steadily increased with each addition of CdS shell thickness with the maximum observed after the first ZnS addition followed by a steady decline as the number of ZnS shell increases as shown in figure 4.2a. Furthermore, the PL spectra indicated a uniform particle size distribution as confirmed by the small full width at half maximum (FWHM) value below 32 nm, as given in figure 4.2b. The absorbance spectral redshift observed (figure 4.2c) was plotting in terms of the first exciton absorption and PL λ_{max} (figure 4.2d) to highlight the gradual increase in wavelength as well as the constant stoke shift as the shell grows. The increase was observed to be larger with CdS shells compared to the ZnS shell counterparts.

It is known that the conduction band offset between CdSe and CdS is very small and this enables electron to leak more easily from the core into the shell while on the other hand, the same band offset for CdSe and ZnS is higher, confining the electron more strongly to the core, thus reducing the degree of the redshift. This redshift strongly supports that the resulting particles are core/shell/shells and not alloyed at any level, otherwise, a blue shift would be observed.[25] The aforementioned features of these material combination explains well the observed trend in the PL quantum yields (PL QYS) and lifetimes as given in figure 4.3a.We attribute the initial increase in PL QY to the passivation of the surface trap states and the confinement of the exciton by the higher band gap shell materials. However, as the shell thickness increases, strain is developed between the different materials resulting into dislocation of the atoms at the interface, generating defects [26] which act as trap states.

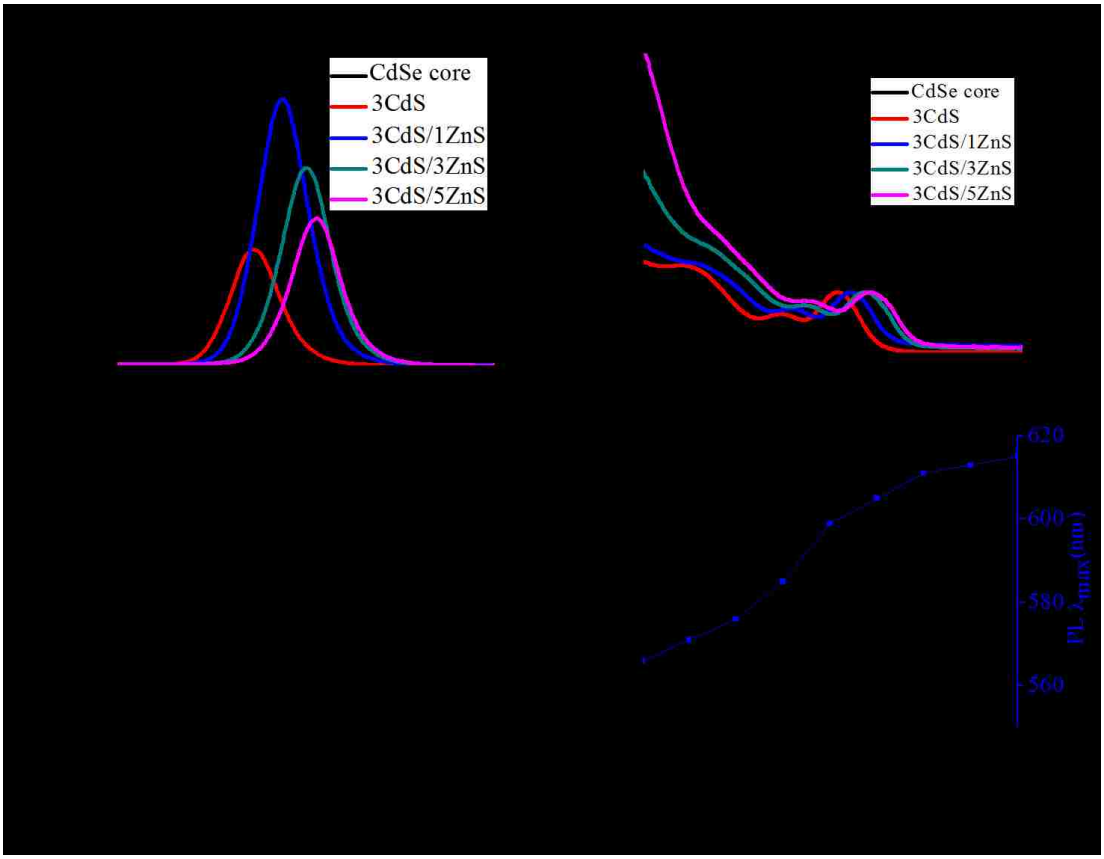

Figure 4.2. (A) Photoluminescence (PL) spectra of selected samples and their respective full width at half maximum (FWHM) (B) plotted as a function of shell thickness. (C) Absorbance spectra of the same samples together with their respective 1st exciton peak of absorption and PL as a function of shell thickness (D).Figures 4.2 (A-C) are plotted in both nm and eV units and are the same samples investigated at single particle level.

The observed decrease in PL QYs as the shell becomes thicker is, therefore, ascribed to these trap states through which non-radiation exciton combinations occur. These defects are expected to be more pronounced in CdS/ZnS than in CdSe/CdS interfaces due to the different lattice mismatch of 7.8% and 3.9%, respectively.

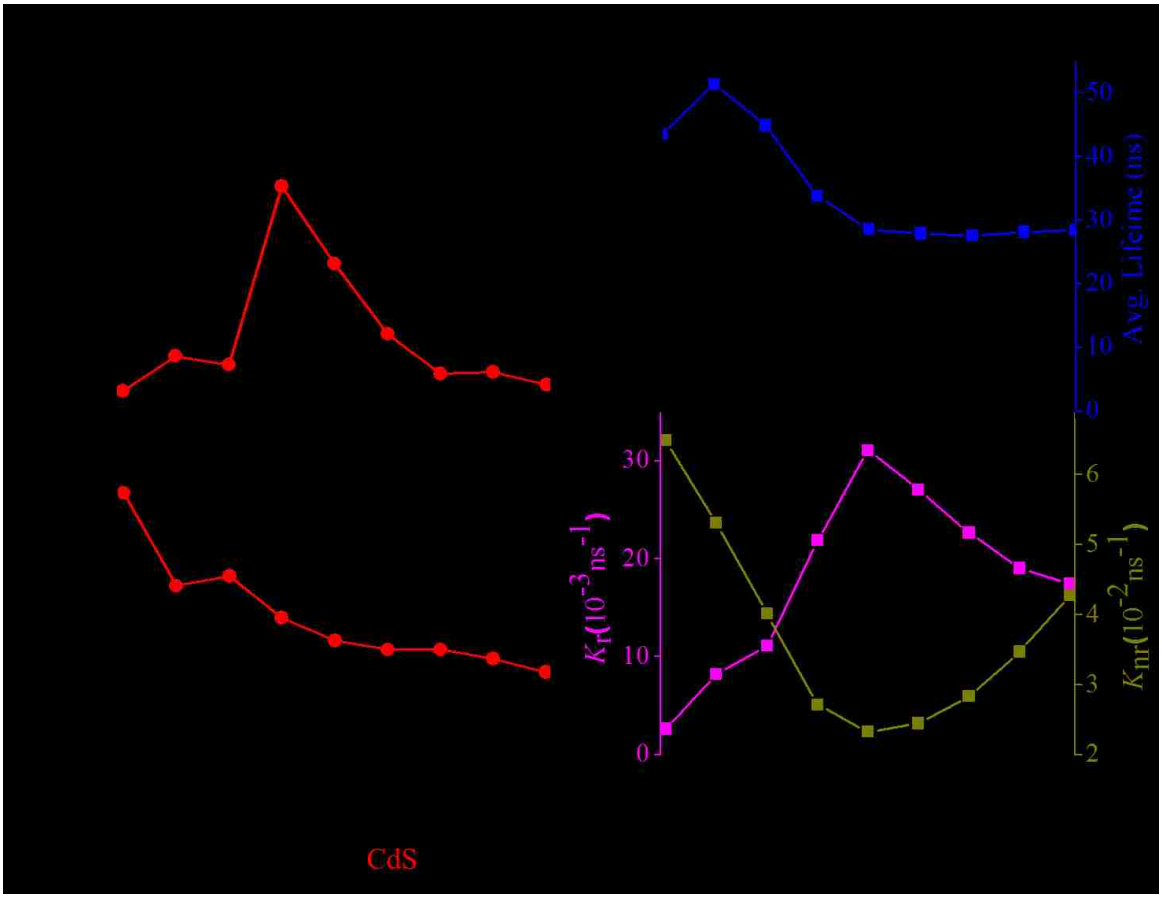

Figure 4.3.(A) PL quantum yields of CdSe/8ML CdS core/shell (red) and CdSe/3CdS/5ZnS core/shell/shell (black) as a function of shell thickness. (B) Average fluorescnec lifetime of CdSe/8ML CdS core/shell (red) and CdSe/3CdS/5ZnS core/shell/shell (black). (C) PL quantum yield and average lifetimes histogram as function of shell thickness (D) Comparison of radiative and non-radiative rates extracted from figure 4.3(C) and plotted as a function of shell thickness.

Figure 4.3a and b show the PL QYs and average fluorescence lifetimes, respectively, of two different samples, CdSe/8 ML CdS core/shell and CdSe/3CdS/5ZnS core/shell/shell samples overlaid together to highlight the overall similar trend as he shell thickness increases. Relating the PL QYs to the average lifetimes of the core/shell/shell samples (figure 4.3c) suggests that the observed trends may be as a result of changes in either or both the radiative and non-radiative rates. Therefore, we separated these two process using equations 4.1 and 4.2 where τ_{fl} is the average

fluorescence lifetime, k_r is the radiative decay rate constant and k_{nr} is the non- radiative decay rate constant respectively, and plotted as shown in figure 4.3d.

$$QY = \tau_{Fl} \kappa_{rad} \quad \textbf{4.1}$$

$$k_{nonrad} = \frac{1}{\tau_{Fl}} - k_{rad} \quad \textbf{4.2}$$

An increase in the radiative rate (k_r) with the first few shell monolayers shows a good passivation of the surface trap states by the shell material. This also results in an initial decrease in non-radiative rate (k_{nr}) as the trap sites through which nonradiative recombination would be enhanced through are eliminated. As discussed above, the increase in shell thickness increases interfacial trap states that further promotes non-radiative decay pathways, as observed by the increase in non-radiative rate (figure 4.3d) as the shell increases after 3ML of CdS and 1ML of ZnS. A closer look at the rates, shows that radiative rate closely follows the same trend as that of the PL QYs indicating that the overall observed PL QYs are more controlled by k_r pathways than the radiative ones, highlighting the importance of controlling lattice strain to improve the fluorescence properties of core/shell and core/shell/shell QDs.

4.5.2. Quantum dots sizes and distributions. A better way of confirming the actual size of QDs besides absorption and PL spectroscopy information is by analyzing TEM images. The TEM images of all the samples described here, therefore, were recorded to confirm the growth and size distribution observed from their optical properties. As shown in figure 4.4a, the increase in quantum dots' size from the CdSe core to CdSe/3CdS/5ZnS samples, further re-affirms the shelling process as observed by redshift in both the absorbance and photoluminescence spectra. Furthermore, the shape of the particles remained spherical even in the largest sample, confirming a well-controlled synthesis when a multi-shell layer is grown.[18] Figure 4.4b shows the size

distribution histograms of the selected quantum dots that were also studied at single molecule level as discussed below. The average diameters of each of the measured samples were agreeable to the expected monolayer definition, whereby, the CdS thickness is 0.34 nm and that of ZnS is 0.31 nm.[27] An interesting observation was on the size distribution of the QDs. As the shell thickness increased, the size distribution relatively remained uniform illustrating a systematically controlled synthesis as explained earlier.

4.5.3. Structural analysis. Elemental distributions of atoms across these QDs was investigated using an annular dark field (ADF) scanning transmission electron microscopy(STEM) coupled with electron energy loss spectroscopy (EELS) techniques. This ADF-STEM technique is based on z- contrast[4], with z referring to the atomic number, so that the denser the nucleus of the atom, the greater the scattering of the beams of electrons which results in brightness being related to the elemental structure. Figure 4.4c and d show the ADF-STEM images of CdSe/3CdS/5ZnS sample where the Cd-rich regions at the centers appear brighter than the Zn-rich regions, as expected given their atomic numbers and further supports the structural quality of the shell. This observation was further evidenced by the EELS spectra from which the collected Cd signal from the center of the QD was greater than from the outer region (figures 4.4d and e), and the opposite for the Zn signal (figures 4.4d and f). Figures 4.4g and h are the histogram plots of the integrated area of the EELS' spectra highlighting this observation.

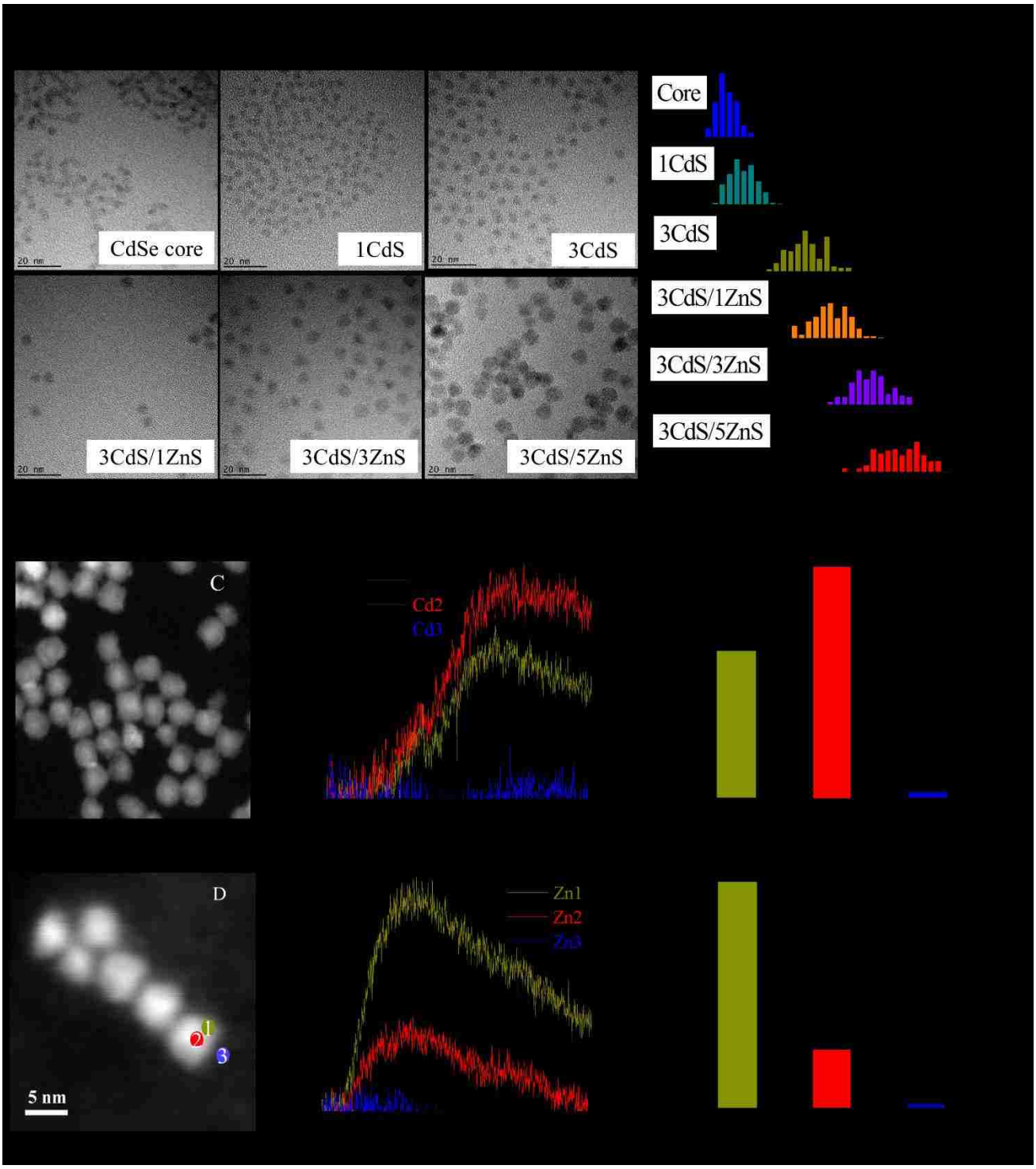

Figure 4.4. (A) TEM images of the selected samples together with their respective size distribution histogram (B)**,** (C and D) Annular dark field (ADF)-STEM images of the CdSe/3CdS/5ZnS core/shell/shell sample. (E and F) are the electron energy loss spectra (EELS) of Cd and Zn signals, respectively, collected at positions indicated in figure 4.4D. (G and H) are the integrated area histograms calculated from the spectra in figures E and F, respectively.

It is worth clarifying here that the recognizable amount of Cd at the shell and Zn at the center is caused by the beam spot overlap within those regions, together with the possible drift during measurements and does not mean that alloying took place. If there was alloying then we would expect to see more equal levels of Cd and Zn in the EELS spectra in addition to a blueshift in the absorbance spectra.[25] In fact, since the inner shell is CdS, it is expected that the outer region, point 1, of the QD would show more Cd that is observed for Zn in the inner region, point 2. Since the STEM image is a 2-D projection of a 3-D particle, there will necessarily be shell material observed even in the inner region, which accounts for the small Zn signal at point 2, since the beam must pass though the upper ZnS shell before reaching the CdS shell and finally the CdSe core. The ADF-STEM images coupled with EELS spectra satisfactory confirmed the elemental distribution in these particles to be mainly core/shell/shell in structure. Each of the QDs used in this analysis were randomly selected and all agreed to the same distribution of the atoms.

4.5.4. Blinking Studies. Fluorescence blinking experiments can provide valuable insights into the trapping mechanisms of the charge carriers as well as the nature and distribution of charge trapping sites[14], which can be used for guiding the development of brighter and non-blinking QDs for optical imaging applications, as well as for more efficient light sources and photovoltaic power generation. As mentioned earlier, for the case of core/shell QDs, it has been suggested that the shell coated onto the core results in lattice strain at the core/shell interface generating defects when the lattice strain energy is being released [17-19]. The defects at the interface will serve as very important trapping sites for the charge carriers, which may play an important role in blinking. Here, we study the blinking behaviors of CdSe/CdS/ZnS core/shell/shell QDs by fixing the CdSe/CdS core/shell size, and growing step-wise the outer ZnS shell from 1ML to 5ML.

Figure 4.5. (A) Schematic structures of CdSe/CdS/ZnS core/shell/shell QDs with 0, 1, 3, and 5 ML ZnS outer shell. (B) The corresponding 300-s fluorescence traces of the synthesized CdSe/CdS/ZnS under cw laser excitation. (C) Photon counting histograms (PCHs) for the fluorescence traces shown in (B). (D) Zoomed in 20-s fluorescence traces showing the details of the fluorescence blinking behaviors of the QDs.

We probe the mentioned lattice strain effect at the CdS/ZnS shell/shell interface, which has lattice mismatch of ~7.78%, by systematically studying the role of the outer ZnS shell thickness on the fluorescence blinking properties of CdSe/CdS/ZnS QDs. In order to study the blinking properties, fluorescence traces on immobilized single CdSe/CdS/ZnS core/shell/shell QDs embedded in a PMMA matrix were recorded as shown in figure 4.5, which typically give high quality on-and-off two-state fluorescence traces with a signal to noise ratio of ~7.

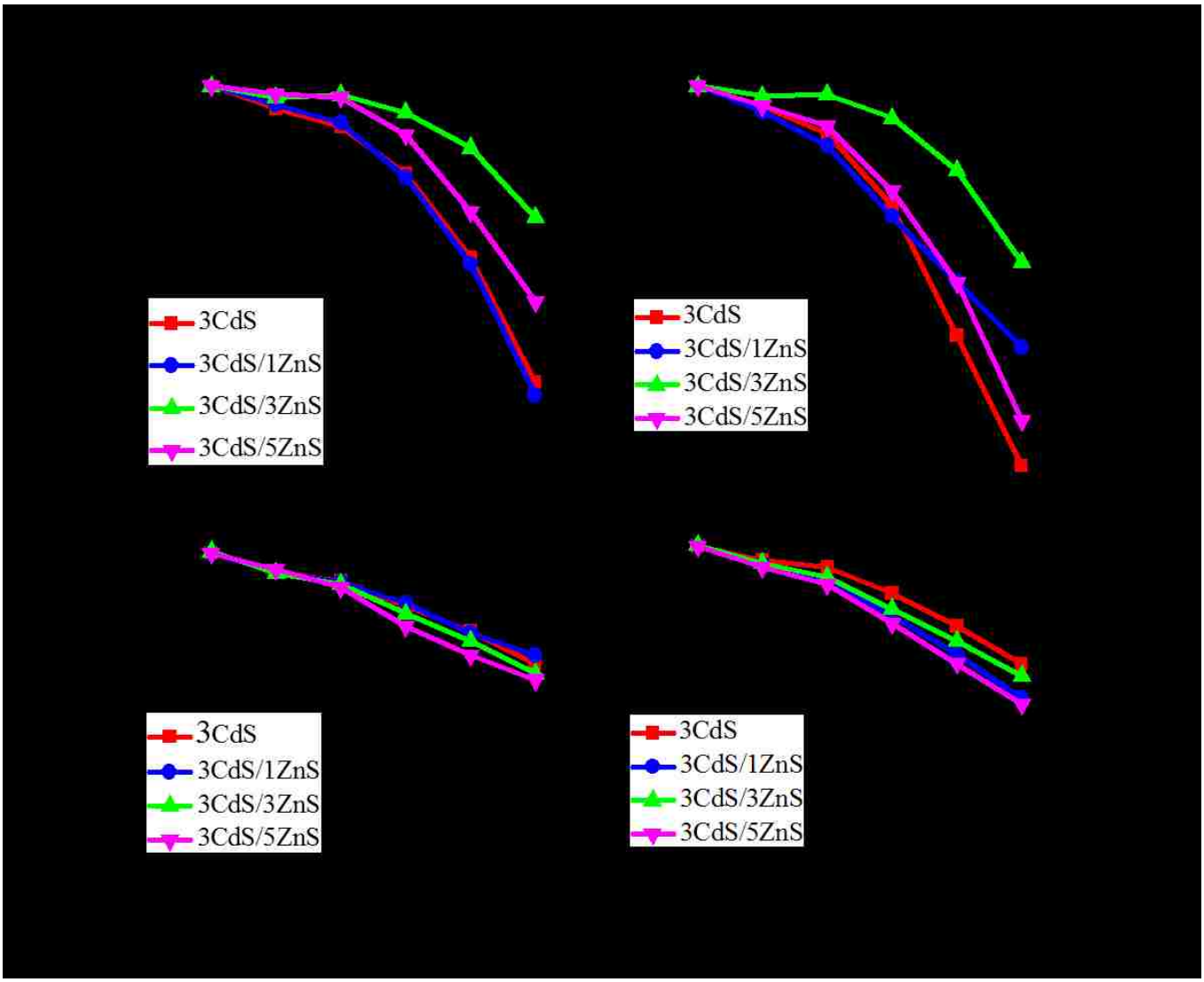

Figure 4.6. Log-log plots of P_{on} (A and C) and P_{off} (B and D) distributions for ~30 CdSe/CdS/ZnS as a function of ZnS shell thickness under cw (A and B) and pulsed laser (C and D) excitation, respectively.

The two states are indicated by the two well-separated peaks in the photon counting histograms (PCHs) of the fluorescence traces. The excellent separation of the fluorescence signal from the background allows us to directly apply a fluorescence threshold to the fluorescence traces to obtaining on-time and off-time distributions (P_{on} and P_{off}), as well as determining the on-fraction (fraction of QDs that are on at any given time) and the relative fluorescence brightness (average fluorescence intensity of the on state) for individual QDs.

Figure 4.6 shows the P_{on} and P_{off} distributions for ~30 CdSe/CdS/ZnS QDs upon varying the ZnS shell thickness from 0 to 5 MLunder both cw and pulsed laser excitation. It is clear that CdSe cores with 3ML CdS and 3ML ZnS shells shows the slowest decrease inP_{on}, meaning that longer on-time events are more probable for these QDs compared to those QDs having thinner or thicker ZnS shells. This trend remains the same under both cw and pulsed laser excitation .The P_{off} distributions, as shown in figures 4.6b and d, are similar for all of the QDs, appearing as straight lines with only small curvature at long off-times in the log-log plots. These results clearly demonstrate that theouter ZnS shell thickness does not affect the off-times, but significantly affects the on-times of the synthesized CdSe/CdS/ZnS core/shell/shell QDs, with 3ML of ZnS showing significantly reduced blinking compared to the other samples. The fact that increasing the ZnS thickness from 3ML ZnS to 5ML ZnS increases blinking rather than further reducing it strongly suggests that, besides the exciton confinement role of the outer ZnS shell[2], the CdS/ZnS shell/shell interfacial lattice strain generates defects that can trap the charge carriers and result in more frequent QD fluorescence blinking.

Figure 4.7 is the proposed model showing the schematic of conduction and valence bands of CdSe/CdS core/shell and CdSe/CdS/ZnS core/shell/shell QDs together with the trap states on the surfaces of the QDs as well as at CdS/ZnS shell/shell interfaces. Since the lattice mismatch between CdSe and CdS is relatively small (~3.8%), the blinking contributions from defects generated by lattice strain at this interface is assumed to be negligible compared to those from the CdS/ZnS interface, which has ~7.8% lattice mismatch. The surface trap states are from the surface sites with unbound ligands and proposed to be approximately the same for CdSe/CdS core/shell and CdSe/CdS/ZnS core/shell/shell QDs.

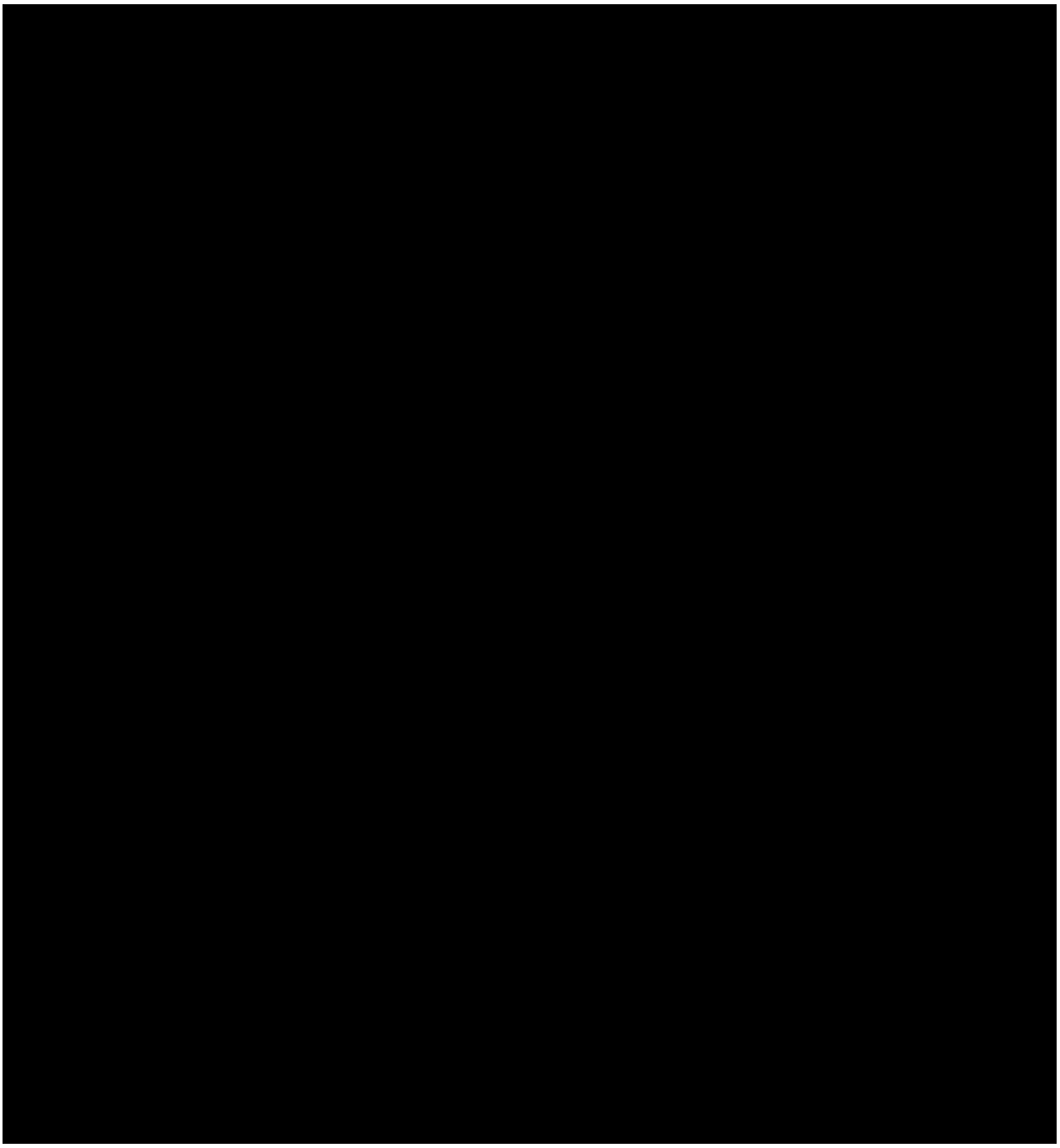

Figure 4.7. The proposed blinking model showing the conduction and valence bands of (A) CdSe/CdS core/shell and (B) CdSe/CdS/ZnS core/shell/shell QDs together with the trap states on the QD surfaces as well as at CdS/ZnS shell/shell interfaces. The number of trap states at the CdSe/CdS interface is proposed to be negligible due to the much smaller lattice mismatch between CdSe and CdS (~3.8%).

Only the exciton electron delocalization is considered, since the valance band energy of CdSe is higher than that of the CdS, so that the hole is well confined within the CdSe core compared to the electron.

Figure 4.7b shows that, with increasing the thickness of the outer ZnS shell, the number of trap states at the CdS/ZnS interface increases due to the defects generated from releasing lattice strain energy caused by the lattice mismatch between CdS and ZnS layers, resulting in more frequent QD blinking. The lattice strain at the CdS/ZnS interface will become stronger when the outer ZnS shell becomes thicker, so that more defects at CdS/ZnS interface are generated for QDs having very thick ZnS shells. However, for a few monolayers of ZnS, it is possible that much fewer defects are generated at the CdS/ZnS interface because the lattice strain energy at the interface is not high enough for it to be released.

For CdSe/CdS/ZnS QDs, there is the possibility that an exciton electron can tunnel to the CdS/ZnS interface defects sites or, if the ZnS shell is thin, to the surface trap sites.The blinking behavior of CdSe/CdS/ZnS QDs reported here should be determined by the total number of trap states at the CdS/ZnS interface and/or on the QD surface, depending on the ZnS shell thickness, as well as the exciton electron accessibilities which are determined by the rate constants[28] $k_{interface\ trap}$ and $k_{surface\ trap}$, respectively. Since ZnS has much higher band gap energy than CdS, it will provide stronger confinement to exciton electron than CdS, thus reducing electron accessibility to the surface trap sites. In other words the rate constant $k_{interface\ trap}$ becomes larger than $k_{surface\ trap}$, particularly when the ZnS shell becomes thicker. When the ZnS shell thickness increases, the accessibility of trap states on the QD surface will decrease, due to the strong confinement potential of the ZnS shell, even though the number of trap states at the CdS/ZnS interface will increase.

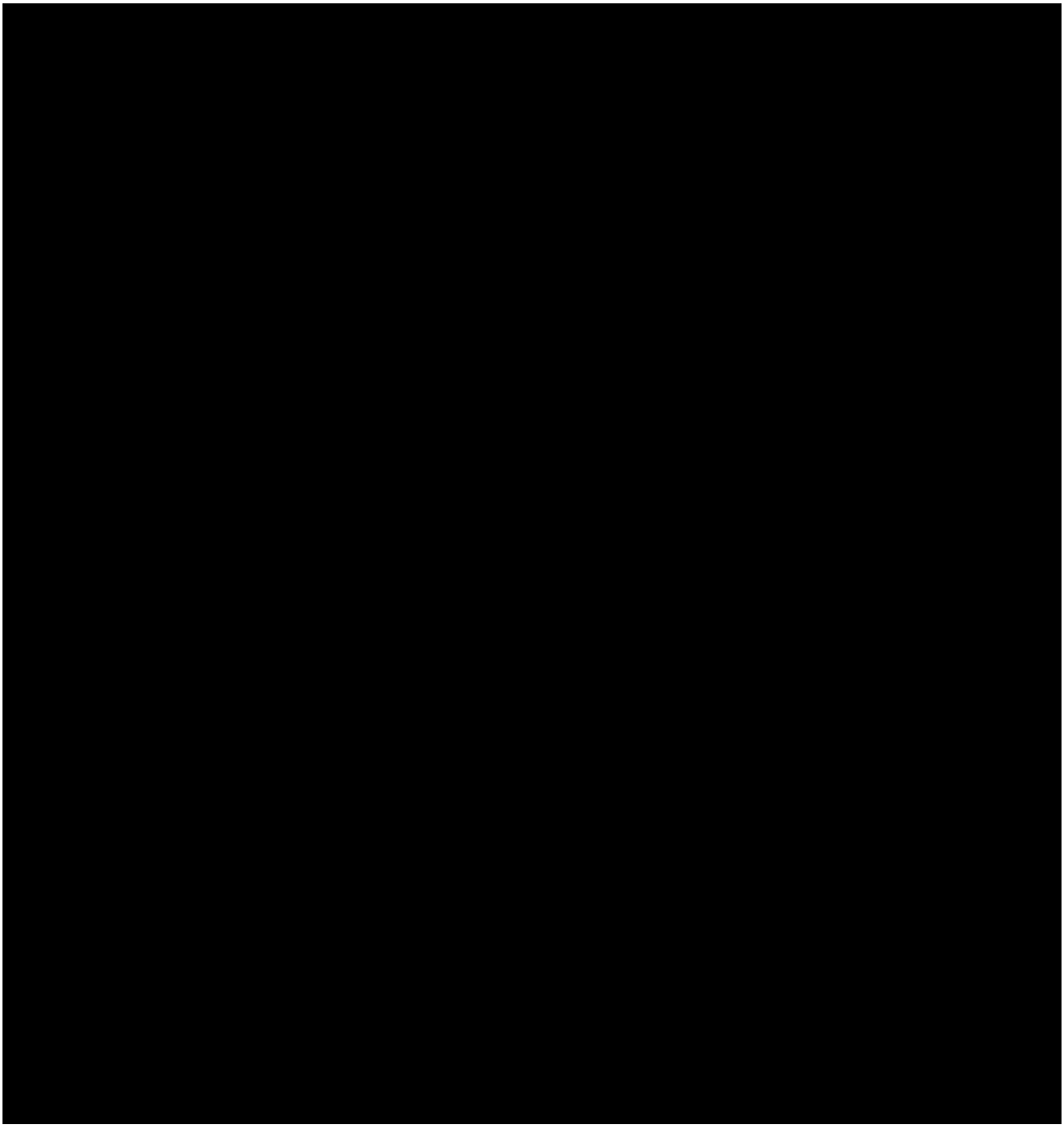

Figure 4.8. On-fraction distributions for CdSe/CdS/ZnS QDs having 3 monolayers of CdS and different thickness of ZnS shells. (A) under cw laser excitation and (B) under pulsed laser excitation.

As highlighted in figure 4.7b, for the case of CdSe/3CdS/3ZnS QDs, the total number of effective trap states is the smallest. This is to say that the accessibility of the surface states has been reduced but the lattice strain is not yet high enough to significantly increase the number of trap states at the CdS/ZnS interface, thus leading to longer on-times , as shown by P_{on} distributions in figure 4.6a and c and by the on-fraction distributions in figure 4.8.

The distributions of on-fraction for CdSe/CdS/ZnS QDs which is calculated by diving the total time at which a quantum dots is on by the total time the blinking trace is collected for each quantum dots having different thickness of ZnS shell are shown in figure 4.8. QDs with 3ML of ZnS shows an average ~40% on-fraction with significant number of QD particles showing ~60% on-fraction and the highest on-fraction is close to 80%. The on-fraction distribution is generally narrow, except for the 3ZnS QDs, indicating that CdSe/3CdS/3ZnS QDs have a large heterogeneity in terms of the probability of accessing trap states .We attribute this either to the time dependent properties of the rate constants $k_{interface\ trap}$ and $k_{surface\ trap}$ for trap state accessibility or probably ~3 ZnS outer shell thickness is the critical thickness at which lattice strain energy starts to be released at the CdS/ZnS interface, leading to some QDs with many trap states, and other with only a few.

Figure 4.9 shows that the average brightness of single QDs in the on-state as a function of outer ZnS shell thickness is very similar, which suggest that the single QD radiative and nonradiative rate constants k_r and k_{nr} in the on-state do not change very much as ZnS shell thickness is increased. This is also supported by the ensemble fluorescence lifetime results showing that k_r is not changing very much with increasing ZnS shell thickness. However, the k_{nr} from ensemble measurements increases when ZnS increases, which suggests that the variation in k_{nr} at the ensemble level is the result of dark particles, i.e. the permanent dark fraction or the blinking particles in the off-state. However this possibility needs to be investigated further.

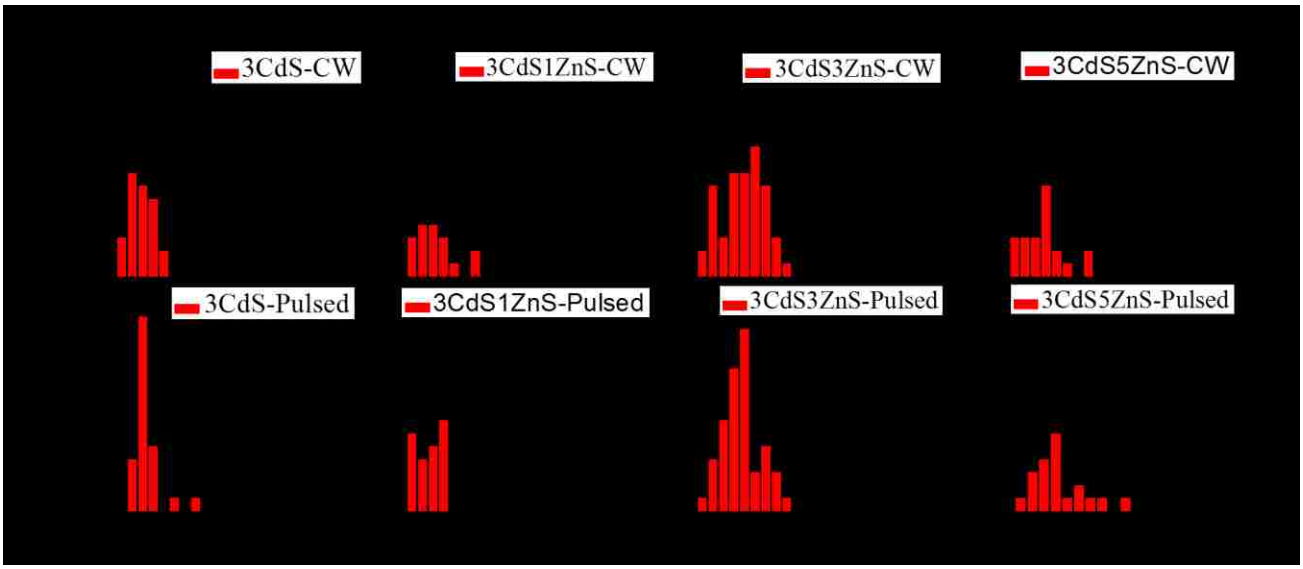

Figure 4.9. Distributions of the brightness of single QDs with different outer ZnS shell thicknesses. (A), (C), (E), (G) are under cw laser excitation, and (B), (D), (F), (H) are under pulsed laser excitation, suggesting that the mode of excitation does not affect the single QD fluorescence.

4.6. Conclusions

The quantum yield and fluorescence lifetime of core/shell/shell QDs were found to be related to trap states, which could either be at the interface between the core and the shell and/or at the surface of the quantum dots at the shell-ligand interface. Elemental distribution data, together with the absorbance and PL spectral redshift, confirmed the growth of core/shell/shell rather than alloyed materials. For the first time, the outer ZnS shell thickness was correlated to the fluorescence blinking of the synthesized CdSe/CdS/ZnS core/shell/shell QDs. Our ensemble fluorescence spectroscopy and single QD fluorescence blinking experimental results suggest that the outer ZnS shell affects CdSe/CdS/ZnS QD fluorescence blinking in two opposite ways, by better confining the exciton away from the outer surface that reduces blinking and by generating CdS/ZnS shell/shell interface defects that increase blinking. Therefore, there is a trade-off between the two roles and there is a balanced ZnS thickness where one can optimize both effects and

achieve significantly reduced QD fluorescence blinking. It can be expected that the strategy of multishell synthesis with better confinement and much less lattice mismatch at each interface can be useful for developing less interface defects and non-blinking QDs, such as CdSe/CdS/ZnSe/ZnS QDs, having relatively small QD sizes with less cytotoxic (i.e. Cd-free) surfaces.

4.7. References

[1]. Dabbousi, B.O., et al., (CdSe)ZnS (Core)Shell Quantum Dots: Synthesis and Characterization of a Size Series of Highly Luminescent Nanocrystallites. The Journal of Physical Chemistry B, 1997. 101(46): p. 9463-9475.

[2]. Hines, M.A. and P. Guyot-Sionnest, Synthesis and Characterization of Strongly Luminescing ZnS-Capped CdSe Nanocrystals. The Journal of Physical Chemistry, 1996. 100(2): p. 468-471.

[3]. Talapin, D.V., et al., Highly Luminescent Monodisperse CdSe and CdSe/ZnS Nanocrystals Synthesized in a Hexadecylamine, Trioctylphosphine Oxide and Trioctylphospine Mixture. Nano Letters, 2001. 1(4): p. 207-211.

[4]. Yu, Z., et al., Shell Distribution on Colloidal CdSe/ZnS Quantum Dots. Nano Letters, 2005. 5(4): p. 565-570.

[5]. Chen, O., et al., Compact high-quality CdSe/CdS core/shell nanocrystals with narrow emission linewidths and suppressed blinking. Nat Mater, 2013. 12(5): p. 445-451.

[6]. Chen, Y., et al., "Giant" Multishell CdSe Nanocrystal Quantum Dots with Suppressed Blinking. Journal of the American Chemical Society, 2008. 130(15): p. 5026-5027.

[7]. Cichos, F., C. von Borczyskowski, and M. Orrit, Power-law intermittency of single emitters. Current Opinion in Colloid & Interface Science, 2007. 12(6): p. 272-284.

[8]. Durisic, N., et al., Probing the Dark Fraction of Core/Shell Quantum Dots by Ensemble and Single Particle pH-Dependent Spectroscopy. ACS Nano, 2011. 5(11): p. 9062-9073.

[9]. Frantsuzov, P.A. and R.A. Marcus, Explanation of quantum dot blinking without the long-lived trap hypothesis. Physical Review B, 2005. 72(15): p. 155321.

[10]. Heyes, C.D., et al., Effect of the shell on the blinking statistics of core-shell quantum dots: A single-particle fluorescence study. Physical Review B, 2007. 75(12): p. 125431.

[11]. Mahler, B., et al., Towards non-blinking colloidal quantum dots. Nat Mater, 2008. 7(8): p. 659-664.

[12]. Spinicelli, P., et al., Non-Blinking Semiconductor Colloidal Quantum Dots for Biology, Optoelectronics and Quantum Optics. ChemPhysChem, 2009. 10(6): p. 879-882.

[13]. Wang, X., et al., Non-blinking semiconductor nanocrystals. Nature, 2009. 459(7247): p. 686-689.

[14]. Cordones, A.A. and S.R. Leone, Mechanisms for charge trapping in single semiconductor nanocrystals probed by fluorescence blinking. Chemical Society Reviews, 2013. 42(8): p. 3209-3221.

[15]. Krauss, T.D. and J.J. Peterson, Bright Future for Fluorescence Blinking in Semiconductor Nanocrystals. The Journal of Physical Chemistry Letters, 2010. 1(9): p. 1377-1382.

[16]. Xie, R., et al., Synthesis and Characterization of Highly Luminescent CdSeâˆ’Core CdS/Zn0.5Cd0.5S/ZnS Multishell Nanocrystals. Journal of the American Chemical Society, 2005. 127(20): p. 7480-7488.

[17]. Talapin, D.V., et al., CdSe/CdS/ZnS and CdSe/ZnSe/ZnS Core/Shell/Shell Nanocrystals. The Journal of Physical Chemistry B, 2004. 108(49): p. 18826-18831.

[18]. Hai, L.B., et al., Preparation and spectroscopic investigation of colloidal CdSe/CdS/ZnS core/multishell nanostructure. Journal of Experimental Nanoscience, 2009. 4(3): p. 277-283.

[19]. Fitzmorris, B.C., et al., Synthesis and Structural, Optical, and Dynamic Properties of Core/Shell/Shell CdSe/ZnSe/ZnS Quantum Dots. The Journal of Physical Chemistry C, 2012. 116(47): p. 25065-25073.

[20]. Xu, S., et al., Effect of Shell Thickness on the Optical Properties in CdSe/CdS/$Zn_{0.5}Cd_{0.5}S$/ZnS and CdSe/CdS/$Zn_xCd_{1-x}S$/ZnS Core/Multishell Nanocrystals. The Journal of Physical Chemistry C, 2011. 115(43): p. 20876-20881.

[21]. Blackman, B., et al., Control of the Morphology of Complex Semiconductor Nanocrystals with a Type II Heterojunction, Dots vs Peanuts, by Thermal Cycling. Chemistry of Materials, 2007. 19(15): p. 3815-3821.

[22]. Li, J.J., et al., Large-Scale Synthesis of Nearly Monodisperse CdSe/CdS Core/Shell Nanocrystals Using Air-Stable Reagents via Successive Ion Layer Adsorption and Reaction. Journal of the American Chemical Society, 2003. 125(41): p. 12567-12575.

[23]. Peng, Z.A. and X. Peng, Nearly Monodisperse and Shape-Controlled CdSe Nanocrystals via Alternative Routes:Nucleation and Growth. Journal of the American Chemical Society, 2002. 124(13): p. 3343-3353.

[24]. Gao, F., et al., 3D Imaging of Flow Patterns in an Internally-Pumped Microfluidic Device: Redox Magnetohydrodynamics and ElectrochemicallyGenerated Density Gradients. Analytical Chemistry, 2013. 85(9): p. 4414-4422.

[25]. Aldeek, F., et al., Enhanced Optical Properties of Core/Shell/Shell CdTe/CdS/ZnO Quantum Dots Prepared in Aqueous Solution. The Journal of Physical Chemistry C, 2009. 113(45): p. 19458-19467.

[26]. Chen, X., et al., Coherency Strain Effects on the Optical Response of Core/Shell Heteronanostructures. Nano Letters, 2003. 3(6): p. 799-803.

[27]. Breus, V.V., C.D. Heyes, and G.U. Nienhaus, Quenching of CdSe/ZnS Core/Shell Quantum Dot Luminescence by Water-Soluble Thiolated Ligands. The Journal of Physical Chemistry C, 2007. 111(50): p. 18589-18594.

[28]. Omogo, B., J.F. Aldana, and C.D. Heyes, Radiative and Nonradiative Lifetime Engineering of Quantum Dots in Multiple Solvents by Surface Atom Stoichiometry and Ligands. The Journal of Physical Chemistry C, 2013. 117(5): p. 2317-2327.

4.8. Appendix 1

UNIVERSITY OF ARKANSAS

J. William Fulbright College of Arts and Sciences
Chemistry and Biochemistry

To whomever it may concern

This is to certify that Benard Omogo is the first author of the manuscript mentioned below and has contributed about 55% of the work reported in this paper.

Benard Omogo, Feng Gao, Mizuho Kaneko and Colin D. Heyes. Effect of Outer Shell Thickness in Core/Shell/Shell Quantum Dots on Blinking. To Be submitted

Colin D. Heyes

Major Advisor

CHEM 119 • 1 University of Arkansas • Fayetteville, AR 72701-1201 • 479-575-4601 • Fax: 479-575-4049 • http://chemistry.uark.edu/

Chapter 5. Conclusion

This thesis has been developed to better understanding the influence of interfacial chemistry in core, core/shell and core/shell/shell quantum dots on their fluorescence properties. In chapter 2, the processes that take place at the interface between the quantum dot cores and the ligands were investigated. Here, the resulting surface atom stoichiometry was controlled by varying the synthetic precursor ratio of Cd and Te to investigate their effect on the radiative and non-radiative relaxation rates, which were found to be anticorrelated. It was found that the density, nature and orientation of the ligand functional groups and the dielectric constant of the solvent play major roles in determining charge carrier trapping and excitonic relaxation pathways which consequently affects the PL QYs and lifetimes of quantum dots. In Chapter 3, the effect of shell growth on different quality quantum dots cores contradicted the traditional belief that higher quality cores result in higher quality core/shells. Starting with five different qualities of CdSe cores, the change in trend of both optical and structural properties with increase in CdS shell thickness up to 8ML were systematically followed and quantified.

In chapter 4, the effect of the outer shell in core/shell/shell quantum dots on both ensemble fluorescence properties and single particle blinking was investigated upon increasing its thickness. This enabled us to control both the lattice strain and exciton confinement effects. It was found that the tradeoff between lattice mismatch and exciton confinement, brought about by the different lattice parameters and band gap energy of the core and shelling semiconductor materials results into different *effective* trap states which affect the quantum dots blinking differently. In this case, 3ML of ZnS outer shell on CdSe cores with 3ML CdS inner shell was observed to be the best compromised thickness which showed less blinking.

Toxicity of cadmium (Cd) results into many complications depending on the amount and route through which it is exposed.[1]The distribution of Cd is mainly through the blood followed by rapid deposition while at the tissue and can stay as long as 29 days as was observed in the liver and kidney showing that they can pass through the kidney.[2] Their distribution especially in form of quantum dots was reported to depend on the size whereby those with sizes below 10 nm can be excreted by the kidneys, but those with approximately 50 nm size penetrate through the endothelial pores, enter the mesangium and accumulate inside mesangial cells.[2]

Comparing the cytotoxicity of different forms of Cd namely, $CdCl_2$, CdO and CdS micro and nano, Ohayon-Courtès *et al* [3] reported that CdS nano appeared to be approximately hundred times less cytotoxic than $CdCl_2$ or CdO, whereas intracellular Cd content in LLC-PK1 was similar for all forms.[3]Since the toxicity results from the release of Cd^{2+} into cells during dissolution, they hypothesized that the cytotoxic effects of Cd are strongly correlated with the intracellular Cd content and that both CdO and $CdCl_2$ with higher content are more soluble. However, the higher toxicity observed for the CdS nano than the micro was attributed to the higher diffusion rate of the nano form compared to the micro.

Several other groups have also reported the cytotoxicity of cadmium based quantum dots.[3-8] For instance, Guo *et al* [4]proved that surface modified CdSe QDs with low cytotoxicity have good potential in biological applications. The quantum dots surface were modified using Fluronic-68 (F 68), cetyltrimethyl ammonium bromide (CTAB) and sodium dodecyl sulfate (SDS) resulting in to samples with nonionic, positive and negative quantum dots, respectively, which were subsequently evaluated for their viability in HepG2 model cells using MTT viability assay.[4]Both of 68 and CTAB surface modified quantum dots showed less cytotoxity while the SDS showed significant cell damage. Fluorescence images obtained by intravenously injecting the F-68 surface

modified quantum dots in to a mice further confirmed on their possibility for biological applications.

Fan *et al*[8]also evaluated the toxicity of CdTe, CdTe/CdS and CdTe/CdS/ZnS quantum dots directly synthesized in aqueous media. They reported that the CdTe QDs are highly toxic for cells due to the release of cadmium ions while the growth of a CdS layer reduced the cytotoxicity of QDs to a small extent. However with ZnS shell on CdTe/CdS, the cytotoxicity was greatly minimized even at very high concentration and over longtime exposure. Almost similar in composition arrangements to our quantum dots as reported in chapter 4 above, these quantum dots were found to be highly biocompatible [8] thus offering quantum dots with better quality for biological applications. Furthermore, the smaller size ~ 8 nm and reduced blinking of our core/shell/shell quantum dots specifically CdSe/3CdS/3ZnS as discussed above further provides promising quantum dots for biological labelling and imaging.

Future work in this area of quantum dots therefore, should incorporate the use of less toxic material basically designed as given in details in section 4.2 for labelling biomolecules. The use of quantum dots in labelling biomolecules is not new [9-12] even though it is still faced with a lot of challenges. For instance, Bawendi et al [10] compared the *in vivo* suitability of their high crystalline CdSe/CdS quantum dots (new generation) with the conventional quantum dots by first modifying the surface through ligand exchange using methoxy-polyethylene-glycol thiol followed by intravenous injection in Tie2-GFP transgenic mice bearing dorsal skinfold chambers. The intravital multiphoton microscopy showed that their new generation quantum dots were ~ 4.7 times brighter than the conventional quantum dots. As discussed earlier, quantum dots with CdS outer shell are relatively toxic which still hinders the aforementioned quantum dots for proper biological applications.

Therefore, designing a similar experiment but using core/shell/shell quantum dots with compositional arrangements as we have reported here may provide an ideal breakthrough to the labelling of biomolecules using quantum dots. For instance, bioconjugating a given protein such as fibroblast growth factor receptor (FGFR) or cpSRP43, as used in our laboratory, with these quantum dots and studying their FRET may provide a better understanding of their behavior.

5.1. References

[1]. Iversen, T.-G., T. Skotland, and K. Sandvig, Endocytosis and intracellular transport of nanoparticles: Present knowledge and need for future studies. Nano Today, 2011. 6(2): p. 176-185.

[2]. Rzigalinski, B.A. and J.S. Strobl, Cadmium-containing nanoparticles: Perspectives on pharmacology and toxicology of quantum dots. Toxicology and Applied Pharmacology, 2009. 238(3): p. 280-288.

[3]. L'Azou, B., et al., Comparative cytotoxicity of cadmium forms ($CdCl_2$, CdO, CdS micro- and nanoparticies) in renal cells. Toxicology Research, 2014. 3(1): p. 32-41.

[4]. Guo, G., et al., Probing the cytotoxicity of CdSe quantum dots with surface modification. Materials Letters, 2007. 61(8-9): p. 1641-1644.

[5]. Nan, C., et al., The cytotoxicity of cadmium-based quantum dots, in Biomaterials. 2012 Feb;33(5):1238 44. doi: 10.1016/j.biomaterials.2011.10.070. 2012.

[6]. Wang, L., et al., Rapid determination of the toxicity of quantum dots with luminous bacteria. Journal of Hazardous Materials, 2010. 177(1-3): p. 1134-1137.

[7]. Wispriyono, B., et al., Protection from cadmium cytotoxicity by N-acetylcysteine in LLC-PK1 cells. Journal of Pharmacology and Experimental Therapeutics, 1998. 287(1): p. 344-351.

[8]. Yuanyuan, S., et al., The cytotoxicity of cadmium based, aqueous phase - synthesized, quantum dots and its modulation by surface coating. Biomaterials, 2009. 30(1): p. 19-25.

[9]. Chen, C.-T., et al., A Triantennary Dendritic Galactoside-Capped Nanohybrid with a ZnS/CdSe Nanoparticle Core as a Hydrophilic, Fluorescent, Multivalent Probe for Metastatic Lung Cancer Cells. Advanced Functional Materials, 2008. 18(4): p. 527-540.

[10]. Chen, O., et al., Compact high-quality CdSe/CdS core/shell nanocrystals with narrow emission linewidths and suppressed blinking. Nat Mater, 2013. 12(5): p. 445-451.

[11]. Gao, X., et al., In vivo cancer targeting and imaging with semiconductor quantum dots. Nat Biotech, 2004. 22(8): p. 969-976.

[12]. Mandal, G., et al., Cadmium-free quantum dots as time-gated bioimaging probes in highly-autofluorescent human breast cancer cells. Chemical Communications, 2013. 49(6): p. 624-626.

[13]. Mahler, B., et al., Towards non-blinking colloidal quantum dots. Nat Mater, 2008. 7(8): p. 659-664.